

INFORMATION TO USERS

The most advanced technology has been used to photograph and reproduce this manuscript from the microfilm master. UMI films the original text directly from the copy submitted. Thus, some dissertation copies are in typewriter face, while others may be from a computer printer.

In the unlikely event that the author did not send UMI a complete manuscript and there are missing pages, these will be noted. Also, if unauthorized copyrighted material had to be removed, a note will indicate the deletion.

Oversize materials (e.g., maps, drawings, charts) are reproduced by sectioning the original, beginning at the upper left-hand corner and continuing from left to right in equal sections with small overlaps. Each oversize page is available as one exposure on a standard 35 mm slide or as a 17" × 23" black and white photographic print for an additional charge.

Photographs included in the original manuscript have been reproduced xerographically in this copy. 35 mm slides or 6" × 9" black and white photographic prints are available for any photographs or illustrations appearing in this copy for an additional charge. Contact UMI directly to order.



300 North Zeeb Road, Ann Arbor, MI 48106-1346 USA

Order Number 8826815

Interfacial phenomena in welding

Sahoo, Purusottam, Ph.D.

The Pennsylvania State University, 1988

U·M·I
300 N. Zeeb Rd.
Ann Arbor, MI 48106

The Pennsylvania State University
The Graduate School

INTERFACIAL PHENOMENA IN WELDING

A Thesis in
Metals Science and Engineering
by
P. Sahoo

© 1988 by P. Sahoo

Submitted in Partial Fulfillment
of the Requirements
for the Degree of

Doctor of Philosophy

August 1988

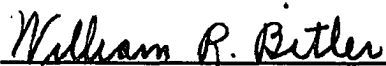
We approve the thesis of P. Sahoo.

Date of Signature



29 April '88

Tarasankar DebRoy
Associate Professor of Metallurgy
Chair of Committee
Thesis Adviser



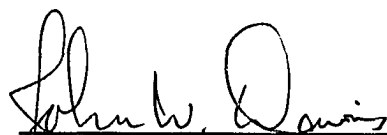
29 April 1988

William R. Bitler
Professor of Metallurgy



29 April 1988

W. Murray Small
Associate Professor of Metallurgy



29 April '88

John W. Davis
Associate Professor of Industrial and
Management Systems Engineering



April 29, 1988

Donald A. Koss
Professor of Metallurgy
In Charge of Graduate Programs in
Metals Science and Engineering

ABSTRACT

A knowledge of the interfacial phenomena in welding is crucial to an understanding of the associated process and weld metal properties. The interfacial tension is the dominant force for fluid flow in welding. The variation of interfacial tension as a function of temperature and composition of the melt is not well understood. Further compounding this effect is the role of plasma during welding. Important questions such as how plasma affects the nature of the interface and thus the interfacial tension forces and vaporization losses of alloying elements remain unanswered. Thus, a rational strategy for the investigation of the welding process and weld metal properties must include an understanding of the interfacial phenomena relevant to welding metallurgy.

Both theoretical and experimental studies were conducted to obtain a fundamental understanding of the nature of the interfacial tension and a physical concept of the weld metal interface in an environment which contains excited and charged species. A combination of Gibbs and Langmuir's adsorption isotherms was used to develop an expression of interfacial tension as a function of both temperature and composition of binary metal-surface active systems. Theoretical predictions of surface tension as a function of temperature and composition were compared with existing data and fair agreement was observed. The variation of the temperature coefficient of surface tension and its effect on fluid flow was examined from a theoretical and experimental standpoint. Using a radio frequency power generator, an inductively coupled plasma was generated and interfacial tension was measured both in the presence and absence of the plasma. The variables studied were temperature, plasma composition and plasma intensity of

emission. A hypothesis was proposed to explain the observed reduction in surface tension in the presence of an argon plasma on the basis of plasma-induced enhanced surface segregation of surface active species. Interfacial tension of pure liquid copper in a hydrogen plasma was not different than that observed in inert gas systems. To further corroborate this effect and to study the nature of the interface, vaporization rate experiments were carried out, in conjunction with emission spectroscopy, to develop a physical concept of the interface in close proximity of the liquid metal.

TABLE OF CONTENTS

LIST OF FIGURES	vii
LIST OF TABLES	xi
ACKNOWLEDGMENTS	xii
Chapter 1. INTRODUCTION	1
1.1 General Introduction	1
1.2 Importance of interfacial tension during welding	3
1.3 Role of plasma during welding	5
1.4 Statement of objectives	7
1.5 Layout of the thesis	8
Chapter 2. CRITICAL REVIEW OF PREVIOUS WORK	10
2.1 Measurement of surface tension	10
2.2 Errors in determining γ	13
2.3 Levitation method of determining γ	18
2.4 Effect of minor elements	20
2.5 Surface tension and fluid flow	24
2.6 Interaction between surface tension behavior and weld shape	26
2.7 Effect of plasma on interfacial tension	27
2.8 Vaporization of alloying elements	28
2.9 Summary	29
Chapter 3. EXPERIMENTAL PROCEDURES	31
3.1 Surface tension measurements	31
3.2 Plasma related experiments	35
3.3 Spectroscopic plasma diagnostics	35
3.4 Weld aspect ratio experiments.	39
Chapter 4. THEORETICAL BACKGROUND	41
4.1 Thermodynamics of interfaces	41
4.1.1 Temperature coefficient of surface tension	48

4.2	Plasma physics relevant to present study	54
4.2.1	Emission spectroscopy	57
4.2.2	Electron temperature estimation	59
Chapter 5.	RESULTS AND DISCUSSION	62
5.1.	Thermodynamic modeling	62
5.1.1	Estimation of enthalpy (ΔH^0) and entropy factor (k_1)	60
5.1.1.1	Fe-S	63
5.1.2	Estimation of heat of adsorption	76
5.1.3	Application to other systems	80
5.1.4	Temperature coefficient of surface tension	86
5.2	Weld Aspect Ratio	91
5.3	Low Pressure Plasma-Liquid Metal Interaction	96
5.3.1	Plasma characterization	96
5.3.2	Electron temperature estimation	100
5.4	Interfacial tension measurements	103
5.5	Role of plasma on metal vaporization rates	115
5.5.1	Experimental and theoretical fluxes	116
5.5.2	Interfacial turbulence - effects of susceptor and surface active elements	123
Chapter 6.	CONCLUSIONS AND SUGGESTIONS FOR FUTURE WORK	131
6.1	Conclusions	131
6.2	Suggestion for future work	134
REFERENCES	136
Appendix	CALCULATION OF BOND NUMBER	143

LIST OF FIGURES

1.1	Representation of the physical processes occurring during welding.	2
2.1	Sessile drop profile and identification of geometrical parameters.	11
2.2	A schematic representation of the sessile drop profile showing the coordinates measured to determine the surface tension.	14
2.3	Fluid flow patterns in the weld pool in the (a) absence and (b) presence of surface active impurities (from reference 8).	25
3.1	A schematic diagram of the experimental set up used for surface tension measurements.	32
3.2	A schematic diagram of the experimental set up used for the plasma work.	36
3.3	Schematic diagram of the experimental set up used for plasma diagnostics.	37
4.1	Variation of a property of a system in going from phase α to phase β .	42
4.2	Variation of interfacial tension as a function of the activity of the solute.	52
4.3	A schematic representation of low pressure low temperature plasma.	56
4.4	Schematic absorption and emission spectrum line series and related atomic energy levels (from reference 60).	58
5.1	Variation of equilibrium constant with temperature for the Fe-S system.	67
5.2	Depression of the surface tension of iron by sulfur and comparison with ideal isotherm (5.1) at 1923 K; surface tension data taken from reference 30.	68

5.3	Depression of the surface tension of iron by oxygen and comparison with ideal isotherm (5.1) at 1823 K; surface tension data taken from reference 70.	70
5.4	Depression of the surface tension of iron by selenium and comparison with ideal isotherm (5.1) at 1873 K; surface tension data taken from reference 34.	71
5.5	Depression of the surface tension of copper by oxygen and comparison with ideal isotherm (5.1) at 1381 K; surface tension data taken from reference 25.	72
5.6	Depression of the surface tension of copper by sulfur and comparison with ideal isotherm (5.1) at 1473 K; surface tension data taken from reference 78.	73
5.7	Depression of the surface tension of copper by selenium and comparison with ideal isotherm (5.1) at 1473 K; surface tension data taken from reference 77.	74
5.8	Depression of the surface tension of copper by tellurium and comparison with ideal isotherm (5.1) at 1473 K; surface tension data taken from reference 77.	75
5.9	Variation of the calculated heat of adsorption for various systems as a function of the difference in electronegativity of the solvent and solute ions.	79
5.10	Calculated surface tension as a function of oxygen concentration for Cr-O alloys at 1973K and comparison with experimental data of Nogi et al. ⁸²	81
5.11	Calculated surface tension as a function of sulfur concentration for Co-S alloys at 1573K and comparison with experimental data of Monma and Suto. ⁸³	83
5.12	Calculated surface tension as a function of sulfur concentration for Ni-S alloys at 1573K and comparison with experimental data of Monma and Suto. ⁸³	85
5.13	The calculated critical solute content in Fe-solute systems as a function of temperature.	88

5.14	Variation of the temperature coefficient of surface tension as a function of temperature for (a) Fe-O and (b) Fe-S systems at various activity levels of the solute.	89
5.15	Weld profile of various samples. Scanning speed: 5 mm/s, Ar gas flow rate: 6 l/min.	92
5.16	Intensity of emission of argon plasma vs wavelength at a chamber pressure of 450 $\mu\text{m Hg}$ and plate current at 1.65 amps.	97
5.17	Intensity of emission of argon plasma vs power (plate current) for various wavelengths at a chamber pressure of 200 $\mu\text{m Hg}$.	98
5.18	Intensity of emission of argon plasma at a particular wavelength vs power (plate current) for various chamber pressures.	99
5.19	Illustration of the principle of determining the electron temperature from relative intensities of spectral lines with known relative transition probability (equation 4.40).	101
5.20	Electron temperatures calculated for various systems.	102
5.21	Interfacial tension between liquid copper and argon with and without the presence of plasma. Plate current and chamber pressure were in the ranges of 1.4 to 1.6 amps and 170 to 200 $\mu\text{m Hg}$, respectively.	104
5.22	Interfacial tension between liquid iron and argon with and without the presence of plasma. Plate current and chamber pressure were in the ranges of 1.2 to 1.4 amps and 150 to 200 $\mu\text{m Hg}$, respectively.	105
5.23	Interfacial tension between liquid copper and hydrogen with and without the presence of plasma. Plate current and chamber pressure were in the ranges of 1.5 to 1.7 amps and 200 to 300 $\mu\text{m Hg}$, respectively.	109
5.24	Interfacial tension between liquid copper and Ar-7% H_2 with and without the presence of plasma. Plate current and chamber pressure were in the ranges of 1.0 to 1.6 amps and 450 to 1200 $\mu\text{m Hg}$, respectively.	110

5.25	Interfacial tension between Cu-0.04 wt% O alloy and argon with and without the presence of plasma. at 1473 K. Plate current and chamber pressure were in the range of 1.2 amps and 240 to 1200 $\mu\text{m Hg}$, respectively.	112
5.26	Interfacial tension between copper and argon plasma at 1473 K as a function of intensity of emission of plasma (plate current) at $200 \pm 10 \mu\text{m Hg}$.	114
5.27	Vaporization flux at 1873 K both in the presence and absence of a graphite susceptor for copper-solute systems. The solute concentration was 0.1 wt% and the chamber pressure was maintained at 80 N/m^2 .	117
5.28	A schematic representation of interfacial turbulence phenomenon. An eddy, A, brings a small volume of solution of a surface active agent to the surface, while an eddy, B in the gas depletes the surface active solute. The surface at A' spreads towards B' and carries some underlying liquid with it (after reference 89).	125
5.29	Vaporization flux at 1873 K both in the presence and the absence of plasma for (a) iron-solute systems where (low) and (high) denote solute concentrations of 0.03 and 0.25 wt%, respectively, and (b) copper-solute systems where (low) and (high) denote solute concentrations of 0.1 and 0.5 wt%, respectively. Chamber pressures were 40 N/m^2 and 80 N/m^2 for iron and copper systems, respectively.	127
5.30	A schematic representation of the space charge effect.	128
5.31	Intensity vs wavelength at a chamber pressure of 300 $\mu\text{m Hg}$ and plate current at 1.6 amps.	129

LIST OF TABLES

3.1:	Various columns and their utility in cleaning gas.	33
3.2	Summary of experimental conditions utilized in doping pure iron with various solutes.	40
5.1:	Area requirements at saturation (from reference 41).	64
5.2:	Summary of the calculated adsorption coefficient of the Fe-S system at various temperatures.	66
5.3:	Summary of calculated entropy and enthalpy factors.	69
5.4:	Summary of values used in calculating surface tension of various systems.	77
5.5:	Summary of the composition, depth(D), width(W) and depth/width (D/W) ratio for various samples. Scanning speed: 5 mm/s, gas flow rate: 6 l/min. Initial sample surface polished to 400 grit.	93
5.6:	Summary of the surface tension, temperature coefficient of surface tension and absorptivity values for various samples.	94
5.7:	Rate of vaporization of copper drops.	119
5.8:	Estimation of vaporization flux under gas phase mass transfer control.	121
A.1:	Typical values of various parameters for laser welding of thin iron plate using a 0.5 KW CO ₂ laser	144

ACKNOWLEDGMENTS

The completion of this dissertation was achieved through the generous help and advice of several people. The author would like to thank Dr. T. DebRoy, as adviser, for his guidance and assistance through the genesis and fulfillment of this investigation. Thanks are also due to Drs. W. R. Bitler, W. M. Small and J. W. Davis for their constructive suggestions during the course of the present study. For the useful discussions with M. M. Collur regarding plasma spectroscopy, the author is grateful.

The author's son, Joshua, provided the much-needed medicine of laughter and relaxation in between the long hours of toil.

The culmination of this thesis is entirely due to the author's parents and his wife, Laureen, whose support and patience made it a labor of love.

Chapter 1

INTRODUCTION

1.1 General introduction

The important physical processes occurring during welding are schematically illustrated in figure 1.1. The energy from a source such as a laser beam penetrates into a layer about 10^{-5} cm thick by thermal conduction. When the surface of the material reaches the melting temperature, a liquid interface propagates and with continued irradiation, the surface begins to vaporize and a molten pool begins to form. If the laser light is intense enough, absorption in the vaporized material leads to the formation of a high temperature opaque plasma. The plasma can grow back along the beam toward the laser as a "laser supported absorption" (LSA) wave. The plasma absorbs the incident light and shields the surface. At relatively low power densities¹ of about 10^5 watts/cm² of a carbon dioxide laser, melting is the dominant effect, while at somewhat higher power densities (10^6 to 2.5×10^7 watts/cm²), vaporization becomes the most important effect. At still higher values of power densities, LSA waves are rekindled and dominate the physical process, whereas vaporization is diminished. Finally, when the power density becomes very high, additional absorption mechanisms may become operative. This includes absorption of the laser light in the laser produced plasma through inverse Bremsstrahlung or through collective plasma effects. The plasma is known to affect weld characteristics. ²⁻⁵ The temperature at the center of the pool is the highest and

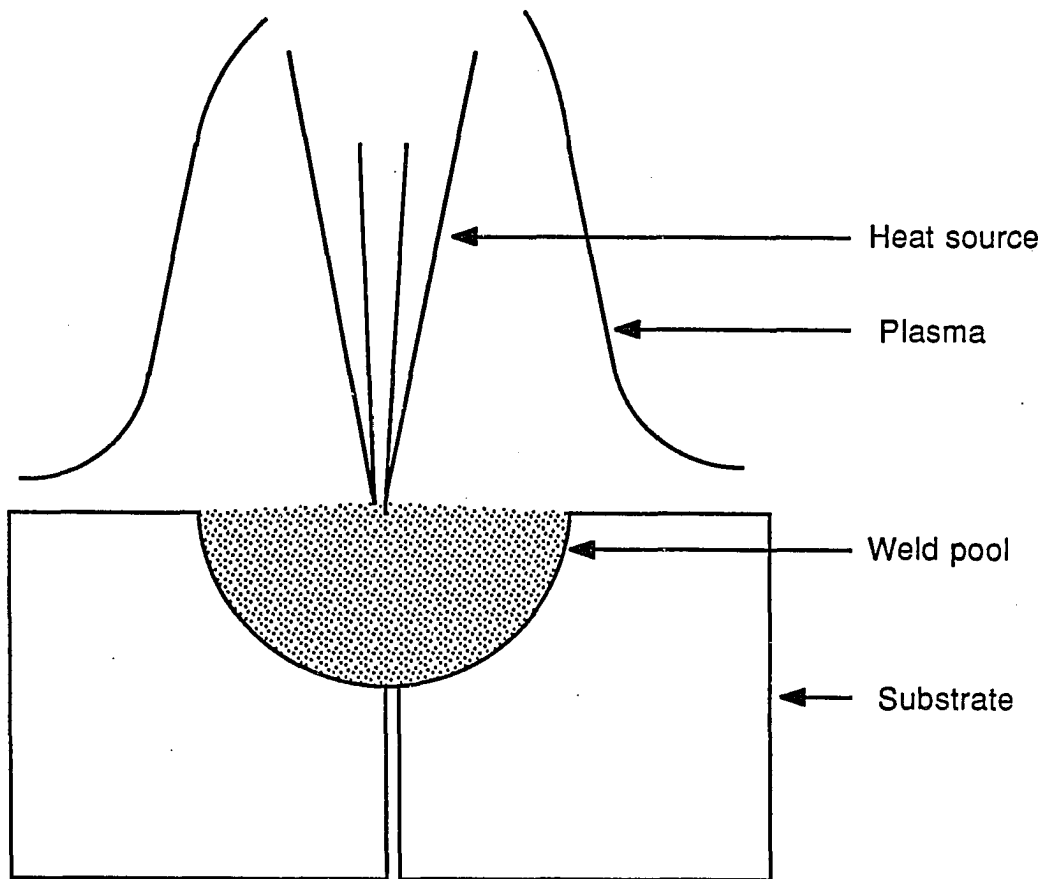


Figure 1.1 Schematic of the important physical processes occurring during welding.

is approximately equal to the boiling point of the material. The temperature decreases from the center to the periphery of the weld pool where the temperature is at about the melting point of the material. This temperature gradient creates a surface tension difference across the pool. Recent studies have demonstrated that, in many cases, the fluid flow, heat transfer, and the resulting weld shape, size and properties are significantly influenced, and in many cases, controlled, by the spatial variation of interfacial tension between the weld pool and the surroundings that contain plasma.^{6,7}

In the current body of literature there are several deficiencies that hinder a complete understanding of the interfacial phenomena under conditions relevant to welding metallurgy. For instance, interfacial tension of liquid metals and alloys at temperatures well in excess of the melting point are not available. Secondly, the interfacial tension of liquid metals in the presence of a plasma is not known. It is thought that this information is crucial for understanding of the welding process.

1.2 Importance of interfacial tension during welding

The driving forces for fluid flow in weld pools include the buoyancy force, the electromagnetic force, the surface tension gradient at the weld pool surface and the impinging force of the arc plasma.⁸ Woods and Milner⁹ studied convection in weld pools by examining the mixing of dissimilar metal droplets in the pools. It was observed that weld pool convection due to buoyancy force is negligible compared to that due to the electromagnetic force. Recently, Heiple et al.^{6,7,10-13} conducted a series of experimental studies on

weld pool convection and weld bead geometry in GTA welding of stainless steels. It was concluded that the surface tension gradient at the weld pool surface is the dominant force driving fluid flow in the weld pool. Brimacombe and Weinberg¹⁴ demonstrated an increase in surface fluid flow velocity by a factor of between 16 and 30 in a pool of liquid tin by imposing a surface tension gradient on the surface of the liquid, when compared to the same set up without an imposed surface tension gradient.

Most commercial alloys contain impurities such as sulfur or oxygen that are surface active in nature. The presence of surface active elements significantly alters the surface tension of the solvent. Furthermore, these elements often change the temperature dependence of surface tension (dy/dT) from a negative value for pure solvents to a positive value for binary systems. This change in the sign of dy/dT has a significant implication in several practical systems. Of particular practical significance is the reversal in the direction of circulation in the weld pool which occurs in steels in the presence of small amounts of surface active impurities. The flow reversal results in deeper weld penetration at particular welding speeds and power levels during welding¹⁵ and it is believed that steels containing small amounts of surface active elements may be more easily fabricated than clean steels which contain very low levels of impurities.

While this effect has been identified, the details of the interactions between temperature, impurity levels, and surface tension are not well understood and optimum impurity levels for different welding processes cannot be specified. Most of the impurity elements which affect surface tension driven fluid flow have deleterious effects on the mechanical properties of steel. If such

elements were to be present in steels for improved weldability, it would be important for the steel to contain the lowest level of surface active element necessary to produce improved weld penetration. Thus, a rational strategy for understanding the the welding process and weld metal properties must include an understanding of the interfacial phenomena relevant to welding metallurgy.

1.3 Role of plasma during welding

Under most welding conditions the interface is formed not between the liquid metal and an inert gaseous atmosphere, but between the liquid pool and the surroundings that contain the plasma. The importance of the role of plasma in welding processes was recognized in the previous works. However, most of the available literature in this field addressed the effect of plasma on weld properties.^{2,3,4} Although weld penetration is known to be related to plasma intensity^{3-5,16} and the penetration is strongly influenced by the nature and intensity of interfacial tension driven flow,^{6,7,10} the effect of plasma on the interfacial tension of liquids was ignored in the previous work. Because of the lack of appropriate interfacial tension data between the plasma and the weld pool, all the previous efforts in the analysis of fluid flow in the weld pool were based, in a rather simplistic way, on the surface tension of gas/metal systems and not on the appropriate interfacial tension between the plasma and the weld pool. In view of the crucial importance of interfacial tension driven flow in the heat transfer, cooling rate and the resulting structure and properties of the weld metal, a rational strategy for the understanding of the welding processes and

weld metal properties must include an understanding of the effect of plasma on the interfacial tension of liquid metals.

Another important effect of the plasma during welding is its effect on the vaporization loss of volatile alloying elements. In fact, one of the major problems in the use of a high power density laser beam for the welding of many important engineering alloys is the loss of volatile alloying elements. The inadequate control of weld composition and properties are familiar difficulties in the welding of several aluminum alloys and high manganese stainless steels.¹⁷⁻¹⁹ The vaporization of alloying elements from the weld pool is influenced by several factors such as the temperature and concentration distributions at the weld pool surface, the extent of surface coverage by the surface active elements, interfacial turbulence and the modification of the nature of the interface due to the presence of plasma²⁰ in close proximity of the vaporizing interface.

Surface active elements such as oxygen and sulfur are known to influence the weld pool fluid motion and aspect ratio which, in turn, affect vaporization rate.^{6,10} Heat-to-heat variations in the concentrations of oxygen and sulfur in several commercial alloys are thought to be responsible for the lack of reproducibility of weld geometry and properties.

The preceding considerations make it imperative that a coherent understanding of the vaporization process must include an understanding of the physical processes at the liquid metal surface in the presence of a plasma. This must take into account the character of the plasma generated in the process and its interactions with a molten pool of metal in an ambient composed of excited and ionized species.

In view of the limitations encountered in the current body of literature pertaining to interfacial phenomena under welding conditions, the present study was initiated to study some of these shortcomings. Both theoretical and experimental studies were conducted to obtain a better understanding of the nature of interfacial tension and a physical concept of the interface within an ambient which contains excited and charged species.

1.4 Statement of objectives

The overall objectives of this research are to understand the interfacial phenomena in welding. More specifically, the objectives of the present study are:

1. To establish a relationship among surface tension, temperature and composition of the binary metal-surface active solute system. This formalism would then be used to see how fluid flow may be affected by a combination of temperature and composition of the melt. To make use of the formalism to predict surface tension for systems in which data are scarce, as a test of the efficacy of the formalism on the basis of the limited amount of published data.
2. Conduct experiments to measure the interfacial tension of liquid metals in the presence of a plasma.
3. Experimental and theoretical considerations to understand the depth of penetration in weld pools in the presence of surface active solutes.

4. Conduct isothermal experiments to investigate the effects of (a) plasma and (b) surface active elements on the vaporization rate of the solvent.

It is hoped that such a study will help in a more complete understanding of the interfacial phenomena that occur during welding.

1.5 Layout of the thesis

The thesis is divided into six chapters.

This chapter introduces, in a concise manner, the importance of interfacial tension in liquid metals and its relevance to some of the important physical processes that occur during welding. The objectives of the investigation are defined and the thesis layout is presented.

Chapter 2 is a comprehensive survey of past work on interfacial tension, plasma effects on liquid metal surface and vaporization kinetics of the alloying elements:

In Chapter 3 the various experimental procedures employed in the course of this investigation are described.

Chapter 4 delves into the mathematical derivation of the thermodynamic model. It also describes some of the basics in low pressure plasma generation and characterization relevant to the present study.

The theoretical and experimental results are presented and discussed in Chapter 5.

Finally, the conclusions of this investigation are presented in Chapter 6. Furthermore, suggestions for future work are documented in this chapter.

Chapter 2

CRITICAL REVIEW OF PREVIOUS WORK

2.1 Measurement of surface tension

The surface tension of liquid metals and alloys can be measured by a variety of techniques. The Young and Laplace equation relating the pressure difference, ΔP , across an interface having principal radii of curvature, R_1 and R_2 which are large compared to atomic dimensions is:

$$\Delta P = \gamma_{LV} \left[\frac{1}{R_1} + \frac{1}{R_2} \right] \quad (2.1)$$

Their derivation of the pressure in terms of the liquid surface tension forms the basis of all liquid surface tension and interfacial tension measurements. For the current study, the sessile drop technique was deemed the most appropriate. This was based on the reasons that the measurements had to be carried out at high temperatures and, secondly, for the plasma related study it was the only viable technique. A schematic representation of this is shown in figure 2.1. The equilibrium at some point, H, below the summit is expressed generally by:

$$\Delta p = \gamma_{LV} \left(\frac{1}{R_1} + \frac{1}{R_2} \right) = g\rho_L Z + p_o \quad (2.2)$$

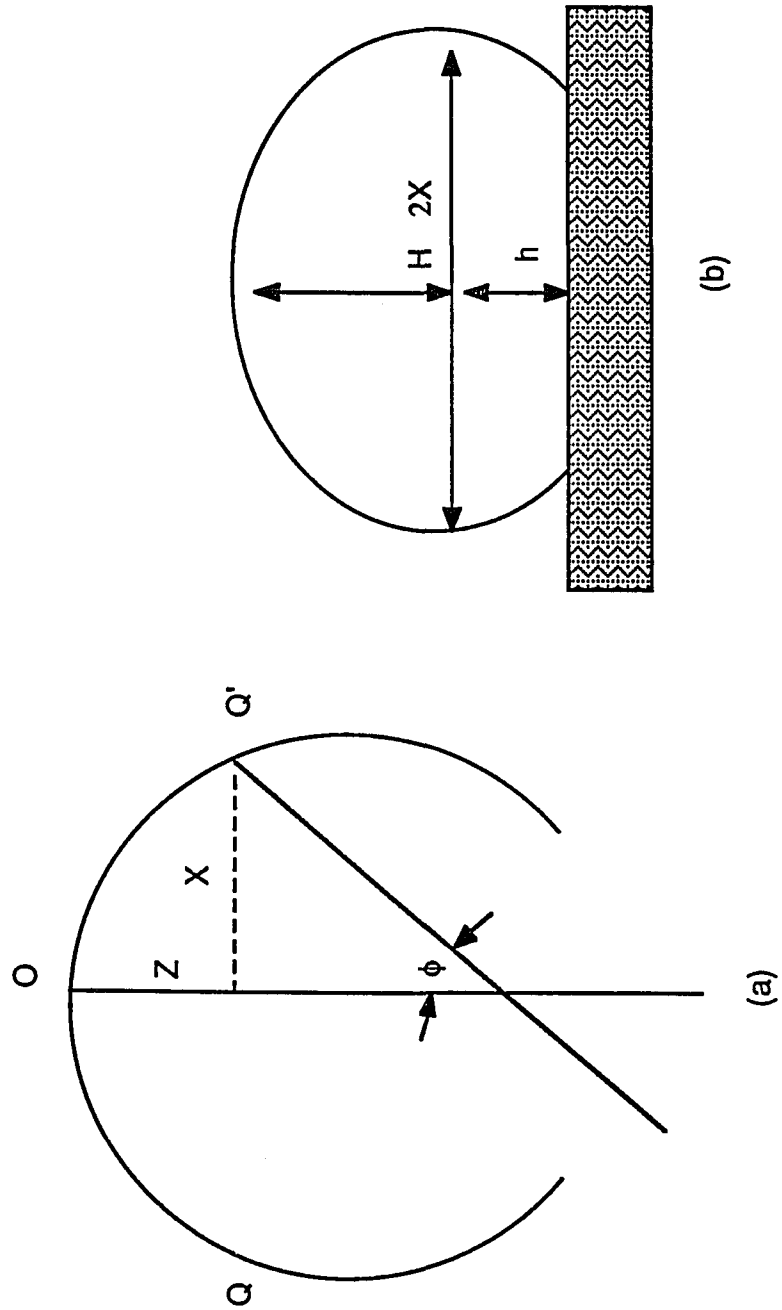


Figure 2.1 Sessile drop profile and identification of geometrical parameters.

where p_0 is the pressure at the apex of the meniscus, where $R_1 = R_2$. Bashforth and Adams²¹ considered the radii of curvature at points Q and Q' to be R in the plane of the figure 2.1a, and $x/\sin\phi$ is a plane perpendicular to the plane of the figure (rotating about the vertical axis). At the apex of the meniscus [figure 2.1a], $R_1 = R_2 = b$, $Z = 0$, and $p_0 = r\gamma_{LV}/b$ in equation 2.2. Thus,

$$\gamma_{LV} \left(\frac{1}{R} + \frac{\sin\phi}{x} \right) = g\rho_L Z + \frac{2\gamma_{LV}}{b} \quad (2.3)$$

Equation 2.3 can be rewritten as:

$$2 + \beta \left(\frac{Z}{b} \right) = \left(\frac{1}{R/b} + \frac{\sin\phi}{x/b} \right) \quad (2.4)$$

$$\text{where } \beta = \frac{b^2 \rho_L g}{\gamma_{LV}} \quad (2.5)$$

These quantities are included in the general equation describing the surface of the sessile drop:

$$\frac{d^2 z}{dx^2} + \left[1 + \left\{ \frac{dz}{dx} \right\}^2 \right] \frac{dz}{x dx} = (2 + \beta z) \left[1 + \left(\frac{dz}{dx} \right)^2 \right]^{\frac{3}{2}} \quad (2.3)$$

which has no analytical solution. For this reason, two main procedures are

currently employed:

- (1) utilizing the tables prepared by Bashforth and Adams²¹ a century ago by the method of quadratures;
- (2) utilizing computerized non-linear fitting methods, which fit the measured drop profile to a theoretical one by optimizing γ and β .

Bashforth and Adams²¹ prepared tables of b and x/Z for $\phi = 90^\circ$, and x/b for values of b and ϕ . For the special case of $\phi = 90^\circ$, the coordinates to be measured are Z and x as shown in figure 2.2. From the tables, β and b are determined and the surface tension is calculated from equation 2.5.

Procedure (2), one of the most recent methods, was developed by Rotenberg et al.²² In this method values of coordinate points of the discretized droplet interface (obtained from an enlarged photograph), the value of the density difference across the interface, and the value of the local acceleration due to gravity are required for the calculations.

2.2 Errors in determining γ

Although, in principle, experimental determination of surface tension appears simple, in practice it is tedious and sometimes difficult to measure accurately because of many sources of error inherent in such measurements. An extensive error analysis has been done by R. Sangiorgi et al.,²³ White²⁴ and Gallois and Lupis.²⁵ A summary of their findings is presented below.

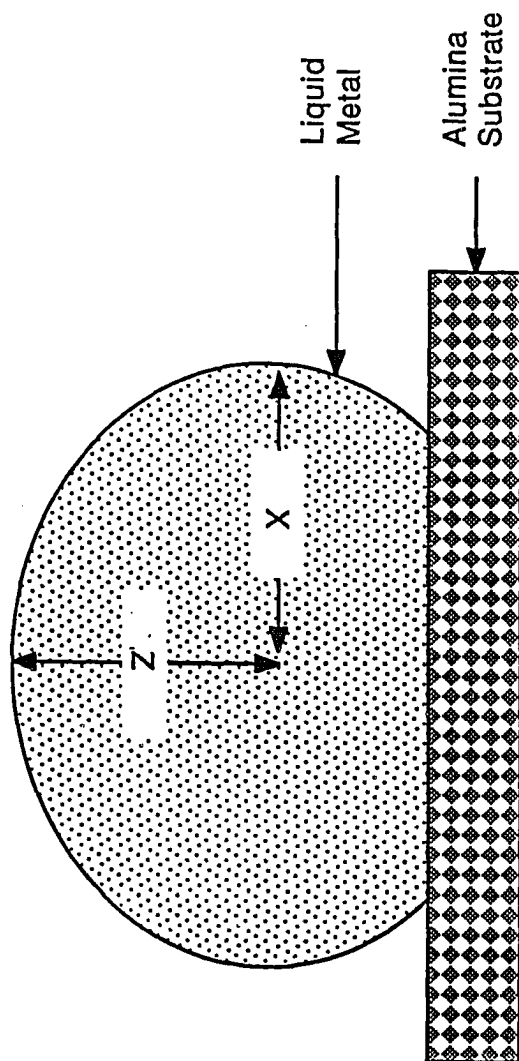


Figure 2.2 A schematic representation of the sessile drop profile showing the coordinates measured to determine the surface tension.

Errors in reading drop coordinates

The value of γ is always affected by a large error (2-5 % when $\beta > 2$) if we can read coordinates with an accuracy of , at least, 0.1 %. If in reading coordinates a precision higher than 0.1 % cannot be obtained, it would be useless to work with drops with β values less than 2, since it would result in errors of 10-50 %. It was also seen that the effect of drop size on the accuracy of surface tension measurements depends on the β factor. For drops of the same material at the same temperature, this effect turns out to be governed by the drop size.

Errors due to magnification factor

The knowledge of the magnification factor, that is, the ratio between the true and measured dimensions of the drop is a necessary condition in computing surface tension from experimental observations. The relative uncertainty in γ is twice as great as the relative uncertainty in the magnification factor.

Geometrical anisotropies

Inaccurate values can arise due to the presence of the following: anisotropy in the optical path; anisotropy in the measuring instrument and anisotropy in the development of the film.

The x and z coordinates have to be measured with an accuracy higher than 0.2 % of each other, in order to let the relative uncertainty in γ be under 1 %.

Recording of the droplet profile requires a parallel beam of light to avoid light beams reflected by the liquid surface which alter the recorded drop profile. This condition is sufficiently fulfilled if a tube of high length to diameter ratio is employed. An error of $\pm 5 \mu\text{m}$ in the positioning of the drop apex, which might be due to spurious reflections, could result in an uncertainty of about ± 1 %.

It is also advisable to use a monochromatic filter to avoid diffraction effects and to exploit the photographic film in its maximum sensitivity range.

Drops must be perfectly levelled and have perfect cylindrical symmetry.

Errors in density

In normal practice, good density values are taken from the literature and used to evaluate γ . However, the temperature of the drop should be known exactly. It is seen that any error in determining the true temperature of the sample is, in part, self-compensated by the effect of the negative temperature coefficient of the sample density.

Physico-chemical effects

The strong influence of adsorption of foreign elements on surface tension values is very well known. The ability to depress surface tension is strictly connected with the difference between the surface tension of the two pure components. Small amounts of surface active elements, like oxygen or sulfur, dramatically depress the surface tension of a pure metal. For example, 0.1 % S lowers the γ of Fe by 30 %. The four principal sources of contamination are:

- 1) impurities in the metal itself,
- 2) reaction with those parts of the apparatus with which the liquid metal comes into contact,
- 3) contamination by impurities contained in gases, and
- 4) contamination by desorbing gases from the internal parts of the apparatus in general and from porous materials in particular.

Errors due to heat induced refraction

In the gas phase, if the radial temperature gradients are not uniform along the furnace tube, a bending of the light rays will result. This could lead to slight deviation in γ from the actual values.²⁵

2.3 Levitation drop method of determining γ

Another method of determining γ of liquid metals at high temperature that has received much attention in recent years²⁶⁻³⁰ is the levitating drop method. The fundamental equation for the levitating drop method was originally developed by Lord Raleigh.³¹ In essence, Lord Raleigh derived the relation between surface tension (γ) and the natural frequency of vibration (ω) of an oscillating drop, by considering the potential energy due to capillarity and relating this to the kinetic energy of motion, which results from a small displacement of the drop surface. From this analysis n different differential equations of motion were obtained, which had the form:

$$\frac{d^2 a_n}{dt^2} + n(n-1)(n+2) \frac{\nu}{\rho a^3} a_n = 0 \quad (2.4)$$

where, a_n = deviation from the equilibrium radius

a = radius of the equilibrium sphere

t = time

ρ = density of drop

n = mode of vibration.

Since $a_n \propto \cos(pt + \epsilon)$ (where $p = 2\pi\omega$), it can be seen that the general solution to this series of equations becomes:

$$p^2 = n(n-1)(n-2) \frac{\nu}{\rho a^3} \quad (2.5)$$

It can be seen from equation 2.5, that the principal mode of deformation occurs when $n = 2$ (in practice, higher modes of deformation do not appear to be stimulated). Whence, equation 2.5 becomes:

$$p^2 = 4\pi^2\omega^2 = \frac{8\pi}{\rho a^3} \quad (2.6)$$

Since the mass of the drop (m) = $\rho \frac{4}{3} \pi a^3$, equation 2.6 can be rewritten as:

$$\gamma = \frac{3}{8} \pi m \omega^2 \quad (2.7)$$

Equation 2.7 is the basic equation used to calculate surface tension using the levitating drop technique.

The two important advantages claimed for this technique are: (1) a knowledge of the density of the melt is not required and (2) there is no physical contact between the melt and any container/support material and hence minimal contamination.

Fraser et al.²⁶ studied the effects of various parameters such as drop size, drop viscosity and vibration amplitude on the values of γ obtained by the levitation drop method. No obvious effects were observed for drop sizes up to 1 g in mass, even though gravitational forces caused drops of this magnitude to show significant departures from a spherical drop. If viscosity effects were significant the oscillations would be aperiodic. For any given viscosity, there is a critical drop size, above which, the vibrations will be periodic. Calculations²⁶ revealed that for pure liquid iron, the critical drop radius was about 10^{-8} cm,

which is well below the drop radii normally encountered. There exist some differences with regard to the effects of vibration amplitude. Lord Raleigh's equation was derived on the basis of small displacements from the equilibrium sphere. Fraser et al.²⁶ observed, that although the amplitude of vibration altered with drop size, the values of γ derived were not affected. However, the study by Soda et al.²⁸ to measure the γ of pure copper revealed that a correction factor was necessary to account for the magnitude of large oscillations.

2.4 Effect of minor elements

The surface tension of pure metals and their alloys can be estimated from a knowledge of factors such as melting point, molar volume, atomic number and heat of vaporization. However, this approach cannot be easily extended to systems with a surface active component because of the radical changes in the nature of the surface layer when these surface active elements are present.

The variation in interfacial tension of binary systems involving a surface active component with temperature has been the subject of various investigators in the past.^{23,25,30,32-36} These have been mostly experimental works aimed at determining the interfacial tension as a function of temperature and composition. One of the first major publications dealing with the effect of surface active agents on the surface tension of solutions was given by

Szyszkowski³⁷ in 1908. He derived the following empirical relation:

$$\frac{\gamma^0 - \gamma}{\gamma} = b \ln \left[\frac{C_2}{c} + 1 \right] \quad (2.8)$$

where γ^0 is the surface tension of the pure solvent, γ is the surface tension of the solution, C_2 is the molality of the solution and b and c are constants. However, it has been shown experimentally that such a relationship is valid for weakly surface active solutes and will not represent true behavior for strongly surface active agents.³⁸

Bernard and Lupis³⁹ developed a monolayer model on the basis of formation of a compound $A_{n-1}B$, where B is the solute element. They introduced two dimensionless quantities, p and ψ , defined as:

$$p = a_B \left(\frac{J_B}{RT\Gamma_A} \right) \quad (2.9)$$

$$\psi = \frac{\gamma - \gamma^0}{RT\Gamma_A} \quad (2.10)$$

where, a_B is the activity of species B in solution, Γ_A is the number of atoms per unit area of the pure solvent and J_B is the surface activity of the solute component. They formulated expressions for the two quantities at both high and low concentrations. At high concentrations, the model yields

$$\ln p = \ln \frac{n\theta}{1-n\theta} + 2n\theta \left(\frac{g}{kT} \right) \quad (2.11)$$

$$\varphi = -\frac{1}{n} \ln (1-n\theta) + n\theta^2 \left(\frac{g}{kT} \right) \quad (2.12)$$

where θ is the fraction of B atoms in the monolayer and g measures the net interatomic forces between the adsorbed solute atoms. At low concentrations, the expression at $n = 2$ is given by:

$$\ln p = \ln\theta + 3 \ln (1-\theta) - 4 \ln (1-2\theta) + 2\theta \left(\frac{g}{kT} \right) \quad (2.13)$$

$$\varphi = 3 \ln (1-\theta) - 2 \ln (1-2\theta) + \theta^2 \left(\frac{g}{kT} \right) \quad (2.14)$$

Application of their formalism to the Fe-O and Ag-O systems produced a semi-empirical correlation between surface activity and surface tension. Although the correlation is useful for predicting the depression of surface tension with concentration, prediction of temperature coefficient of interfacial tension using the current form of the correlation is not straightforward.

In the model developed by Fowler and Guggenheim,⁴⁰ the derivation of the model yields the following equation:

$$Ka_i = \frac{\theta}{1-\theta} \exp \left[-2 \left(\frac{Z\omega}{kT} \right) \theta \right] \quad (2.15)$$

where Z is the number of nearest neighbors within the surface layer, ω is equal to the regular solution parameter $U_{AB} - 1/2(U_{AA} + U_{BB})$, where U_{ij} is the

bonding energy between two surface atoms i and j . The term K is a constant with respect to composition, but is temperature dependent. Lupis⁴¹ pointed out that this model predicts surface saturation only at $\theta = 1$. However, surface saturation is known to occur at lower values of θ corresponding to surface stoichiometries such as A_3B , A_2B and AB .⁴¹

Belton³² has used a combination of Gibbs and Langmuir adsorption isotherms to develop a formalism which describes the interfacial tension of liquid metal in the presence of a surface active element. The relationship is given by:

$$\gamma^0 - \gamma = RT\Gamma_s \ln [1 + Ka_i] \quad (2.16)$$

where, Γ_s is the surface excess at saturation, K is the adsorption coefficient and a_i is the activity of the species in solution.

Although equation 2.16 is derived to express interfacial tension as a function of both temperature and composition from first principles, the variation of the adsorption coefficient K with respect to temperature is not explicitly defined.

2.5 Surface tension and fluid flow

Late in the nineteenth century, Marangoni⁴² demonstrated that if a surface tension gradient existed on the surface of a liquid, fluid will be drawn along the surface from the region of lower surface tension to those of higher

surface tension. This phenomenon is generally referred to as Marangoni convection.

According to the theory proposed by Friedman⁴³ an increase in penetration of the weldment is a result of the reduction in surface tension brought about by the addition of surface active elements. According to his finite element heat transfer model for GTA welding process, the distortion of molten metal under the action of arc pressure and gravitational forces is inhibited by the surface tension existing at the interface between puddle and atmosphere.

In the model put forward by Heiple and Roper⁶, the increase in penetration in the presence of surface active impurities is due to positive $d\gamma/dT$ existing at the surface of the pool. As shown in figure 2.3, a pure element A has a negative $d\gamma/dT$, whereas a binary solution B can, under certain conditions, have a positive $d\gamma/dT$. The indicated surface flow patterns for the two systems, A and B, are shown in the lower part of the figure. For the pure metal, the metal flows radially outward from the center of the pool, descends, and returns beneath the surface to the center of the weld. This motion transfers heat to the toe (edge) of the weld and produces wide, shallow welds. When a surface active element is added, the fluid direction is reversed, with the metal flowing inward to the center and then down. This flow pattern efficiently transfers heat to the weld root and produces deep, narrow welds. In spite of the steep temperature gradients created during welding, the buoyancy force is negligible in comparison to the surface tension force. This has been shown mathematically in the appendix where the dimensionless Bond number has been calculated under typical welding conditions.

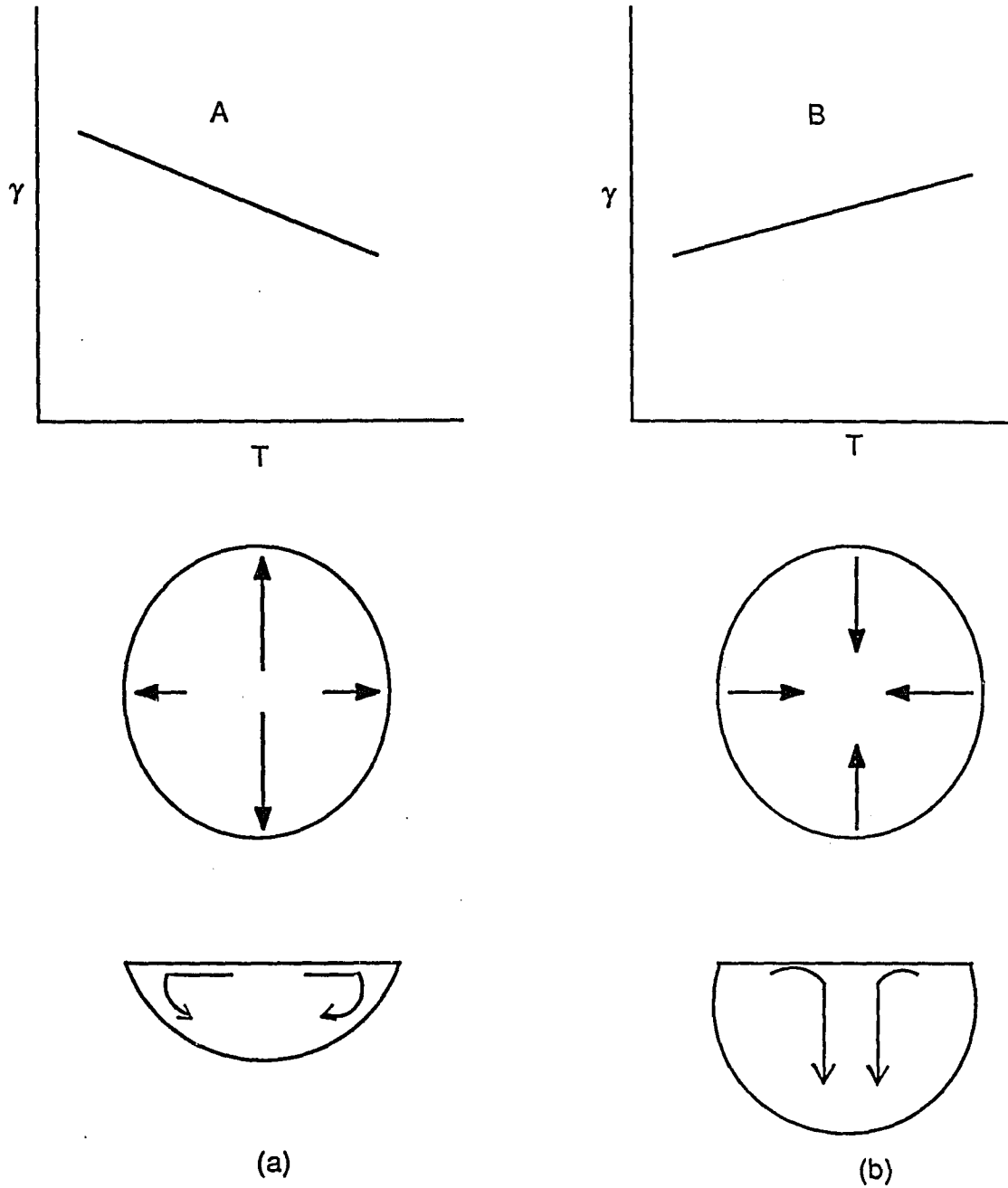


Figure 2.3 Fluid flow patterns in the weld pool in the (a) absence and (b) presence of surface active impurities (from reference 6).

2.6 Interaction between surface tension behavior and weld shape

The surface tension driven fluid flow model which has been used to explain the effects of surface active residual elements on weld shape can also be used to understand the effect of changing welding parameters on weld shape.⁴⁴ The effect of a change in welding parameters which increases the temperature gradient (and thus the surface tension gradient) from center to edge of weld pool is to drive the existing fluid flow patterns more strongly. Heiple et al.^{6,10,11} have demonstrated that addition of surface active elements such as O, S, Se and Te to stainless steel in small concentrations (less than 150 ppm) substantially increases the weld depth to width ratio (d/w), as predicted by their model. All these elements, known to be highly surface active in iron, are either known (O, S) or expected (Se, Te) to produce positive temperature coefficients of surface tension in iron. Recent measurements of the temperature dependence of the surface tension for steels with different weld penetrations have produced an impressive correlation between a positive temperature coefficient and a high d/w ratio in welds.⁴⁵ In addition, it has also been shown that¹⁰ when oxygen is removed from solution in the steel (by aluminum additions) or oxygen and sulfur are removed from solution (by cerium additions), the weld d/w ratio is decreased, as expected.

However, in the investigation carried out by Sundell et al.,⁴⁶ it was reported that although oxygen increases both the width and the depth of the pool, it does not affect the d/w ratio. Sulfur, in contrast, decreases width and increases depth, greatly increasing d/w . Nitrogen was found to have an effect similar to, but more subdued than that of oxygen. Cerium forms stable oxides

and sulfides (Ce_2O , CeS , $\text{Ce}_2\text{O}_2\text{S}$) with melting points in excess of the base material. These compounds would effectively remove surface active materials from the weld pool and reduce the surface tension driven flow fostered by these elements.

Experiments carried out by Pollard⁴⁷ indicated that other factors besides the temperature coefficient of surface tension must be taken into account to explain penetration behavior. In his experiments in which silicon was added to Type 304 stainless steel, an increase in penetration was noticed up to a maximum value beyond which further additions of Si caused a reduction in penetration. It was proposed that the beneficial effect of the initial silicon addition was most likely due to silicon reducing the viscosity of the molten steel.⁴⁸ If a downward pattern already existed because of the 0.014 % sulfur content, then a reduction in the viscosity of the molten steel would increase the flow velocity and hence increase penetration. However, with increasing silicon additions a point was eventually reached where the soluble oxygen content became the dominant factor, the temperature coefficient of surface tension was reduced sufficiently to more than offset any further decrease in viscosity by silicon, and penetration subsequently decreased.

2.7 Effect of plasma on interfacial tension

Although the importance of the role of plasma in the welding processes was recognized in the previous works, most of the available literature was addressed to the effect of plasma on weld properties.^{2,3,4} Although the weld penetration is known to be related to the plasma intensity^{3,4,5,16} and the

penetration is strongly influenced by the nature and intensity of interfacial tension driven flow^{6,7,10}, the effect of plasma on the interfacial tension of liquids was ignored in the previous works. Because of the lack of appropriate interfacial tension data between the plasma and the weld pool, all the previous efforts in the analysis of fluid flow in the weld pool were based, in a rather simplistic way, on the surface tension of gas/metal systems and not on the appropriate interfacial tension between the plasma and the weld pool.

2.8 Vaporization of alloying elements

The presence of surface active elements such as sulfur or oxygen in the base metal affects the surface area and temperature distribution in the weld pool - factors that strongly influence vaporization rate. In a recent paper⁴⁹ it has been demonstrated that the rate of alloying element vaporization during conduction mode laser welding of stainless steels is controlled by plasma induced intrinsic vaporization at the weld pool surface.

Previous emission spectroscopic investigations by Savitskii and Leskov⁵⁰ indicated that during GTA welding of stainless steels, the rates of vaporization of iron and manganese increased with the increase in the sulfur and oxygen concentrations in steel. Similar effects were observed by Dunn et al.⁵¹ who found that the presence of sulfur in the base plate enhanced the intensity of emission of Fe, Cr and Mn peaks. Although alloying element vaporization is regarded as an important problem during laser processing and the presence of surface active elements are known to affect the vaporization, no systematic investigation of the role of oxygen and sulfur on alloying element

vaporization rates have been undertaken so far. Although there have been studies to examine vaporization effects during welding, it is difficult to determine from the welding data if the changes in the vaporization rate due to the presence of surface active elements in the base metal are attributable exclusively to changes in the weld pool surface area and temperature distribution or are contributed by additional interfacial effects due to the presence of these elements. In either case, the primary interfacial effect of sulfur cannot be easily separated from the secondary effects of sulfur manifested in changes in surface area and temperature distribution. To determine the true interfacial effect of sulfur on the metal vaporization rate, a series of experiments was designed where iron and copper drops doped with oxygen or sulfur were allowed to vaporize isothermally both in the presence and absence of a low pressure argon plasma. The rates were compared with the rate of vaporization of ultrapure metal drops under appropriate conditions.

2.9 Summary

During welding, the fluid flow, heat transfer, and the resulting weld shape, size and properties are significantly influenced by surface tension driven flow. The presence of surface active elements often changes the temperature dependence of surface tension which results in flow reversal and, consequently, deeper weld penetrations. While this effect has been identified, the details of the interactions between temperature, impurity levels and surface tension are not well understood. Further compounding this effect is the fact that

the interfacial tension is established between the liquid metal and the surrounding environment that contains the plasma.

Another major problem that has not received much attention is the loss of volatile alloying elements during the use of a high power density laser beam for welding. Recently, it has been demonstrated that the rate of alloying element vaporization during conduction mode laser welding of stainless steels is controlled by plasma induced intrinsic vaporization at the weld pool surface. However, no systematic investigation of the role of oxygen and sulfur on the alloying element vaporization rates has been undertaken so far.

The work reported in this thesis is aimed at partially alleviating this lack of understanding on interfacial phenomena during welding. Although the scope of the present study is not to provide answers that are all encompassing, it is an attempt to better quantify some of the effects that occur at the interface of liquid metals. It is hoped that such a study will enhance, to some degree, our current knowledge of interfacial effects and their significance in welding.

Chapter 3

EXPERIMENTAL PROCEDURES

3.1 Surface tension measurements

The materials used for the initial measurements were puratronic grade tin and copper supplied by Johnson Matthey Chemical Company.

For the initial experiments a Fisher Model 472 High Temperature furnace with molybdenum disilicide (MoSi_2) heating elements was utilized. The furnace temperature was controlled to $\pm 10^\circ\text{C}$ using solid state circuitry. A schematic diagram of the experimental set up employed for the measurement of surface tension is shown in figure 3.1. Argon was used in most of the experiments. It was purified by passing it through various columns to be cleansed of its various impurities. The types of impurities that were removed by the various columns indicated in table 3.1. The gas flow rate was measured by a rotameter prior to its entry in the furnace.

The photography unit consisted of a Minolta X-370 camera, a Starblitz 2X teleconverter, a Minolta bellows and a Soligor 85-210 mm zoom lens. This unit was mounted on a camera tripod and levelled horizontally with a spirit-level. The cross-hairs of the lens was used to check the sample position for horizontal placement.

For a typical run a sample weighing approximately 0.5 g would be cleaned in dilute HCl, degreased in acetone and placed on a horizontal substrate inside the furnace tube. Sufficient time was allowed for the drop to

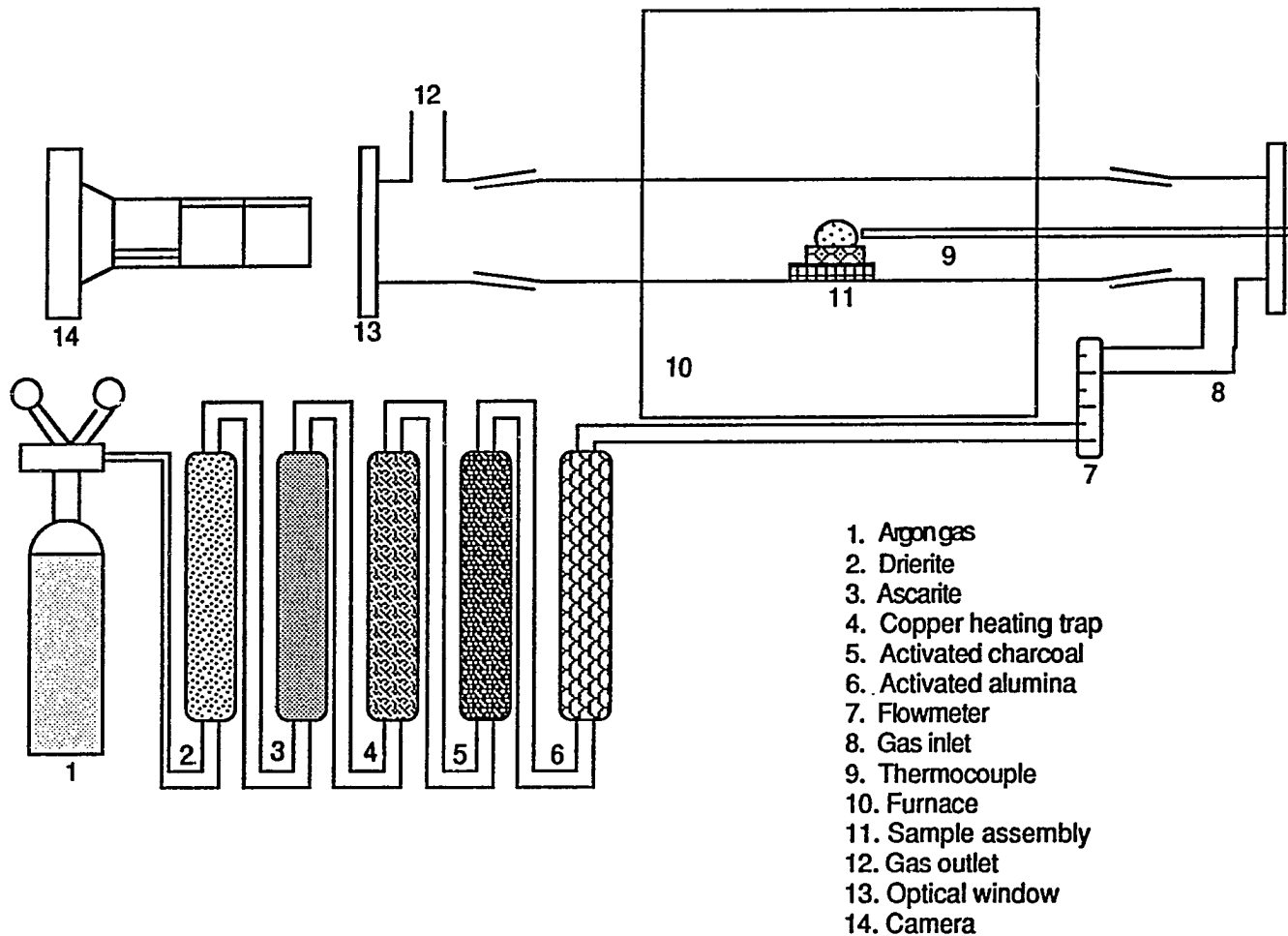


Figure 3.1 A schematic diagram of the experimental set up used for surface tension measurements.

Table 3.1 Various columns and their utility in cleaning gas.

Column	Use
Drierite	remove H ₂ O
Ascarite	remove CO ₂
Copper heating trap	remove O ₂
Activated charcoal	remove C _n H _n
Activated alumina	remove CO

equilibriate at a predetermined temperature prior to photography. The drop profile was then analyzed from the photograph to calculate the surface tension. The variables studied were temperature and the vertical and horizontal coordinates of the drop profile along the meridional section. In the determination of surface tension values several preliminary runs were conducted on samples with accurately known g values to establish a reliable procedure of measurements. Since these experiments are extremely tedious it was not easy to repeat experiments under the same conditions. However, the following error analysis indicates the precision of such measurements. From equation 2.6, the surface tension is given by:

$$\gamma_{LV} = \frac{b^2 \rho_L g}{\beta} \quad (3.1)$$

Differentiating the logarithm of equation 3.1, and rewriting in finite difference notation one obtains:

$$\frac{\Delta\gamma_{LV}}{\gamma_{LV}} = \frac{2 \Delta b}{b} + \frac{\Delta\rho_L}{\rho_L} + \frac{\Delta\beta}{\beta} \quad (3.2)$$

where $\Delta\gamma_{LV}$, Δb , $\Delta\rho_L$ and $\Delta\beta$ are the errors in measurement of γ_{LV} , b , ρ_L and β , respectively. It has been estimated that $\Delta b/b$, $\Delta\rho_L/\rho_L$, and $\Delta\beta/\beta$ are approximately $\pm 0.1\%$, $\pm 0.6\%$ and $\pm 5\%$, respectively. Substituting these values in equation 2.7, $\Delta\gamma_{LV}/\gamma_{LV}$ is calculated to be approximately $\pm 6\%$. Further details are given in chapter 2.

3.2 Plasma related experiments

For the plasma related experiments a different furnace was used. A schematic diagram of the set up is shown in figure 3.2. The ultra high purity argon used for the experiments had a maximum impurity content of 10 ppm with no more than 2 ppm of oxygen and and 3 ppm of water vapor. High purity copper and iron (maximum 10 ppm impurities) supplied by Aesar were used in the experiments. The samples weighing about 0.5 g were cleaned, degreased in acetone, placed on a polished alumina substrate. The substrate was placed horizontally in a graphite susceptor tube as shown in figure 3.2. The RF power was supplied through a 3.4 cm internal diameter coil made up of 0.32 cm diameter copper tube. The coil had seven turns with 0.15 cm spacing between the adjacent turns. Because of the high frequency used for heating, the skin depth of the induced current was very small and the graphite susceptor ensured that the shape of the metal drop was not disturbed by the induced currents. The metal drops were photographed through an optical window fitted at one end of the vycor tube.

3.3 Spectroscopic plasma diagnostics

Figure 3.3 is a schematic diagram of the experimental set up used for this study. As can be seen from the figure, the radiation emitted from the plasma is focussed on the slit of a monochromator through a convex lens. A kinematically mounted diffraction grating is used to obtain a high resolution spectrum. An intensified silicon intensified target (ISIT) detector was used to

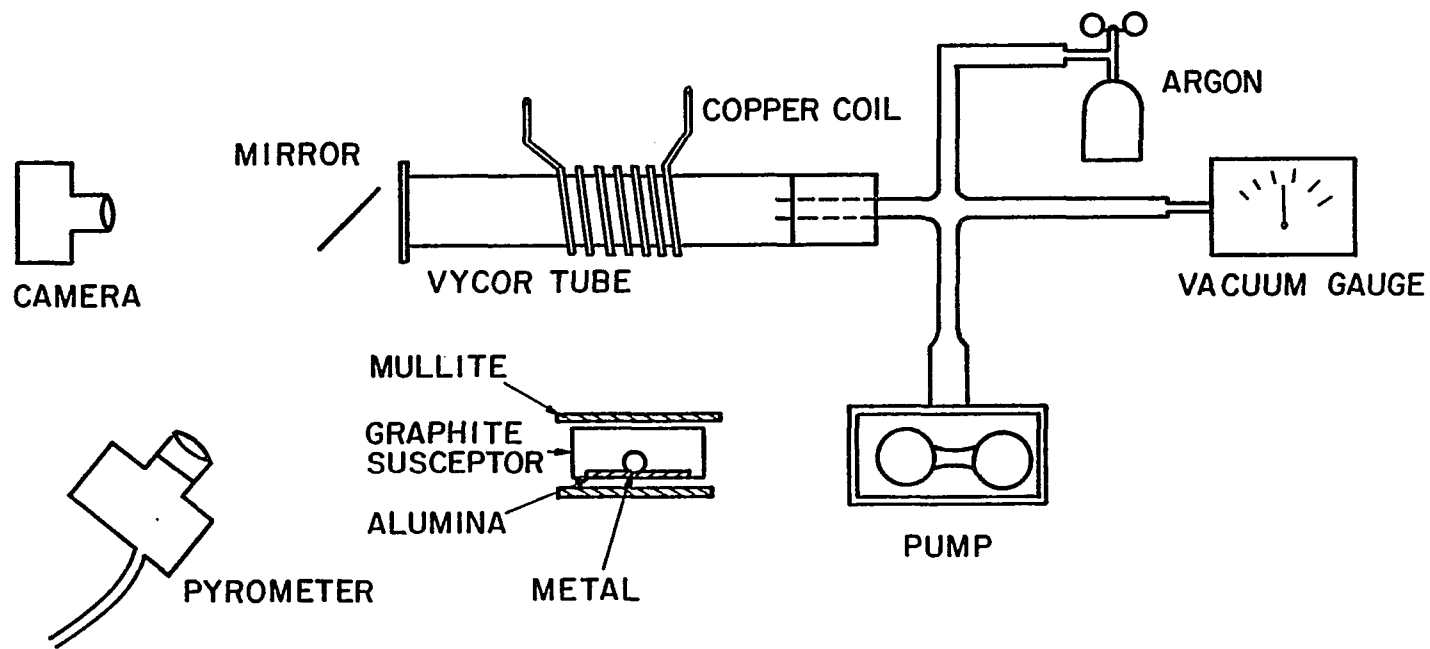


Figure 3.2 A schematic diagram of the experimental set up used for the plasma work.

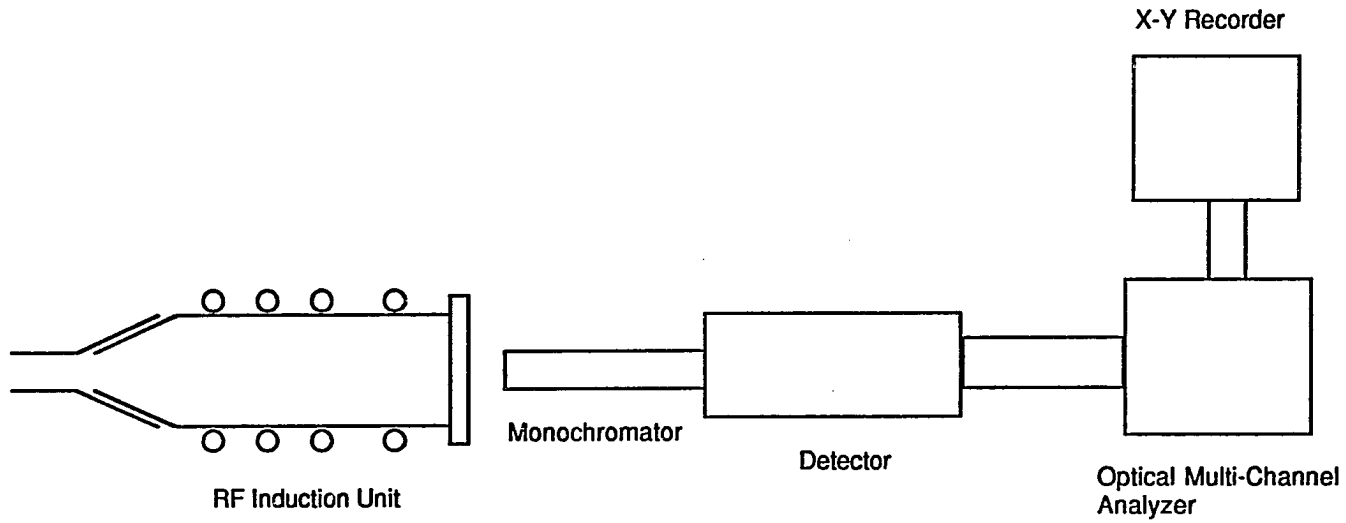


Figure 3.3 A schematic diagram of the experimental set up used for plasma diagnostics.

detect the emission from the plasma through a monochromator. The detector in turn was connected through a controller to the optical multi-channel analyzer (OMA-3). A 2.5 mm high band at the center of the 12.5 mm x 12.5 mm square ISIT target was monitored in order to avoid peripheral effects due to aberrations to prevent increased linewidth and thus reduced resolution.⁹¹ However, the full width of the ISIT target was monitored allowing about 300 to 600 angstroms wavelength range of the spectrum to be recorded at one time. Information from the detector was transferred to the OMA as plots of intensity versus wavelengths. Since the plasma was fairly stable and intense, the emission spectroscopy data were collected in the single track single scan mode.

The monochromator was first calibrated using an argon lamp (ORIEL Model 6030) and atomic absorption hollow cathode tubes as calibration standards such that each channel of the OMA corresponded to a particular wavelength. Intensities of the peaks were calculated by subtracting the background noise from the observed intensities automatically.

Surface tension and vaporization rate measurements were carried out both in the presence and absence of plasma. The surface tension measurement procedure was explained previously in the first section of this chapter.

For the vaporization rate experiments, the samples weighing between 0.5 g to 1.0 g were cleaned, degreased in acetone and placed on an alumina substrate inside a vycor reaction tube. Some of the samples were doped with a small quantities of oxygen or sulfur. The rate of vaporization was determined from the weight change of the sample and exposure time.

3.4 Weld aspect ratio experiments.

For the determination of weld morphology a carbon dioxide laser, Coherent Model Everlase 525-1, was used in the continuous mode. All welding was carried out inside a Plexiglas box using a 2.54 cm diameter and 12.7 cm focal length Zn-Se lens with an antireflection coating. Samples of dimensions 3 cm length, 1.5 cm width and 0.8 cm thickness were used for the experiments. Helium was used as the shielding gas. The weld pool width and depth were determined by optical microscopy. Samples were doped with sulfur by using appropriate H_2S/H_2 ratios calculated on the basis of data of Turkdogan⁵² and Rosenqvist.⁵³ Oxygen doping was done by using appropriate CO/CO₂ mixtures based on the oxygen content achieved at equilibration.⁵⁴ Tellurium and tin doping was done by covering the surface of the flat plate iron sample with a slurry composed of the powder in acetone and heating the sample to just above the melting point of the dopant under a stagnant hydrogen atmosphere. A summary of the experimental parameters employed in the doping processes is outlined in table 3.2.

Table 3.2 Summary of experimental conditions utilized in doping pure iron with various solutes.

System	Temperature	Experimental procedures	Solute concentration
Fe-O	1473	Oxygen doping using CO ₂ /CO flow rate ratio = 0.277	0.0186 wt%
Fe-S	1473	Sulfur doping using H ₂ S/H ₂ flow rate ratio = 5.02x10 ⁻³	0.02 wt%
Fe-Te	728	Tellurium slurry on sample plate	0.01 wt%
Fe-Sn	513	Tin slurry on sample plate	0.3 wt%

Chapter 4

THEORETICAL BACKGROUND

4.1 Thermodynamics of interfaces

An interface is a boundary or region of discontinuity between bulk phases or orientations. A surface is an interface between a condensed phase and a vapor phase. Because atomic coordination at a surface is incomplete (8 degrees of freedom: 6 vibrational and 2 translational), there is a surface tension force perpendicular to the boundary tending to minimize its area. This means that atomic bonds must be broken in bringing an atom from the interior of the condensed phase (9 degrees of freedom: 6 vibrational and 3 translational) to the surface and that energy is required to create additional surface. The potential energy of a molecule would be lowered if it moved from the surface to the bulk, and so the molecules are under the influence of a force which tends to draw them into the bulk. This force is attractive, and is termed a tension, the surface tension.

Consider a liquid in equilibrium with its vapor. The two bulk phases α and β do not change sharply from one to the other at the interface, but rather, as shown in figure 4.1, there is a region over which the density and local pressure vary.⁵⁵ Because the actual interfacial region has no sharply defined boundaries it is convenient to invent a mathematical dividing surface.⁵⁶ One then handles the extensive properties (G , E , S , n , etc.) by assigning to the bulk phases the values of these properties that would pertain if the bulk phases

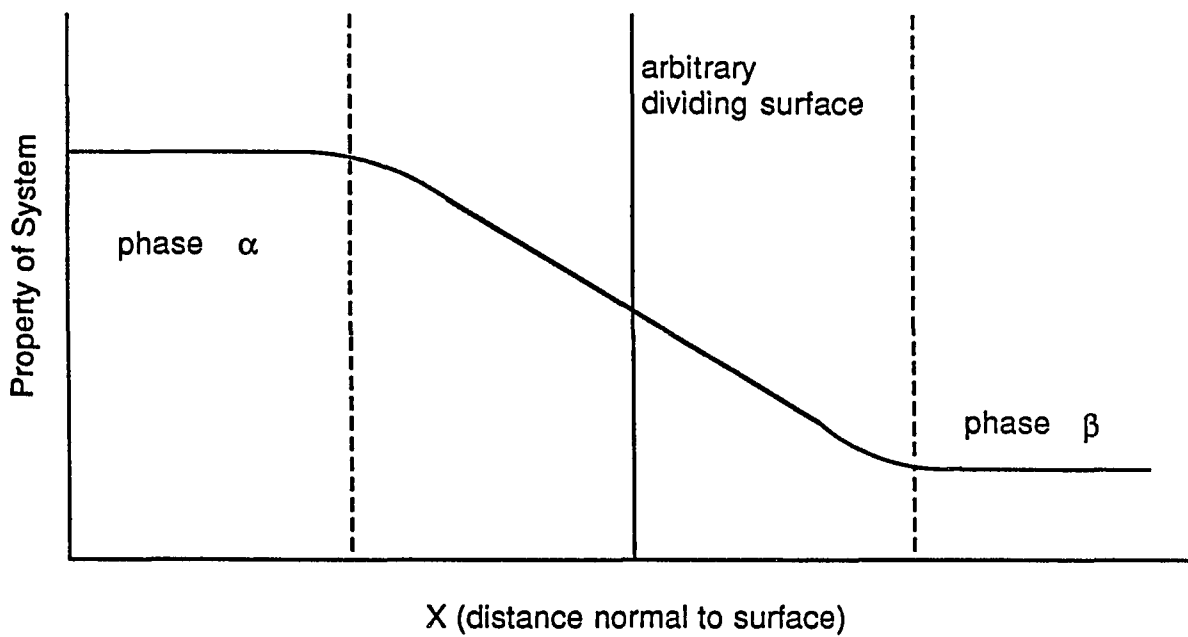


Figure 4.1 Variation of a property of a system in going from phase α to phase β .

continued uniformly up to the dividing surface. The actual values for the system as a whole will then differ from the sum of the values for the two bulk phases by an excess or deficiency assigned to the surface region. The following relations will then hold:

$$\text{Volume: } V = V^\alpha + V^\beta \quad (4.1)$$

$$\text{Internal energy: } E = E^\alpha + E^\beta + E^\gamma \quad (4.2)$$

$$\text{Entropy: } S = S^\alpha + S^\beta + S^\gamma \quad (4.3)$$

$$\text{Moles: } n_i = n_i^\alpha + n_i^\beta + n_i^\gamma \quad (4.4)$$

The superscript γ is used to denote surface quantities calculated on the above assumptions that the bulk phases continue unchanged to an assumed mathematical dividing surface. For an arbitrary set of variations from equilibrium,

$$dE = TdS + \sum_i \mu_i dn_i - P^\alpha dV^\alpha - P^\beta dV^\beta + \gamma dA + C_1 dc_1 + C_2 dc_2 \quad (4.5)$$

where c_1 and c_2 denote the two curvatures (reciprocals of the radii of curvature) and C_1 and C_2 are constants. The last two terms may be written as $1/2(C_1 + C_2) d(c_1 + c_2) + 1/2(C_1 - C_2) d(c_1 - c_2)$, and these plus the term γdA give the effect of variation in area and curvature. Because the actual effect might be independent of the location chosen for the dividing surface, a condition may be put on C_1 and C_2 , and this may be taken to be that $C_1 + C_2 =$

0. This particular condition gives a particular location of the dividing surface such that it is now called the surface of tension.

For the case where the curvature is small compared to the thickness of the surface region, $d(c_1 - c_2) = 0$ (this will be exactly true for a plane or for a spherical surface), and equation 4.5 reduces to:

$$dE = TdS + \sum_i \mu_i dn_i - P^\alpha dV^\alpha - P^\beta dV^\beta + \gamma dA \quad (4.6)$$

Because

$$G = E - TS + P^\alpha V^\alpha + P^\beta V^\beta \quad (4.7)$$

where G is the Gibbs free energy, it follows that:

$$dG = -SdT + \sum_i \mu_i dn_i + V^\alpha dP^\alpha + V^\beta dP^\beta + \gamma dA \quad (4.8)$$

Equation 4.8 is obtained by differentiating equation 4.7 and comparing with equation 4.6. At constant temperature and pressure:

$$dG = \sum_i \mu_i dn_i + \gamma dA \quad (4.9)$$

Therefore,

$$G = \sum_i \mu_i n_i + \gamma A \quad (4.10)$$

Differentiating equation 4.10:

$$dG = \sum_i \mu_i dn_i + \sum_i n_i d\mu_i + \gamma dA + A d\gamma \quad (4.11)$$

Comparing equation 4.11 with equation 4.9, it follows that :

$$A d\gamma + \sum_i n_i d\mu_i = 0 \quad (4.12)$$

$$\text{or, } d\gamma = - \sum_i \frac{n_i}{A} d\mu_i \quad (4.13)$$

Since $\sum \frac{n_i}{A}$ is the surface excess Γ_i , equation (4.13) can be written as :

$$d\gamma = - \sum_i \Gamma_i d\mu_i \quad (4.14)$$

Equation 4.14 is known as the Gibbs adsorption isotherm.

For a two component system, the portion of the dividing surface is so located such that the surface excess of the solvent is equal to zero. Thus, for a solute species i in a binary system, equation 4.14 can be written as:

$$d\gamma = - \Gamma_i RT d \ln a_i \quad (4.15)$$

where a_i is the activity of the species i in the solution. Equation 4.15 can be written as:

$$\Gamma_i = - \frac{1}{RT} \frac{d\gamma}{d \ln a_i} \quad (4.16)$$

$$= - \frac{a_i}{RT} \frac{d\gamma}{d a_i} \quad (4.17)$$

Langmuir's isotherm model is based on the assumptions that the surface has a number of well-defined sites which may be occupied by only one

atom (or molecule) of the surface active species. The adsorbed atoms have no mutual interactions. Formally, it can be represented thus:



for which the dissolved solute component i segregates to surface site V^S in order to form an occupied sites i^S . The standard free energy change of the above reaction can be written as:

$$\Delta G^0 = -RT \ln K \quad (4.19)$$

where K is the equilibrium constant for reaction 4.18. Thus:

$$K = \exp\left(\frac{-\Delta G^0}{RT}\right) = \frac{\theta_i}{a_i(1 - \theta_i)} \quad (4.20)$$

where $\theta_i = \Gamma_i/\Gamma_s =$ fraction surface coverage of i and Γ_s is the surface coverage at saturation. The Langmuir isotherm permits calculation of Γ_i as a function of a_i as:

$$K a_i - K \theta_i a_i = \theta_i \quad (4.21)$$

or,

$$\theta_i = \frac{K a_i}{1 + K a_i} \quad (4.22)$$

or,

$$\Gamma_i = \Gamma_s \frac{K a_i}{1 + K a_i} \quad (4.23)$$

Combining equation 4.17 and 4.22, which is essentially a combination of Gibbs

and Langmuir's isotherms, we obtain:

$$-\frac{a_i}{RT} \frac{d\gamma}{da_i} = \Gamma_s \frac{K a_i}{1 + K a_i} \quad (4.24)$$

or,

$$d\gamma = -\Gamma_s \frac{RTK}{1 + K a_i} da_i \quad (4.25)$$

Integrating equation 4.25 from $\gamma = \gamma^0$ in the pure metal to $\gamma = \gamma$ in impure metal:

$$\int_{\gamma^0}^{\gamma} d\gamma = -\int_0^{a_i} \Gamma_s \frac{RTK}{1 + K a_i} da_i \quad (4.26)$$

$$\text{or,} \\ \gamma - \gamma^0 = -RT \Gamma_s \ln(1 + K a_i) \quad (4.27)$$

or,

$$\gamma = \gamma^0 - RT \Gamma_s \ln(1 + K a_i) \quad (4.28)$$

The form of the above equation was found empirically by Szyszkowski³⁷ in 1908 and bears his name. Equation 4.20 can also be written as:

$$K = \exp\left(\frac{-\Delta G^0}{RT}\right) = \exp\left(\frac{\Delta S^0}{R}\right) \exp\left(\frac{-\Delta H^0}{RT}\right) \quad (4.29)$$

If we assume, as a first approximation, that both the entropy and enthalpy values are constants independent of temperature, then equation 4.29 can be

modified as :

$$K = k_1 \exp\left(\frac{-\Delta H^\circ}{RT}\right) \quad (4.30)$$

where k_1 is a constant. For a pure metal, the temperature dependence of surface tension is given by:

$$\gamma^0 = \gamma_m - A(T - T_m) \quad (4.31)$$

where γ_m is the surface tension of pure metal at the melting point, A is the negative of $d\gamma/dT$ for pure metal and T_m is the melting point of the material.

Combining equations 4.28 and 4.31, we have:

$$\gamma = \gamma_m - A(T - T_m) - RT \Gamma_s \ln \left[1 + k_1 a_i \exp\left(\frac{-\Delta H^\circ}{RT}\right) \right] \quad (4.32)$$

which gives the surface tension of metal-solute (i) alloys as a function of both temperature, T , and activity, a_i .

4.1.1 Temperature coefficient of surface tension

The temperature coefficient of surface tension, $d\gamma/dT$, for an alloy containing a surface active element can be obtained by differentiating equation 4.32 with respect to T and remembering that $K = k_1 \exp(-\Delta H^\circ/RT)$.

Differentiating γ with respect to T,

$$\frac{d\gamma}{dT} = -A - \left[R\Gamma_s \ln \left\{ 1 + k_1 a_i e^{\frac{-\Delta H^\circ}{RT}} \right\} + \frac{RT\Gamma_s}{\left(1 + k_1 a_i e^{\frac{-\Delta H^\circ}{RT}} \right)} \frac{d}{dT} \left(k_1 a_i e^{\frac{-\Delta H^\circ}{RT}} \right) \right] \quad (4.33)$$

Now,

$$\frac{d}{dT} \left(1 + K a_i \right) = \frac{d \left(1 + k_1 a_i e^{\frac{-\Delta H^\circ}{RT}} \right)}{dT} = k_1 e^{\frac{-\Delta H^\circ}{RT}} \frac{da_i}{dT} + k_1 a_i e^{\frac{-\Delta H^\circ}{RT}} \left(\frac{\Delta H^\circ}{R} \frac{1}{T^2} \right) \quad (4.34)$$

Therefore,

$$\frac{d\gamma}{dT} = -A - \left[R\Gamma_s \ln \{ 1 + K a_i \} + \frac{RT\Gamma_s}{1 + K a_i} \left(K \frac{da_i}{dT} + K a_i \frac{\Delta H^\circ}{RT^2} \right) \right] \quad (4.35)$$

To take into account the variation of the activity with respect to temperature, it will be necessary to carry out the following operations. For any real solution, the partial molar free energy of mixing, $\Delta \bar{G}_i^m$, is given by

$$\Delta \bar{G}_i^m = RT \ln a$$

then,

$$a = \exp \left(\frac{\Delta \bar{G}_i^m}{RT} \right)$$

Differentiating with respect to temperature we obtain:

$$\begin{aligned}\frac{da}{dT} &= \exp\left(\frac{\Delta\bar{G}_i^m}{RT}\right) \times \frac{\Delta\bar{G}_i^m}{R} \left(-\frac{1}{T^2}\right) \\ &= a \times \frac{RT \ln a}{R} \left(-\frac{1}{T^2}\right) \\ &= -\frac{a \ln a}{T}\end{aligned}$$

Substituting these in equation 4.35, we have:

$$\frac{d\gamma}{dT} = -A - R\Gamma_s \ln(1 + Ka_i) - \frac{RT\Gamma_s}{1 + Ka_i} \left(-K \frac{a \ln a}{T} + Ka_i \frac{\Delta H^\circ}{RT^2} \right) \quad (4.36)$$

$$= -A - R\Gamma_s \ln(1 + Ka_i) - \frac{R\Gamma_s}{1 + Ka_i} \left\{ Ka_i \left(\frac{\Delta H^\circ}{RT} - \frac{\bar{G}_i^m}{RT} \right) \right\} \quad (4.37)$$

Replacing $\Delta\bar{G}_i^m$ by $\Delta\bar{H}_i^m$ ($= RT \ln \gamma$), we have :

$$\frac{d\gamma}{dT} = -A - R\Gamma_s \ln(1 + Ka_i) - \frac{Ka_i}{1 + Ka_i} \frac{\Gamma_s}{T} \left(\Delta H^\circ - \Delta\bar{H}_i^m \right) \quad (4.38)$$

The derivative consists of 3 terms:

Term 1. This is equivalent to $d\gamma/dT$ for pure metals and is negative since A is positive.

Term 2. This term is related to the entropy of segregation. It must be negative because the entropy change for segregation must be negative.

Term 3. This term is related to the enthalpy change of segregation. This term is negative if ΔH^0 is positive (i.e. endothermic process) and is positive if ΔH^0 is negative (i.e. exothermic process).

Thus, $d\gamma/dT$ can only be positive if ΔH^0 is highly negative i.e. surface segregation is an exothermic reaction. It should be noted that terms (2) and (3) also depend on T and a_j .

Consider the variation of γ with a_j . Figure 4.2 shows the variation of surface tension with additions of a surface active species. Consider two extreme cases.

Region I: In this case, $\theta/(1-\theta) = 0$ i.e., a very clean surface is prevalent. In this case $Ka_j \ll 1$ and equation 4.35 reduces to

$$\frac{d\gamma}{dT} = -A - Ka_j \frac{\Gamma_s (\Delta H^0 - \Delta \bar{H}_i^m)}{T} \quad (4.39)$$

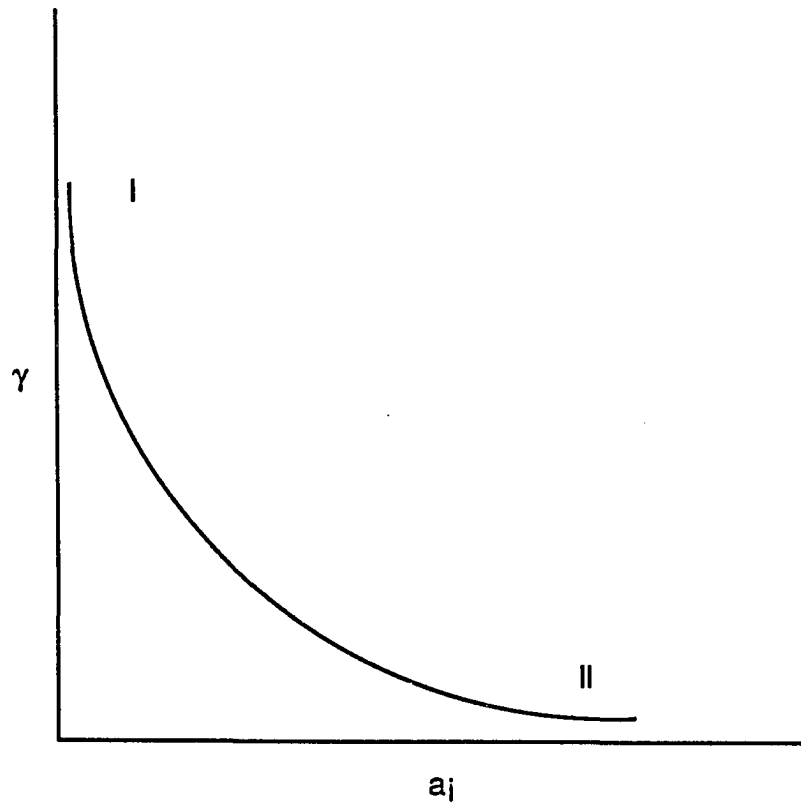


Figure 4.2 Variation of interfacial tension as a function of the activity of the solute.

Region II: Here $\theta/(1-\theta) = 1$, i.e. a saturated surface is prevalent.

In this case $Ka_i \gg 1$, and equation 4.35 reduces to:

$$\frac{d\gamma}{dT} = -A - R\Gamma_s \ln(k_1 a_i) + \frac{\Gamma_s \Delta \bar{H}_i^m}{T} \quad (4.40)$$

From equations 4.39 and 4.40 it is seen respectively that in case I, $d\gamma/dT$ depends on a_i , while in case II, it depends on $\ln(a_i)$. In case I, $d\gamma/dT$ can be positive if ΔH^0 has a sufficiently high negative value. In case II, the $d\gamma/dT$ value is usually negative. Under low surface coverage conditions the Langmuir isotherm represents the effect of adsorbed atoms on the surface tension very well so that interactions between adsorbed atoms need not be considered.⁴¹ On continued addition of the surface active element a saturation stage is reached. This is manifested by a practically constant value of Γ_s or, by a constant slope of γ vs. $\ln a_i$. Generally, the saturation stage corresponds to the formation of a two-dimensional compound. The nature and structure of such compounds have been investigated extensively in the case of solid surfaces by techniques such as "low energy electron diffraction" (LEED), field ion microscopy and Auger spectroscopy.⁵⁷

Studies by Germer et al.⁵⁸ and Mac Rae⁵⁹ on oxygen adsorption on nickel yields results which are fairly typical of many other systems. Their studies indicated that depending on the plane of nickel on which oxygen is being adsorbed a two-dimensional compound with a superlattice structure is formed. For example, on the (100) plane of nickel, the superlattice has the stoichiometry NiO. After the formation of this two-dimensional compound, no further adsorption of oxygen is observed.

In the case of liquid metals, there is experimental evidence that a short range is retained.⁴¹ Similar adsorption phenomena with formation of superlattices of stoichiometry $A_{n-1}B$ may therefore be assumed. Clearly, however, such structures would not cover the entire surface as a coherent compound. Direct experimental observation of the surface structure and chemistry is, however, more difficult than in the case of solid surfaces. Increasing the temperature has the effect of causing adsorbed atoms to desorb from the surface resulting in an increase in the surface tension.

Therefore ΔH^0 , the heat of adsorption of the surface active species at low surface coverages, is the most important parameter for determining the conditions under which the temperature coefficient of the surface tension can be positive.

The minimum activity of solute required to obtain a positive value of dy/dT at various temperatures can be calculated by equating dy/dT to zero in equation 4.35.

4.2 Plasma physics relevant to present study

The word "plasma" was coined in 1928 by Irving Langmuir of the General Electric Laboratory who was working with low pressure electric discharges which have since become familiar in fluorescent tubes and neon signs. Plasma has been recognized as a fourth state of matter, apart from solid, liquid and gas. Just as the solid is characterized by a rigid, dense lattice structure, a liquid by a non-rigid fluid and a gas by a low density randomized collection of atoms or molecules; so a plasma is characterized by a collection of

charged particles (ions and electrons) of low density.⁶⁰ The plasma is a collection of particles which can range from a few percent to complete ionization. Today, the word plasma covers a wide variety of conditions in electrically conducting gases. They range from the low-pressure discharges to fully ionized extremely high temperature thermonuclear plasmas.⁶¹ The plasma, as a whole, is electrically neutral since there are substantially equal number of electrons and gas ions present. The mechanism of formation of a low-pressure plasma is schematically illustrated in figure 4.3. The positively charged ions and the negatively charged electrons are accelerated in opposite directions by the applied electric field, E . In low-pressure plasmas (10^{-3} atm or less), collisions are relatively rare, and an electron travels a considerable distance between collisions. When it finally collides with an atom, it has gained enough energy from the electric field to produce an ion by knocking off an electron or at least to excite the atom and cause it subsequently to emit light. The nature of the plasma produced depends on the gas used, the pressure and the energy supplied to it. In plasmas normally used in the electronic technology, the electron concentration varies from 10^{12} to 10^{14} cm^{-3} .⁶² The primary difference between the plasmas produced during welding and an RF inductively coupled plasma is the absence of local thermal equilibrium in the RF produced plasma. However, under welding conditions, the plasma produced is essentially in local thermal equilibrium in which case the electron, ion and gas temperatures are equivalent to each other. Another difference is the existence of an electric field in the inductively coupled plasma.

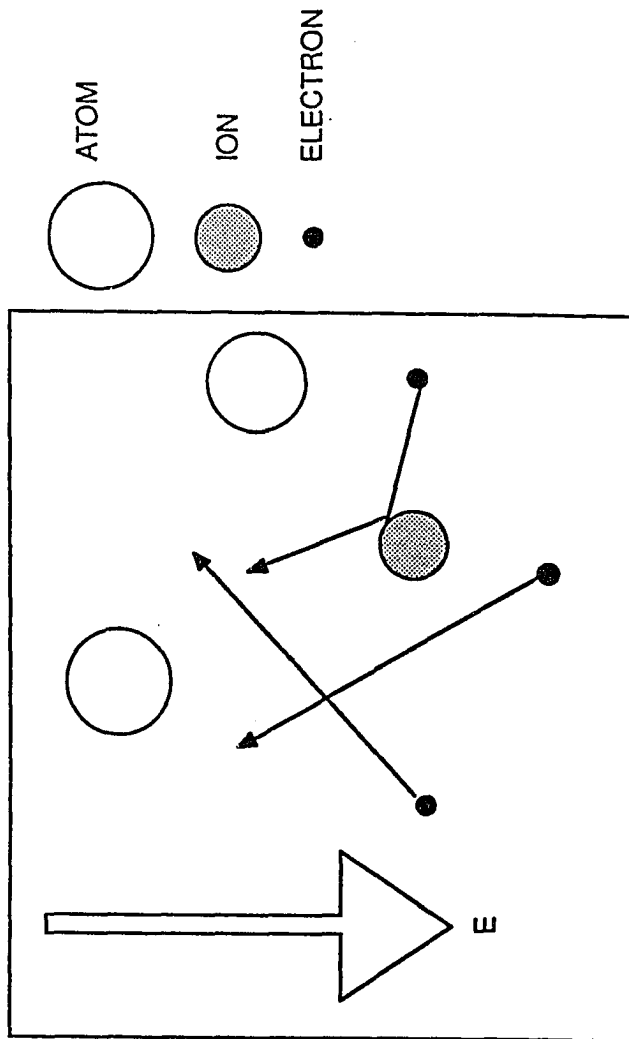


Figure 4.3 A schematic representation of low pressure low temperature plasma.

4.2.1 Emission spectroscopy

When an atom is placed in a sufficiently strong electric field or is hit by a sufficiently swift electron (as in a discharge tube), or collides violently with another atom (as at high temperatures), it may have an electron displaced from the normal orbit (energy level) to an outer one. As the disturbed (unstable) electron falls to a lower energy level orbit, it will radiate this acquired energy as a monochromatic light⁶³ consisting of photons.

The actual change in energy (ΔE) between the two energy levels in an atom is related to the frequency and wavelength of the radiation absorbed or emitted by the following equation:

$$E' - E'' = \Delta E = h\nu = hc/\lambda \quad (4.41)$$

where h is Planck's constant (cm^{-1}s), ν is the frequency in hertz (s^{-1}), E' is the energy (cm^{-1}) of the lower level of the electron, c is the velocity of light or electromagnetic radiation (cm s^{-1}) and λ is the wavelength of emission (cm). This transition from an upper energy level is known as bound-bound transition, wherein the electron makes a transition from one bound state to another of lower energy. This can be understood from figure 4.4 which shows the emission and absorption spectrum lines, wherein each of the transitions corresponds to a particular wavelength.

The study of plasmas using emission spectroscopy enables us to obtain a large amount of information about the plasma of various species in terms of their number density and temperatures without disturbing or perturbing

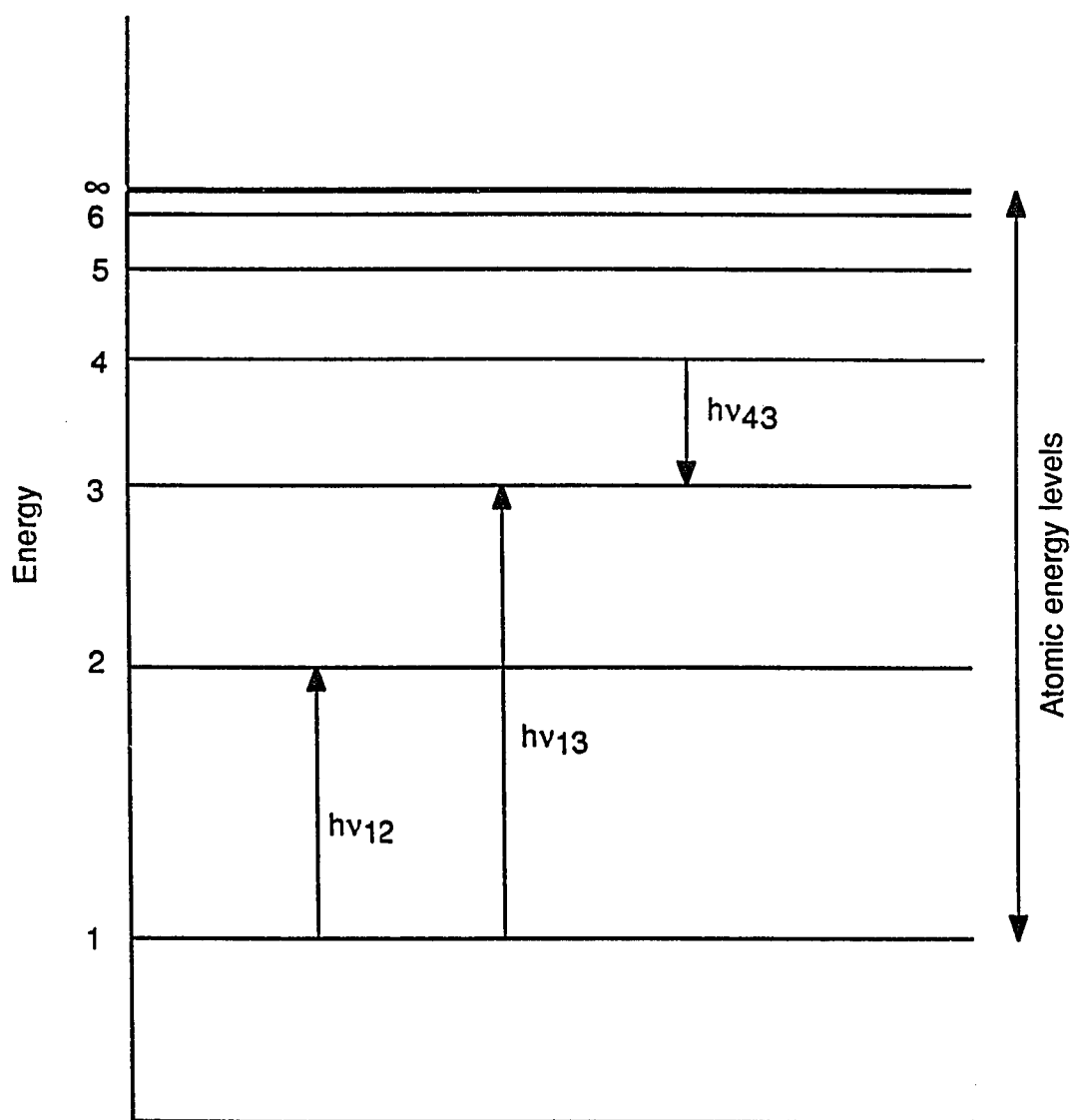


Figure 4.4 Schematic absorption and emission spectrum line series and related atomic energy levels (from reference60.)

it. This non-invasive technique was utilized in the present study to characterize the plasma.

Glow discharge plasma can be generated in a tubular type reactor with external ring electrodes or a coil energized with a 50 Hz to 13 MHz excitation. Regardless of the power supply and electrode configuration, the important parameters that characterize plasma include the nature of the various species, the energy of the electrons (electron temperature), the energy of molecular vibration and rotation and the gas temperature.⁶⁴ In the low temperature glow discharge plasma, the electron temperature is much higher than the temperatures of the ions and atoms and the plasma is generally highly ionized.

Recent work has shown that the electron temperature is an important parameter in various plasma processing operations. For example, the electron temperature is known to affect the oxidation rate in an oxygen plasma and solid surface interactions.⁶⁵ The electron temperature also has a strong influence on the anodization rate in glow discharge anodization of silicon.⁶⁵

4.2.2 Electron temperature estimation

The method for measuring the electron temperature is based on the assumption that the population of atoms, ions, or molecules of the thermometric species at the different energy levels follow a Boltzmann distribution. The equation for the absolute intensity of a spectral line involved in the transition from an upper energy level q to a lower energy level p is given by:⁶⁶

$$I_{qp} = \frac{d}{4\pi} A_{qp} h \nu_{qp} n \frac{g_q \exp\left(\frac{-\epsilon_q}{kT}\right)}{Z} \quad (4.42)$$

where I_{qp} is the intensity at a particular frequency, A_{qp} is the average transition probability, h is Planck's constant, ν_{qp} is the frequency of emission from upper energy level to lower level, g_q is the degeneracy of upper level, k is Boltzmann's constant, ϵ_{qp} is the integrated intensity, n is the number density, T is the absolute temperature and Z is the partition function. Taking logarithms and rearranging we have:

$$\ln \frac{I_{qp}}{g_q A_{qp} \nu_{qp}} = \ln \frac{d}{4\pi} h + \ln \frac{n}{Z} - \frac{\epsilon_q}{kT} \quad (4.43)$$

Inserting relative intensity I'_{qp} and relative transition probability A'_{qp} we write:

$$\ln \frac{I'_{qp}}{g_q A'_{qp} \nu_{qp}} = \ln \frac{n}{Z} - \frac{\epsilon_q}{kT} \quad (4.44)$$

Applying equation 4.44 to a group of spectral lines emitted by atoms, ions or molecules of one and the same kind, we see that $\ln\left(\frac{I'_{qp}}{g_q A'_{qp} \nu_{qp}}\right)$ is a linear function of ϵ_q because n and Z are now constants, that is, n and Z have the same values for all the lines involved. Consequently, if for a series of spectral

lines of a particular type of atom, ion or molecule, $\ln\left(\frac{I'_{qp}}{g_q A'_{qp} \nu_{qp}}\right)$ or equivalently $\ln\left(\frac{I'_{qp} \lambda}{g_q A_{qp}}\right)$ is plotted against the corresponding excitation energy ϵ_q , a straight

line with slope proportional to $1/T$ will result, provided self-absorption is negligible.

Chapter 5

RESULTS AND DISCUSSION

5.1 Thermodynamic modeling

It was explained in the previous chapter that the interfacial tension of binary metal-surface active solute systems can be thermodynamically represented by equation 4.32 which is repeated here as:

$$\gamma = \gamma_m - A(T - T_m) - RT\Gamma_s \ln \left[1 + k_1 a_i \exp\left(\frac{-\Delta H^0}{RT}\right) \right] \quad (5.1)$$

This formalism gives a quantitative relationship between surface tension to the temperature and composition of the melt. This makes it much more amenable to use in various mathematical modeling studies of fluid flow in weld pools which, hitherto, relied on approximate values of γ .

Examination of equation 5.1 reveals that four factors (A , Γ_s , k_1 and ΔH^0) must be known before the surface tension of the binary solution can be calculated. The term A , which is the negative of the temperature coefficient of surface tension of a pure metal can be determined from the surface tension values at two or more temperatures. This constant can also be estimated by means of expressions based on Eotvos' Law and procedures are discussed by Allen.⁹² The surface excess of the solute species at saturation, Γ_s , can be determined by applying Gibbs isotherm to a surface tension versus activity plot. In the absence of experimental data, Γ_s may be estimated from a knowledge of

the surface structure. Table 5.1 shows that such an estimation indeed yields fairly satisfactory values⁴¹, especially when one considers the uncertainty in the experimental data. In fact, both A and Γ_S have been extensively studied for most systems and are either readily available or can be calculated easily.^{35,41,67-69} The means of estimating the two other factors, ΔH^0 and k_1 are now discussed.

5.1.1 Estimation of enthalpy (ΔH^0) and entropy factor (k_1)

At a given temperature the equilibrium constant for the adsorption reaction (reaction 4.18) otherwise referred to as the adsorption coefficient, K , is determined by fitting experimental surface tension data versus composition data to equation 4.28 in which all the parameters except K are known. If the natural logarithm of the equilibrium constant K is plotted as a function of $1/T$, the values of ΔH^0 and k_1 can be determined from the slope and the intercept of the straight line respectively.

Since the evaluation of K requires a series of surface tension measurements on high purity liquid metals at various concentrations of surface active impurities at two, or preferably more temperatures, such data are available for very few systems.

5.1.1.1 Fe-S system

The Fe-S system has been one of the most thoroughly studied and the surface tension data for this system is used to calculate K as a function of

Table 5.1: Area requirements at saturation (from reference 41).

System	T, K	[Å ² /atom, 1 Å = 10 ⁻¹⁰ m]			Ionic radius(Å)		Ionic charge	
		Experimental	Calculated ^a	Calculated ^b	r	r ⁺	Z ⁻	Z ⁺
Fe-O	1823	10.3	6.0	8 (111)	1.33	0.83	2	2
Fe-S	1823	15.1	10.5	12 (010)	1.74	0.83	2	2
Fe-Se	1823	14.7	13	13 (010)	1.91	0.83	2	2
Fe-Te	1823	15.0	14.6	18 (100)	2.11	0.83	2	2
Cu-O	1273	29	6.0	30 (111)	1.32	0.96	2	1
Cu-S	1393	14.5	10.5	14.5 (100)	1.74	0.96	2	1
Cu-Se	1423	11.9	13	16.8 (111)	1.91	0.96	2	1
Cu-Te	1423	13.8	14.6	23 (100)	2.11	0.96	2	1
Ag-O	1253	34	6.0	38 (111)	1.32	1.13	2	1

^a On the basis of monolayer of close-packed solute anions

^b On the basis of the solid compound.

temperature. Sources for raw data were extracted from references 70-72. The calculated values of K at various temperatures are given in table 5.2 and are plotted as a function of $1/T$ in figure 5.1. From this plot the values of the heat of adsorption, ΔH^0 and the entropy factor, k_1 , are determined to be -1.66×10^5 KJ/kg mole and 3.18×10^{-3} respectively by regression analysis.

The utility of the previous calculations lies in the fact that the enthalpy and entropy factors, along with the temperature coefficient of surface tension and the surface excess at saturation can give a relationship for the surface tension of a binary solution as a function of temperature and composition. As an example, the expression for the interfacial tension of Fe-S alloys as a function of both temperature and composition is given by:

$$\gamma = 1.943 - 4.3 \times 10^{-4} (T - 1809) - RT \times 1.3 \times 10^{-8} \ln \left\{ 1 + .0032 a_s e \left(\frac{1.66 \times 10^6}{RT} \right) \right\} \text{ N/m (5.2)}$$

In order to demonstrate the validity of the above equation, the predictions from equation 5.2 are compared with the experimental values reported by Keene et al.³⁰ for the pseudo-binary Fe-S system in figure 5.2. It may be observed that a fairly good agreement is achieved between the experimental data and the computed values. Table 5.3 summarizes the results of similar calculations for various other systems studied and the data sources. In figures 5.3 to 5.8 the predicted interfacial tension values are presented as a function of solute concentration for the Fe-O, Fe-Se, Cu-O, Cu-S, Cu-Se and Cu-Te systems respectively. The predicted curves are calculated on the basis

Table 5.2: Summary of the calculated absorption coefficient in the Fe-S system at various temperatures.

Temperature, K	K	$1/T \times 10^4$ (K^{-1})	ln K
1843	166	5.43	5.11
1823	185	5.49	5.22
1723	325	5.80	5.78

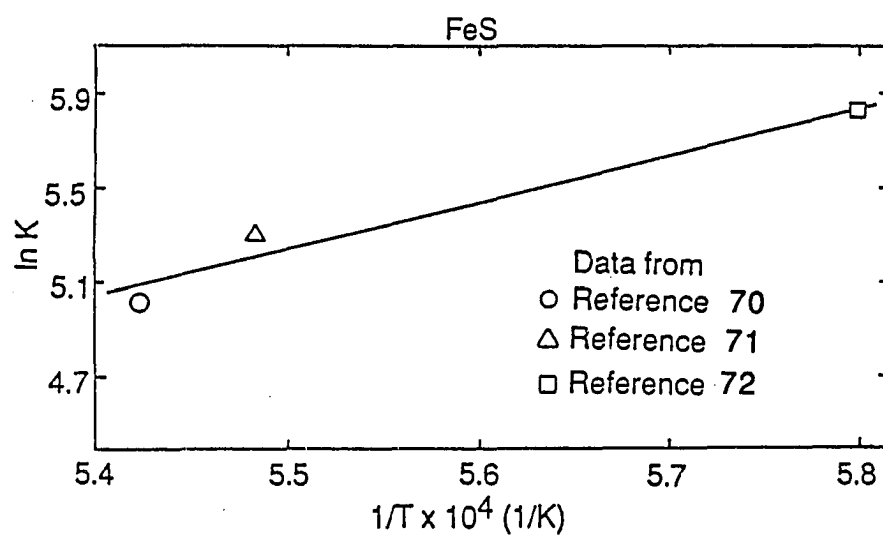


Figure 5.1 Variation of equilibrium constant with temperature for the Fe-S system.

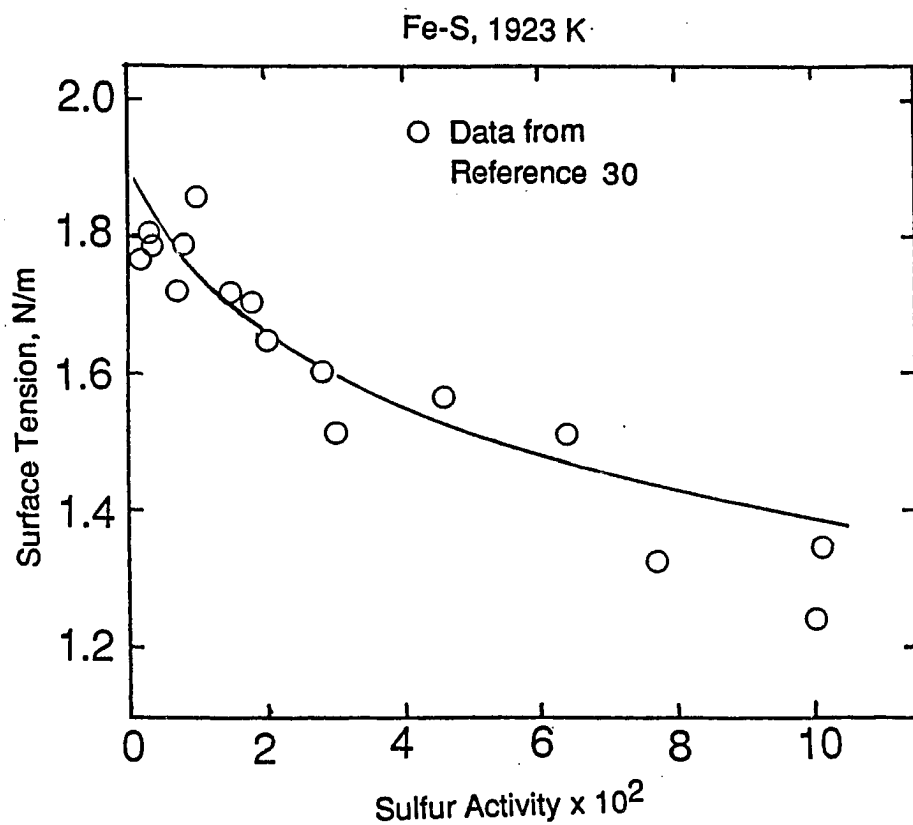


Figure 5.2 Depression of the surface tension of iron by sulfur and comparison with ideal isotherm (5.1) at 1923 K; surface tension data taken from reference 30.

Table 5.3: Summary of calculated entropy and enthalpy factors.

System	k_1	$-\Delta H^0$ KJ/Kg mole	Activity Calculations	References
Fe-O	1.38×10^{-2}	1.46×10^5	$a_O = \text{wt}\% \underline{O}$	27,30,33, 70,73,74
Fe-S	3.18×10^{-3}	1.66×10^5	$a_S = \text{wt}\% \underline{S}$	70-72
Fe-Se	8.57×10^{-1}	1.09×10^3	$a_{Se} = \text{wt}\% \underline{Se}$	34,72
Cu-O	3.29×10^{-1}	1.73×10^5	$a_O = X_O \times \text{activity coefficient}$	25,36,75
Cu-S	7.94×10^{-5}	1.67×10^5	$a_S = \text{Atom \% } \underline{S}$	75,76
Cu-Se	1.45×10^{-3}	1.25×10^5	$a_{Se} = \text{wt}\% \underline{Se}$	77
Cu-Te	1.02×10^{-3}	1.29×10^5	$a_{Te} = \text{wt}\% \underline{Te}$	77
Ag-O		1.42×10^5	$a_O = X_O \times \text{activity coefficient}$	67
Sn-Te	1.68×10^{-2}	3.78×10^4	$a_{Te} = \text{wt}\% \underline{Te}$	71

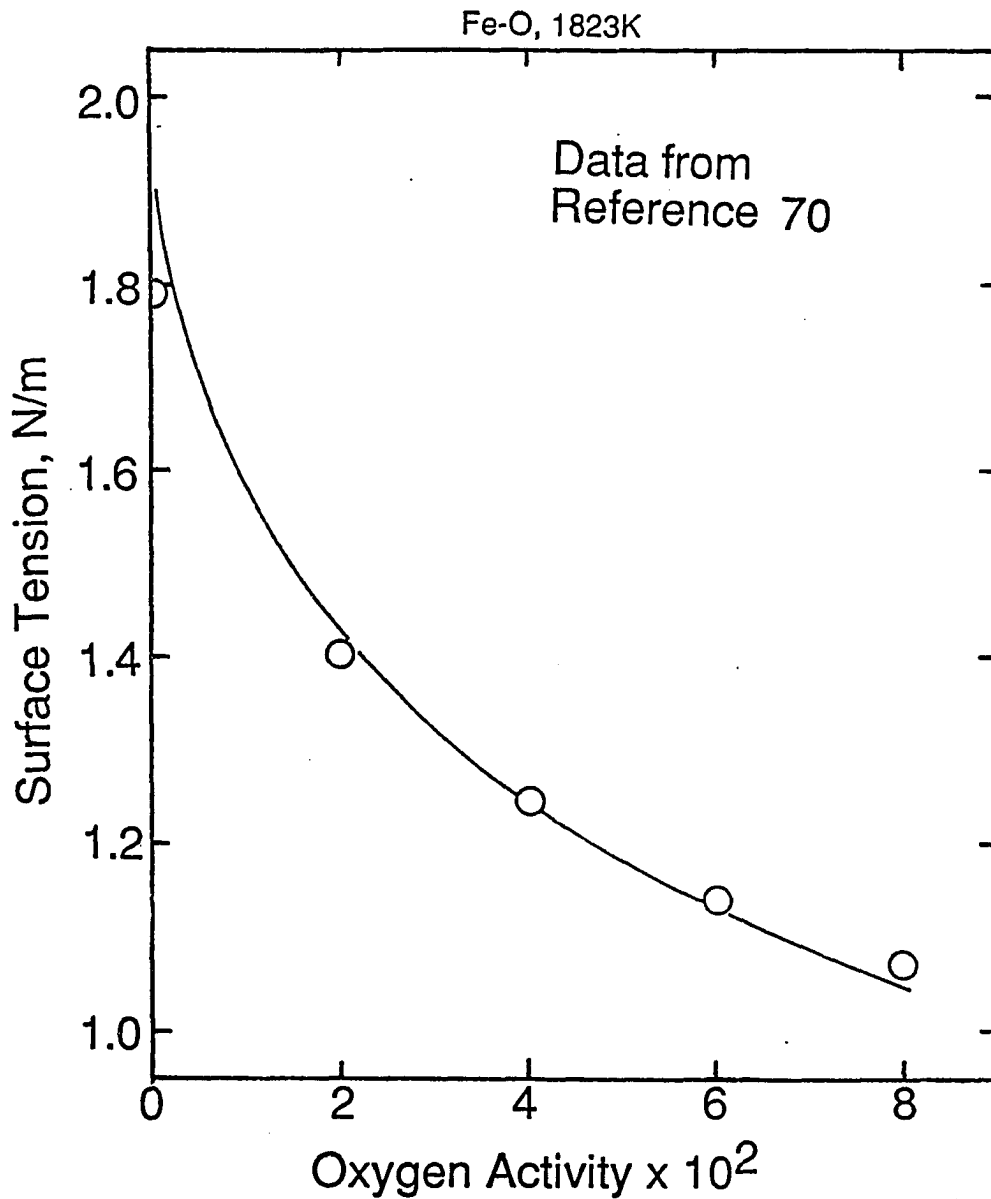


Figure 5.3 Depression of the surface tension of iron by oxygen and comparison with ideal isotherm (5.1) at 1823 K; surface tension data taken from reference 70.

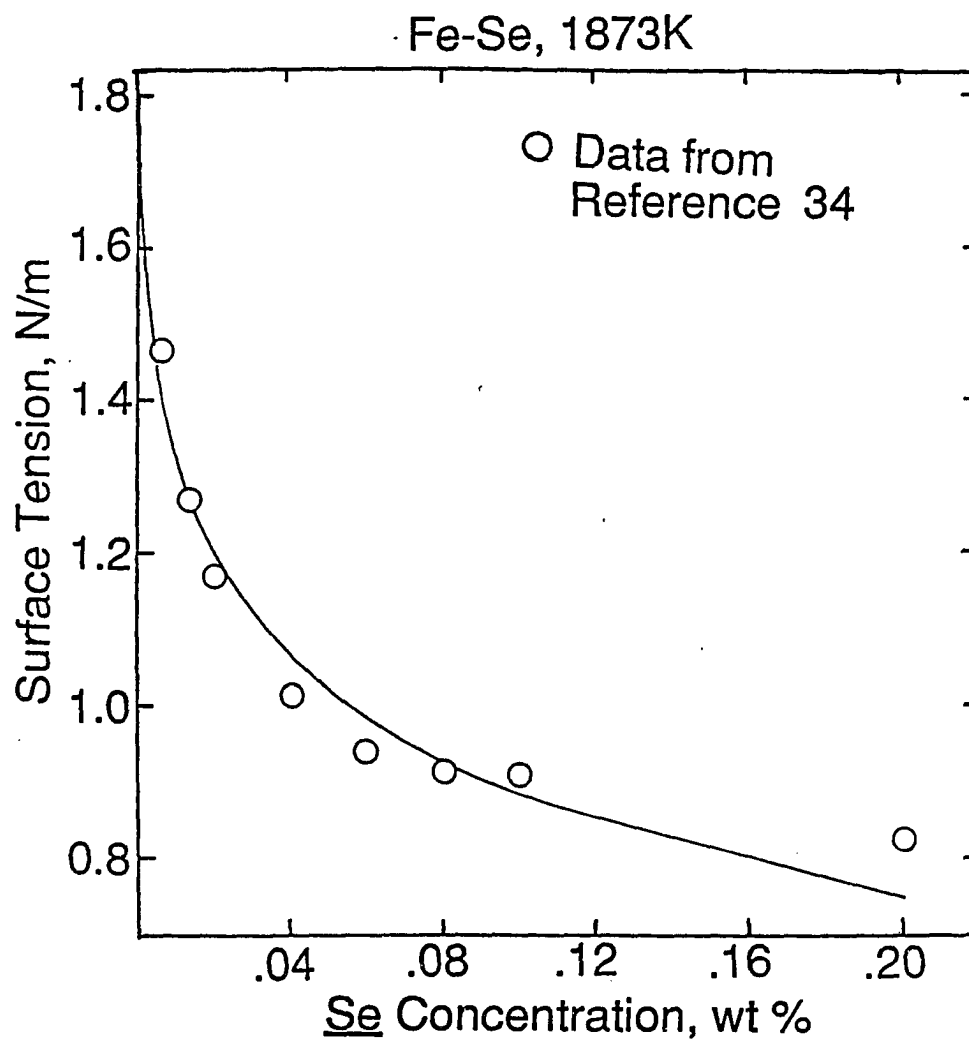


Figure 5.4 Depression of the surface tension of iron by selenium and comparison with ideal isotherm (5.1) at 1873 K; surface tension data taken from reference 34.

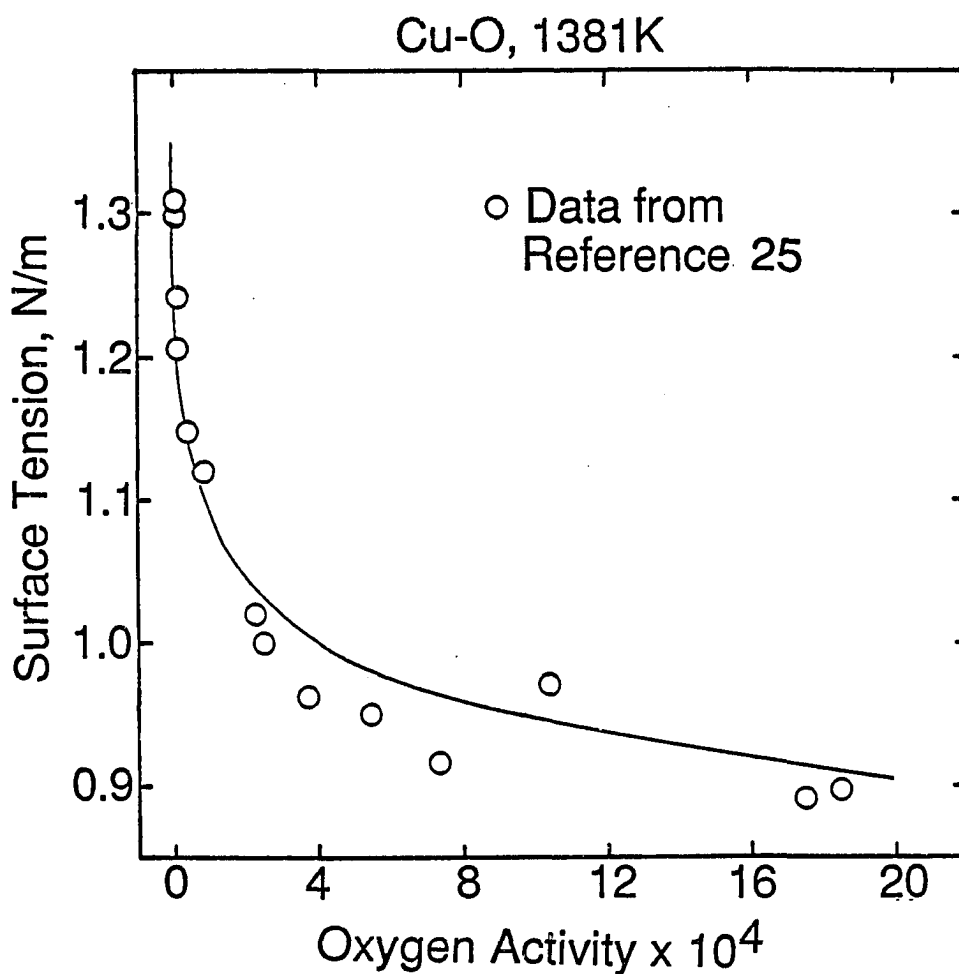


Figure 5.5 Depression of the surface tension of copper by oxygen and comparison with ideal isotherm (5.1) at 1381 K; surface tension data taken from reference 25.

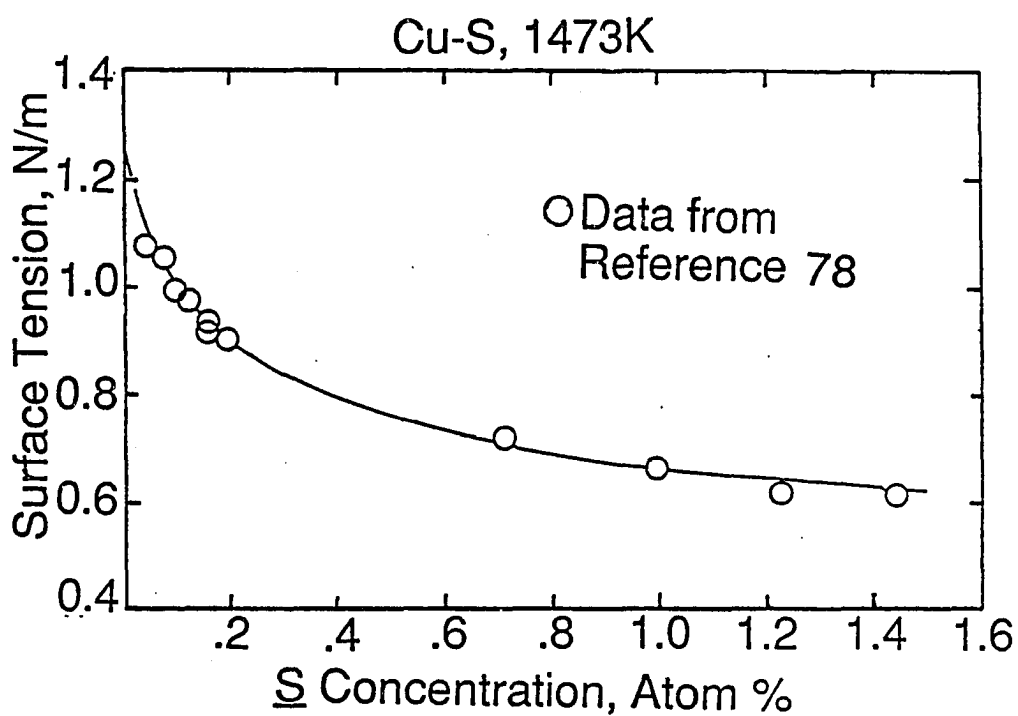


Figure 5.6 Depression of the surface tension of copper by sulfur and comparison with ideal isotherm (5.1) at 1473 K; surface tension data taken from reference 78.

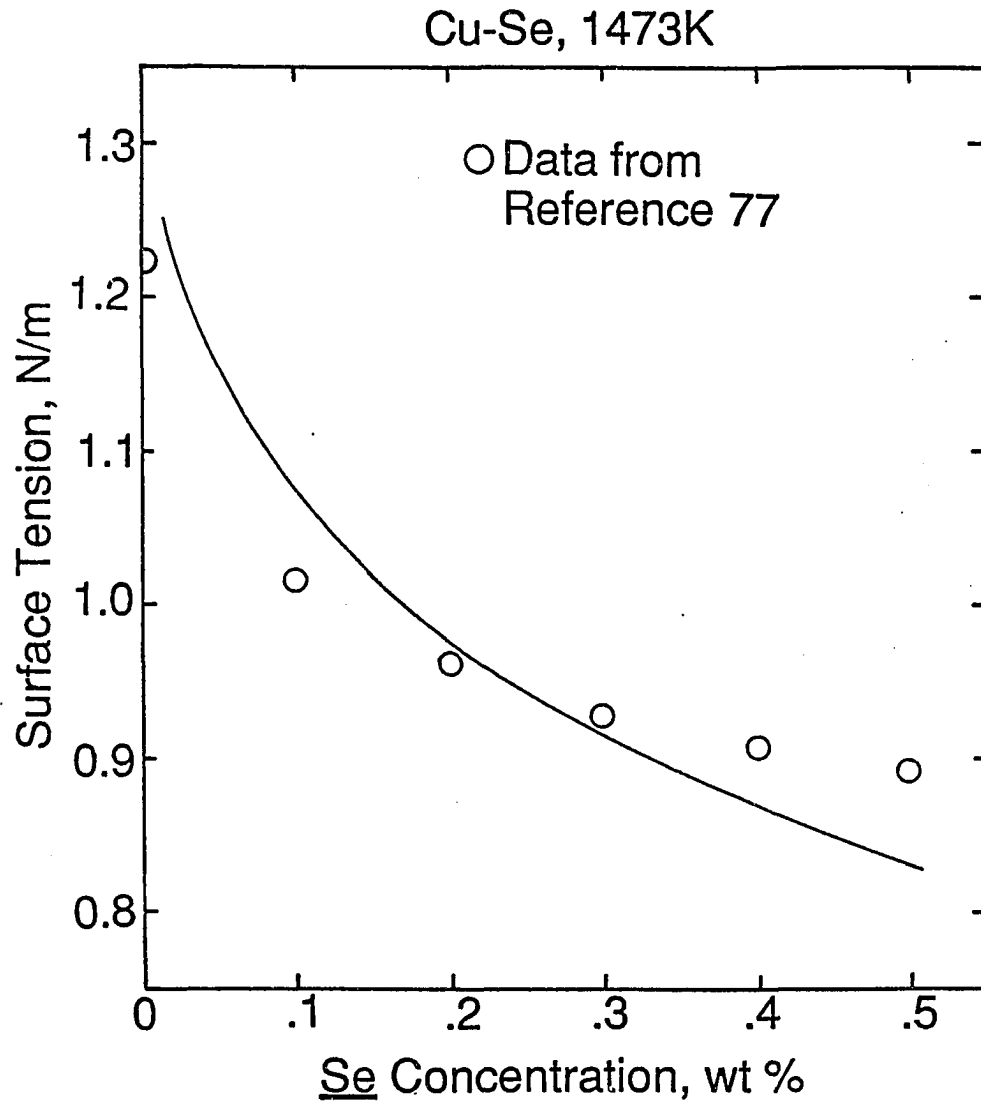


Figure 5.7 Depression of the surface tension of copper by selenium and comparison with ideal isotherm (5.1) at 1473 K; surface tension data taken from reference 77.

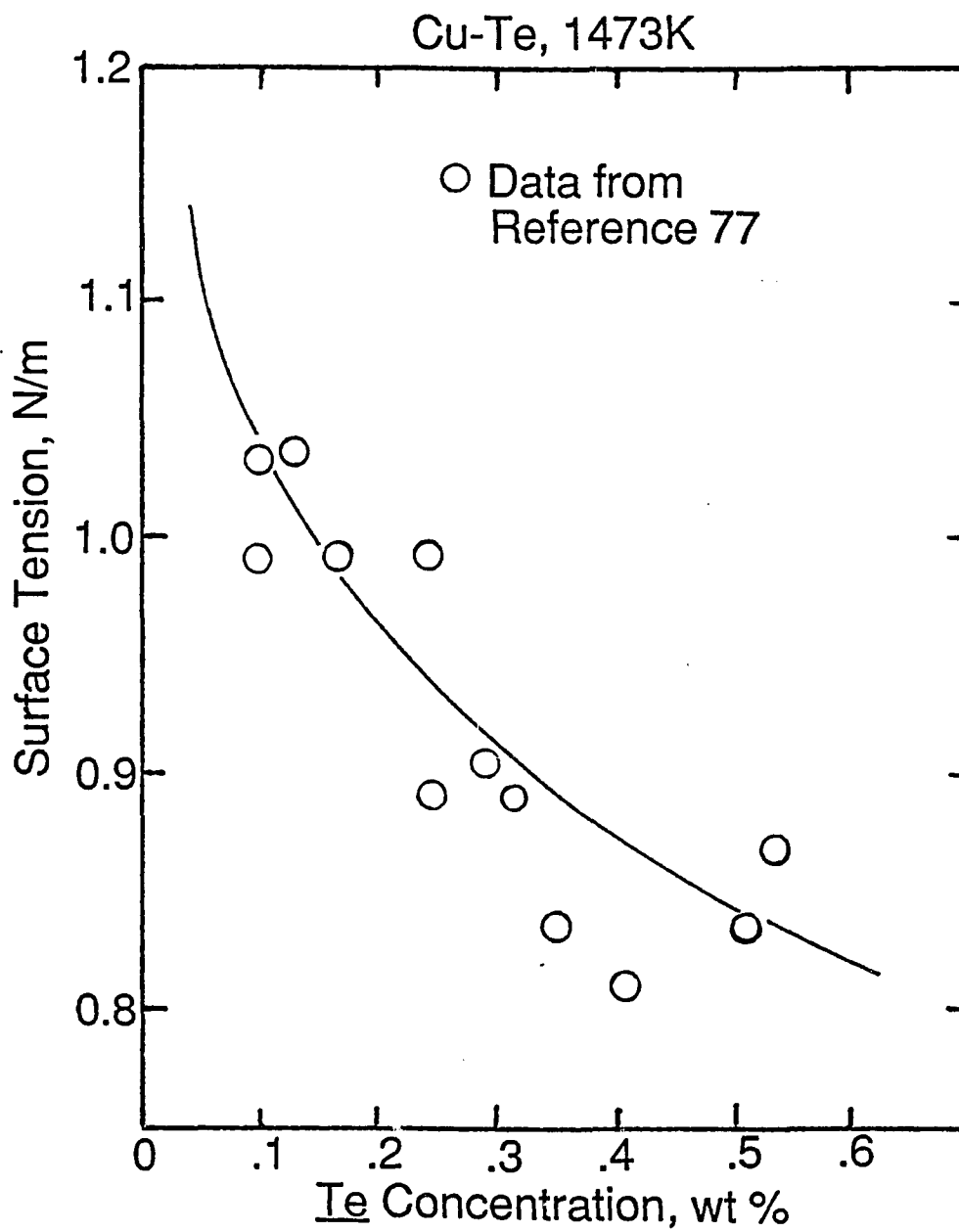


Figure 5.8 Depression of the surface tension of copper by tellurium and comparison with ideal isotherm (5.1) at 1473 K; surface tension data taken from reference 77.

of equation 5.1 and the values used for the various systems are summarized in table 5.4. It can be observed from figures 5.3 to 5.8 that in all cases good correlations are obtained between the predicted and the experimental surface tension values. The good agreements are testimonies of the usefulness of equation 5.1 in predicting the variation of surface tension as a function of composition and temperature.

5.1.2 Estimation of the heat of adsorption

Unlike the heat of solution data for various systems, the heat of adsorption data is not generally available in the literature. From the previous work, it is known that the heat of adsorption depends on diverse factors such as the difference in electronegativity of the ions, the size difference, type of bonding and the degree of attraction between the ions, the structure of the surface layer and other parameters of interaction between the solute and the solvent. Since the temperature dependence of interfacial tension is significantly influenced by ΔH^0 , we have tried to relate the values of ΔH^0 presented in table 5.3 with various properties of the system. It is difficult to draw truly general conclusions from this information, since all of the data available apply to transition metals and group VIB surface active solutes. However, these are the systems for which surface tension driven flow phenomena in welding would be of the greatest practical importance. In particular, we have attempted to seek correlations between the value of ΔH^0 and factors such as size difference, ion-ion attraction and difference in electronegativity between the cation and the anion. In plotting ΔH^0 as a function of the ionic size difference or as a function

Table 5.4: Summary of values used in calculating surface tension of various systems.

System	γ_m N/m	$A \times 10^4$ N/m K	$\Gamma \times 10^8$ Kg mole/m ²
Fe-O	1.943	4.3	2.03
Fe-S	1.943	4.3	1.30
Fe-Se	1.843	4.3	1.28
Cu-O	1.382	2.7	0.53
Cu-S	1.382	2.7	1.14
Cu-Se	1.382	2.7	1.40
Cu-Te	1.282	2.7	1.10

of the ion-ion attraction no coherent trends could be observed. This could possibly be due to the fact that such correlations do not take into account more complex interactions between the ions or the electronic distribution within the ion. However, by plotting $-\Delta H^0$ as a function of the difference in electronegativity of the cation and the anion⁷⁹, as shown in figure 5.9, the results seem to indicate a small measure of correlation with significant scatter in the data.

It has been shown previously for silicate melts⁸⁰ that the heat of formation increases with the difference in electronegativity. From the works of Otsuka and Kozuka⁸¹ it is observed that the heat of solution increases with the heat of formation. Since the heat of adsorption is the sum of the heat of solution and the heats of segregation, it is expected that the heat of adsorption should increase as the difference in electronegativity increases, as observed in figure 5.9. The scatter in the plot indicates the complexity of the systems and emphasizes the fact that factors other than electronegativity are important in determining the heat of adsorption. However, when the difference in electronegativity is greater than about 0.5, the heat of adsorption lies between -1.21×10^5 and -1.72×10^5 KJ/kg mole. These values are consistent with the heats of adsorption derived by Belton for the Fe-S, Cu-S and Ag-O systems which are -1.47×10^5 , -1.67×10^5 and -2.0×10^5 KJ/kg mole, respectively.³² This information is of particular interest for welding systems since the temperature coefficient of surface tension is significantly influenced by the heat of adsorption, and in most systems the difference in electronegativities is greater than 0.5 in Pauling's scale.

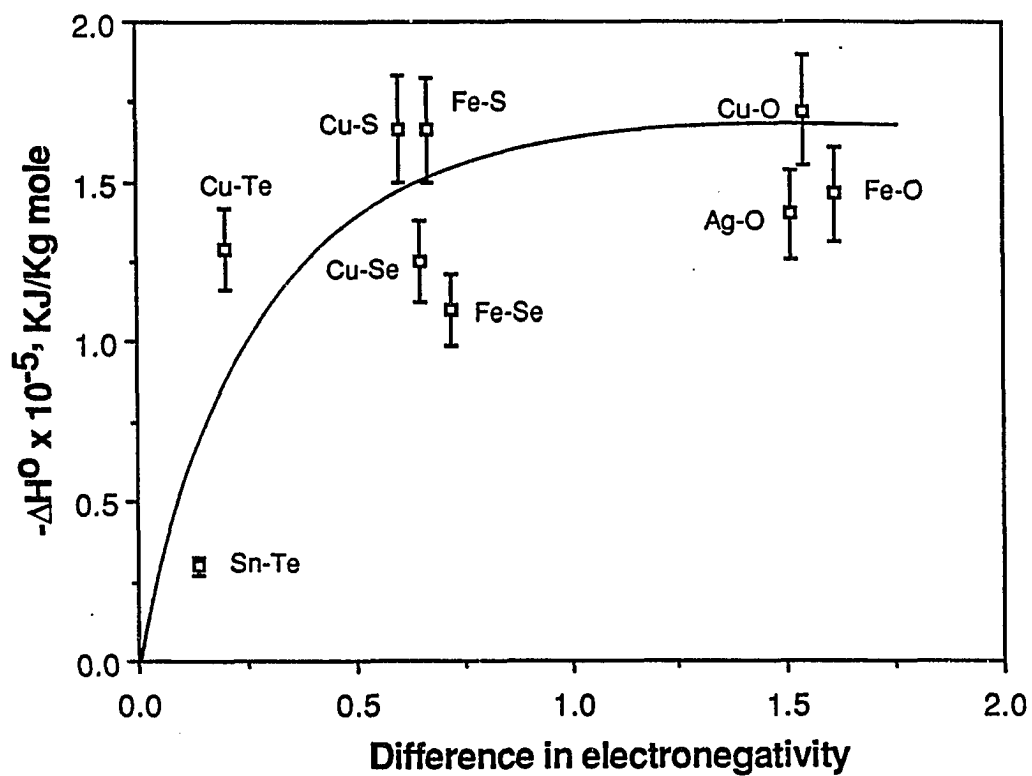


Figure 5.9 Variation of the calculated heat of adsorption for various systems as a function of the difference in electronegativity of the solvent and solute ions.

5.1.3 Application to other systems

Surface tension was predicted for several systems in which very limited experimental work has been done. In all the examples presented the values of k_1 and ΔH^0 are not readily available. Because of this, the two parameters are estimated for each system based on certain simplifying assumptions and these are mentioned separately for each case.

Cr-O

Nogi et al.⁸² determined the surface tension of pure Cr as $\gamma = 2.032 - 5.4 \times 10^{-4} (T - 2133)$ N/m and the surface excess at saturation, Γ_S , to be 5.1×10^{-9} kg mole/m². The heat of adsorption is taken equal to -1.67×10^5 KJ/kg mole from the plot of figure 5.9 with the difference in electronegativity taken as 1.78 in Pauling's scale. The value of k_1 for the Cr-O system is taken to be the same as that for the Fe-O system since Fe and Cr are both transition elements. Based on these data, the interfacial tension of Cr-O system can be expressed as a function of temperature and composition as:

$$\gamma = 2.032 - 5.4 \times 10^{-4} (T - 2133) - RT \times 5.1 \times 10^{-9} \ln \left[1 + .0138 a_O e \left(\frac{1.67 \times 10^8}{RT} \right) \right] \text{ N/m} \quad (5.3)$$

Predictions of interfacial tension from the above equation were checked against the available experimental data⁸² of interfacial tension vs. oxygen concentrations at 1973 K. It is observed from figure 5.10 that good

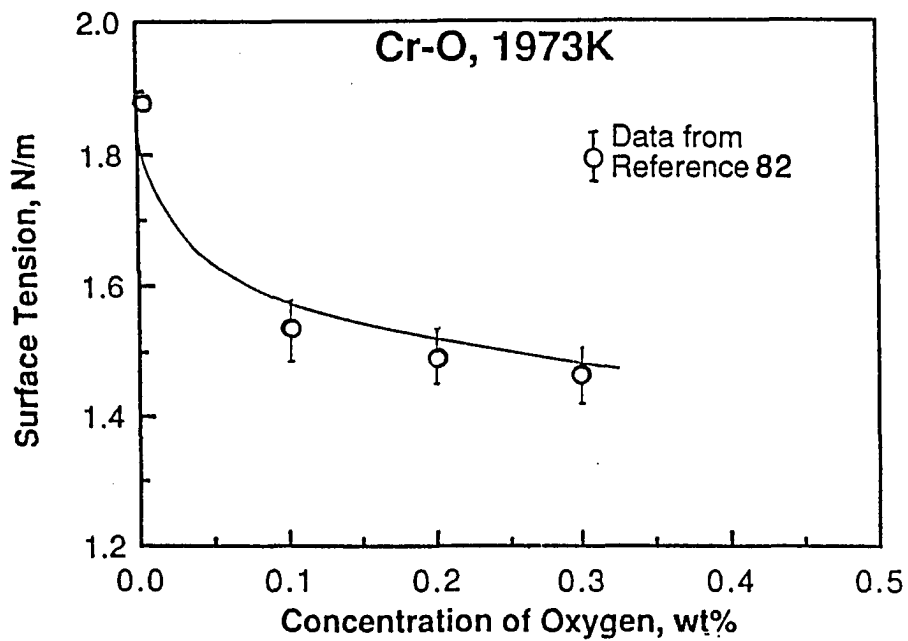


Figure 5.10 Calculated surface tension as a function of oxygen concentration for Cr-O alloys at 1973K and comparison with experimental data of Nogi et al.⁸²

agreement is achieved between the experimental data and the predicted results.

Co-S

Monma and Suto⁸³ have calculated Γ_s to be 1.6×10^{-8} kg mole/m² and Nogi et al.⁸² determined surface tension of pure cobalt as $\gamma = 1.993 - 5.7 \times 10^{-4} (T - 1768)$ N/m. In the Co-S system the difference in electronegativity is equal to 0.62 and using this value, the heat of adsorption is interpolated from figure 5.9 to be -1.55×10^5 KJ/kg mole. The entropy factor k_1 is assumed to be the same as for the Fe-S system since both Co and Fe belong to the same group in the periodic table. Based on these simplifying factors, the surface tension relationship for the Co-S system was calculated as:

$$\gamma = 1.993 - 5.7 \times 10^{-4} (T - 1768) - RT \times 1.6 \times 10^{-8} \ln \left[1 + .00318 a_s e \left(\frac{155 \times 10^6}{RT} \right) \right] \text{ N/m} \quad (5.4)$$

In figure 5.11 the calculated values of surface tension at 1573 K are compared with the experimental data of Monma and Suto⁸³ as a function of sulfur concentration. It is observed that there is fair agreement between the predicted and experimental values.

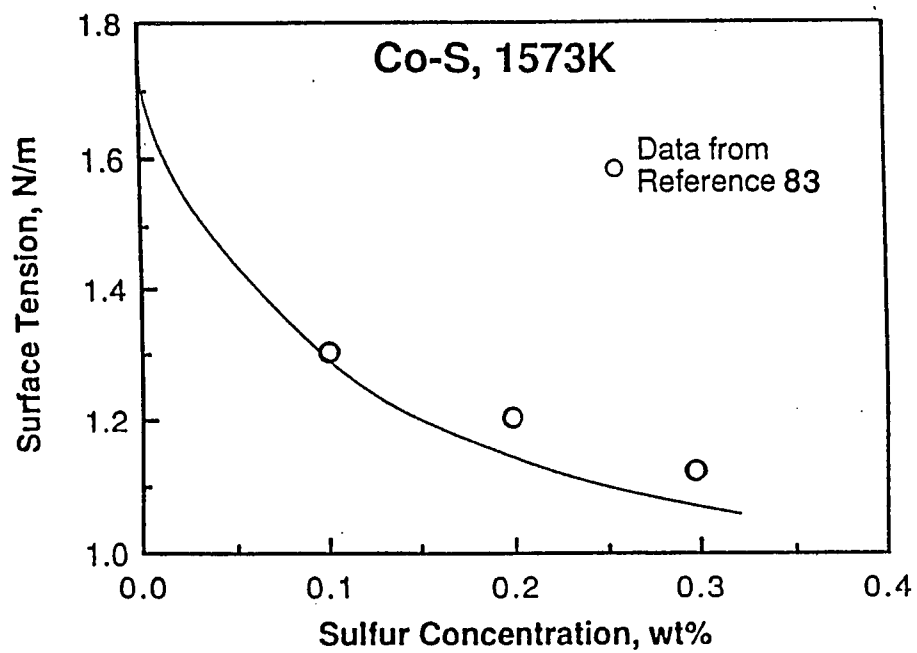


Figure 5.11 Calculated surface tension as a function of sulfur concentration for Co-S alloys at 1573K and comparison with experimental data of Monma and Suto.⁸³

Ni-S

Surface tension of pure nickel has been calculated by Nogi et al.⁸² as $\gamma = 1.845 - 4.3 \times 10^{-4} (T - 1726)$ N/m and Γ_S has been calculated by Monma and Suto^[16] to be 1.6×10^{-8} kg mole/m². From the difference in electronegativity values in this system (0.59) the heat of adsorption was interpolated from figure 5.9 to be -1.47×10^5 KJ/kg mole. The entropy factor was assumed same as for the Fe-S system, since both nickel and iron belong to the same group in the periodic table. Based on these approximations, the surface tension of Ni-S system as a function of temperature and composition is given by:

$$\gamma = 1.845 - 4.3 \times 10^{-4} (T - 1726) - RT \times 1.5 \times 10^{-8} \ln \left[1 + .00318 a_S e^{\left(\frac{1.47 \times 10^8}{RT} \right)} \right] \text{ N/m} \quad (5.5)$$

Figure 5.12 shows a plot of surface tension as a function of weight percent sulfur at 1573 K. Comparison of the predicted curve with the experimental values of Monma and Suto⁸³ show fair agreement.

The study of the three systems mentioned above shows that in the absence of extensive experimental data in these systems it is possible to use equation 5.1 in combination with certain simplifying assumptions to predict the surface tension of these metal-solute systems.

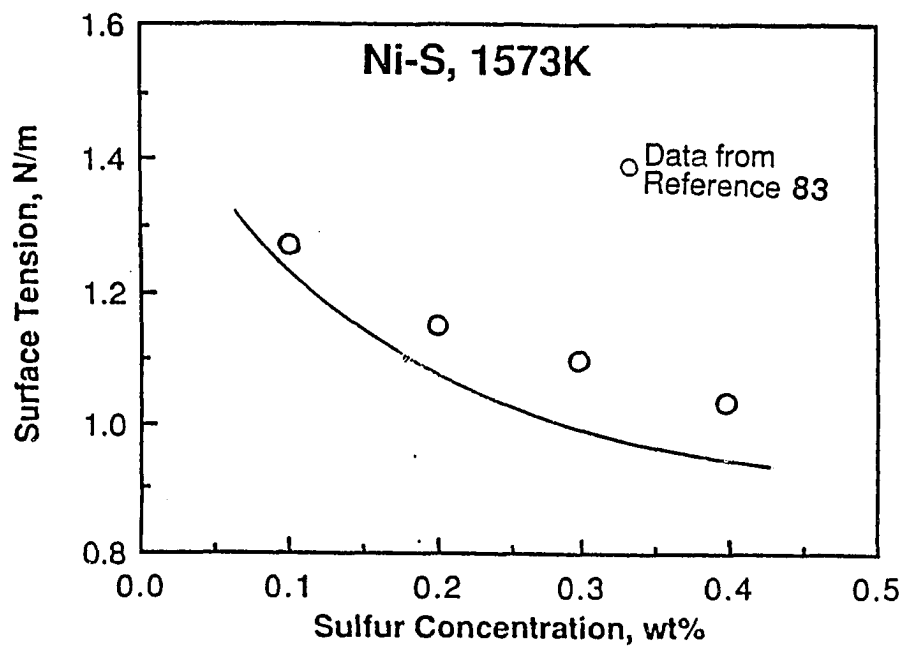


Figure 5.12 Calculated surface tension as a function of sulfur concentration for Ni-S alloys at 1573K and comparison with experimental data of Monma and Suto.⁸³

5.1.4 Temperature coefficient of surface tension

The values of $d\gamma/dT$ can be obtained by differentiating equation 5.1 with respect to T as:

$$\frac{d\gamma}{dT} = -A - R\Gamma_s \ln(1 + Ka_i) - \frac{Ka_i}{1 + Ka_i} \frac{\Gamma_s (\Delta H^\circ - \Delta \bar{H}_i^m)}{T} \quad (5.6)$$

where $\Delta \bar{H}_i^m$ is the partial molar enthalpy of mixing of species i in the solution. From equation 5.6 it is seen that $d\gamma/dT$ is a function of both temperature and composition and is negative for pure metals. In alloys containing surface active solutes $d\gamma/dT$ depends on temperature, T , the equilibrium constant for segregation, K and the activity of the surface active species a_i . For metals with a high surface coverage of the adsorbed species ($Ka_i \gg 1$), equation 5.6 will reduce to:

$$\frac{d\gamma}{dT} = -A - R\Gamma_s \ln(k_1 a_i) + \frac{\Gamma_s \Delta \bar{H}_i^m}{T} \quad (5.7)$$

and this value is usually negative. However, for metals with a low surface coverage of the surface active species ($Ka_i \ll 1$), equation 5.6 will simplify to:

$$\frac{d\gamma}{dT} = -A - Ka_i \Gamma_s \frac{\Delta H^\circ - \Delta \bar{H}_i^m}{T} \quad (5.8)$$

and can be positive for a sufficiently large negative value of ΔH^0 . Under these conditions the Langmuir isotherm represents the effect of adsorbed atoms on the surface tension very well so that interactions between adsorbed atoms need not be considered. Increasing the temperature has the effect of causing adsorbed atoms to desorb from the surface resulting in an increase in the surface tension. Therefore, ΔH^0 , the heat of adsorption of the surface active species at low surface coverages, is the most important parameter for determining the conditions under which the temperature coefficient of surface tension can be positive.

The minimum activity of solute (O or S) required to obtain a positive value of $d\gamma/dT$ at various temperatures can be calculated by equating $d\gamma/dT$ to zero in equation 5.6. For these calculations ΔH_i^m was taken as zero since the activity coefficients were taken to be unity. The calculated critical concentration values corresponding to these activities are presented in figure 5.13 for Fe-O and Fe-S systems. It is observed that as the temperature increases, progressively larger amounts of the solute are required to produce a positive $d\gamma/dT$. In welding processes where the peak temperature is high, relatively high amounts of these surface active solutes will be required to ensure deep penetration of the weld.

Since a steep temperature gradient exists at the surface of a weld pool, calculations were carried out to examine how $d\gamma/dT$ changes with temperature, given a particular amount of solute. Figure 5.14 shows how $d\gamma/dT$ varies with temperature at a given solute content for the Fe-O and Fe-S systems, respectively. In this figure the curves corresponding to higher concentrations of solute may intersect, i.e., a solution containing lower amounts

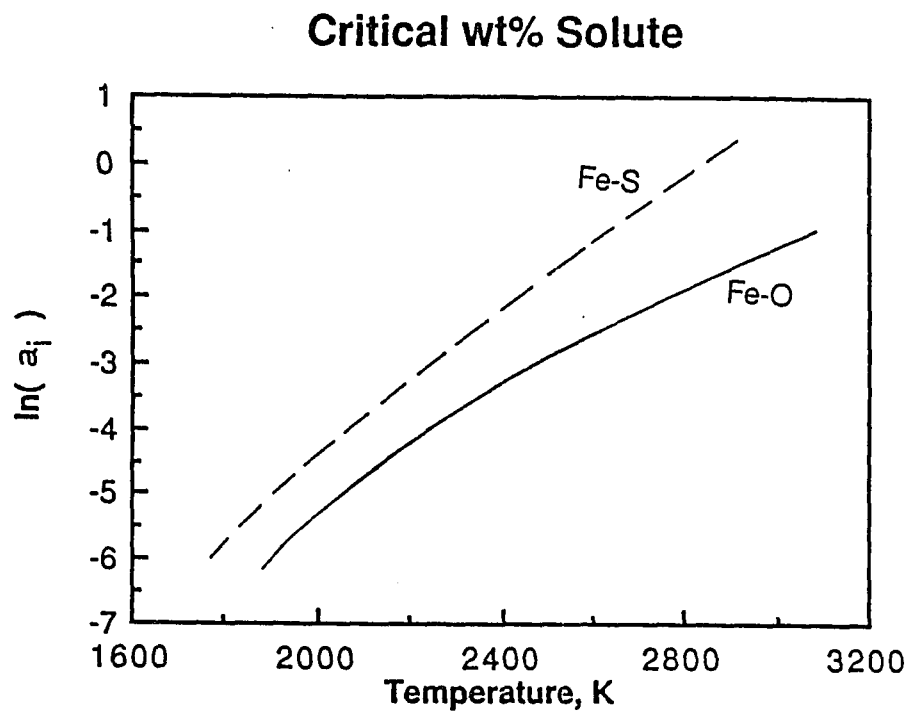


Figure 5.13 The calculated critical solute content in Fe-solute systems as a function of temperature.

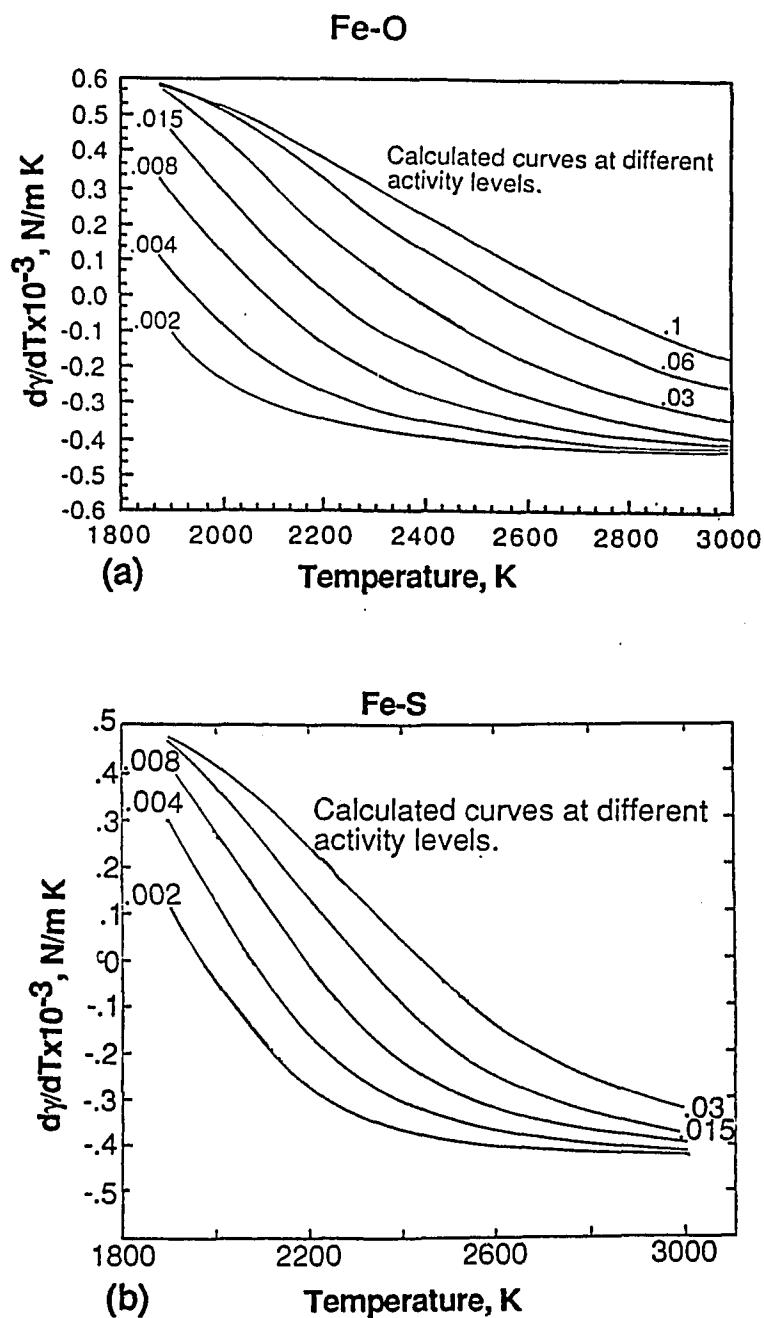


Figure 5.14 Variation of the temperature coefficient of surface tension as a function of temperature for (a) Fe-O and (b) Fe-S systems at various activity levels of the solute.

of solute can have a higher $d\gamma/dT$ than that for a solution having a higher concentration of the solute. Since the values of $d\gamma/dT$ are contributed by the three terms in equation 5.6, the sign and magnitude of $d\gamma/dT$ depends on relative values of these three terms. As the amount of solute in solution increases, the surface tension is lowered because more of the solute segregates to the surface. This means that the second term becomes larger in magnitude with increasing solute content. Also, this term is more important at lower temperatures, since at high temperatures the solute atoms tend to desorb. Thus, at relative low temperatures, if the solute content is high, the large negative value of the second term dominates and $d\gamma/dT$ can be lower for a solution with high solute content as compared to one with a low solute content. However, with increase in temperature, the positive enthalpy term dominates and $d\gamma/dT$ will be higher for a solution with a higher solute content than for one with a lower solute content.

It is interesting to note that at very low oxygen contents (<0.002 wt%), $d\gamma/dT$ will practically always be negative across the weld pool, whereas, at higher oxygen contents, $d\gamma/dT$ can change from a positive value at relatively low temperatures to a negative value at higher temperatures. A similar trend is also observed for the Fe-S system. This implies that in a weld pool containing fairly high oxygen or sulfur contents, $d\gamma/dT$ may go through an inflection point somewhere on the surface of the pool. Under these conditions the fluid flow in weld pools is likely to be much more complicated than a simple recirculation.³⁰

5.2 Weld aspect ratio

Pure iron and iron doped with various surface active elements were irradiated with a CO₂ laser beam operating in the CW mode at 475 W total power. The scanning speed was 5 mm/s and the argon shielding gas flow rate was 6 l/min. The samples were subsequently analyzed using optical microscopy for profile characterization. Figure 5.15 shows the fusion zone geometry for various samples studied and table 5.5 summarizes the composition, depth, width and depth/width values. From figure 5.15 it is observed that the pure iron sample had the least depth and width values whereas those of the others showed substantial increases in both width and depth values. Oxygen, sulfur and tellurium belong to the Group VIB in the periodic table and are known to be surface active. A comparison among the samples doped with these elements show a progressive increase in the aspect ratio (D/W) in the following order: O --- S --- Te. Lupis⁴¹ has related the adsorption coefficient to surface activity and from values compiled by him, surface activity increases as we consider elements in higher period in the Group VIB elements. Also, these elements create a positive temperature coefficient of surface tension when added to iron. Table 5.6 lists all the available values for surface tension (γ), temperature coefficient of surface tension ($d\gamma/dT$) and absorptivity (ρ) values for various pure elements and binary systems. It can be seen that the addition of any of these elements drastically reduces the surface tension of pure iron. According to Friedman's model,⁴³ these values indicate that the depth of penetration should increase on addition of these elements. These results also substantiate the model proposed by

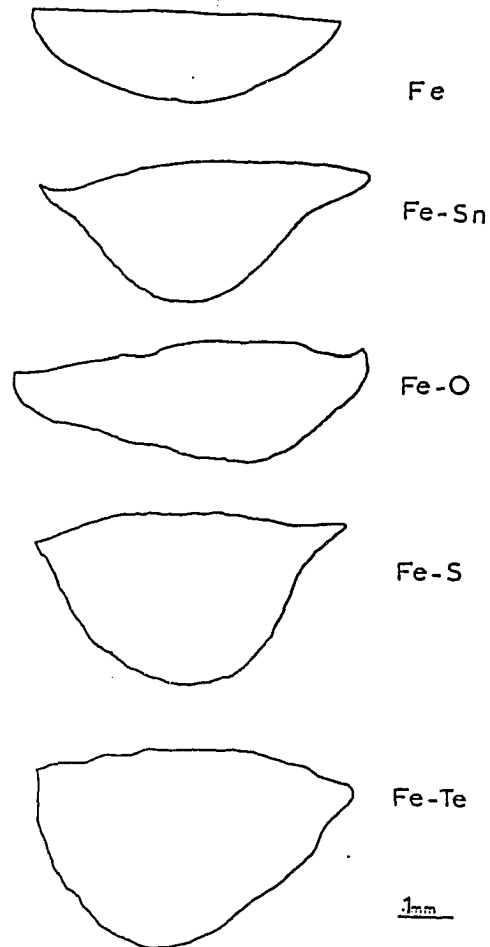


Figure 5.15 Weld profile of various samples. Scanning speed: 5 mm/s, Ar gas flow rate: 6 l/min.

Table 5.5 Summary of the composition, depth(D), width(W) and depth/width (D/W) ratio for various samples. Scanning speed: 5 mm/s, gas flow rate: 6 l/min. Initial sample surface polished to 400 grit.

System	Wt % solute	D, cm	W, cm	D/W	(D/W) _{average}
Fe		0.0169	0.0598	0.283	
Fe		0.0188	0.0603	0.312	0.298
Fe-O	.02	0.0217	0.0648	0.335	
Fe-O	.02	0.0198	0.0619	0.320	0.328
Fe-S	.02	0.0323	0.0582	0.555	
Fe-S	.02	0.0286	0.0603	0.474	
Fe-S	.02	0.0257	0.0587	0.438	0.515
Fe-Te	.01	0.0368	0.0601	0.613	
Fe-Te	.01	0.0381	0.0603	0.632	
Fe-Te	.01	0.0333	0.0587	0.567	0.604
Fe-Sn	.3	0.0262	0.0500	0.524	
Fe-Sn	.3	0.0269	0.0635	0.424	0.474

Table 5.6 Summary of the surface tension, temperature coefficient of surface tension and absorptivity values for various samples.

System	Temperature K	γ N/m	$d\gamma/dT$ mN/m K	Absorptivity
Fe	1823	1.94	-0.43	.13
Fe-Sn	1823	1.5	-.4	~ .13
Fe-S	1823	1.62	+.25	~ .17
Fe-O	1823	1.5	+.48	~ .2
Fe-Te	1873	1.12	+(?)	~ .2

Heiple and Roper,^{7,10} since a positive dy/dT is created on addition of any of these Group VIB elements. Two other factors that normally are not frequently taken into account when discussing penetration behavior are the viscosity and absorptivity effects. Experiments of Pollard⁴⁷ showed that addition of silicon to type 304 stainless steel increased penetration which was attributed to the reduction in viscosity of the molten steel. The reduction in viscosity leads to higher flow velocities and hence bigger pools. The other factor, namely absorptivity, which can influence the depth of penetration is dependent on various factors such as temperature, surface condition, presence of plasma and its composition and the type of the shielding gas.¹⁷ The absorptivity of a substance can be related to its resistivity and the wavelength of the irradiating source, and is related by Bramson's equation.⁸⁴ From table 5.6 we note that the absorptivity of the pure metal is the least and increases when alloyed. Because of the minute quantities of dopant additions to pure iron it would be safe to assume that viscosity and absorptivity effects will be much less important compared to surface tension effects.

It is interesting to note that for the sample doped with tin, there is a substantial increase in the D/W ratio. Interfacial tension studies on Fe-Sn alloys by Dyson⁸⁵ indicated that tin is slightly surface active in iron. The drastic reduction in the surface tension of iron in the presence of tin is attributed to the very low surface tension of pure tin (370 mN/m at 1823 K).⁸⁶

Based on these observations it is safe to say that both the lowering of surface tension and the positive temperature coefficient of surface tension can contribute to increased depth of penetration during welding. The importance of the absolute value of interfacial tension stems from the fact that the depression

of the liquid pool surface due to the arc pressure is resisted by the force due to interfacial tension. It is thought that the lowering of interfacial tension of iron due to the presence of argon plasma during arc welding would be useful in explaining the depression of the weld pool surface and the resulting weld penetration.

5.3 Low pressure plasma-liquid metal interaction

5.3.1 Plasma characterization

Figure 5.16 shows a typical plot of intensity in arbitrary units as a function of wavelength for the argon plasma utilized in this work. It is observed from the wavelengths that both ionized and excited neutral argon atoms are present in the plasma. The plasma produced during the arc and laser welding processes is known to contain both ionized and excited neutral atoms of the inert shielding gas.

The intensity of the various peaks in the plasma could be controlled by varying the input power (plate current) and the chamber pressure. The increase in the intensity of the three major argon peaks with the increase in the power (plate current) is shown in figure 5.17. In figure 5.18 the influence of the chamber pressure on the intensity is observed in the pressure range 0.20 to 0.45 torr. The intensity of emission is a function of both the kinetic energy of the colliding molecules and the total number of collisions. In this pressure range, the population density is fairly high and the kinetic energy of the molecules increases as the pressure is reduced. At pressures lower than a critical value

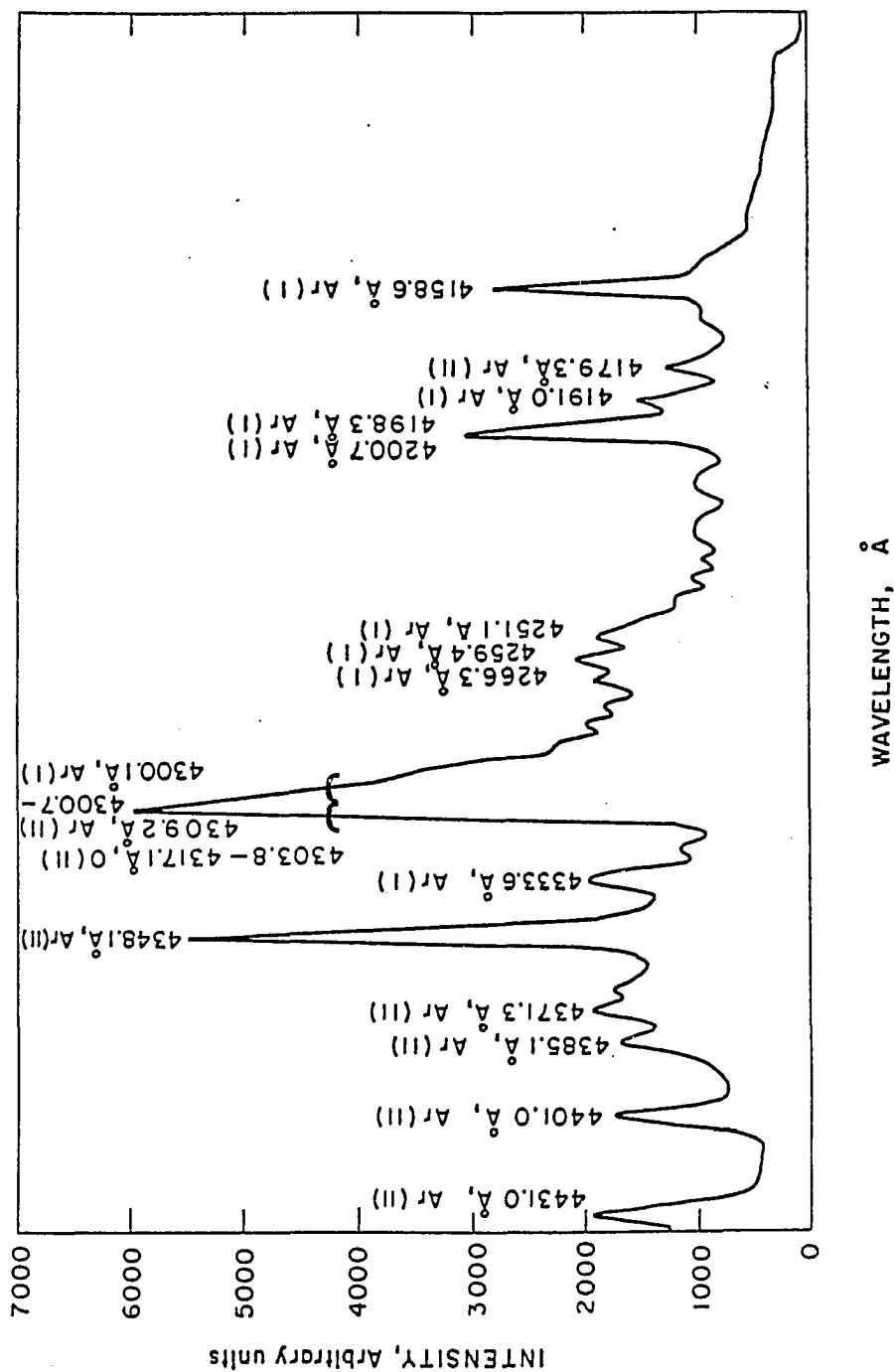


Figure 5.16 Intensity of emission of argon plasma vs wavelength at a chamber pressure of 450 $\mu\text{m Hg}$ and plate current at 1.65 amps.

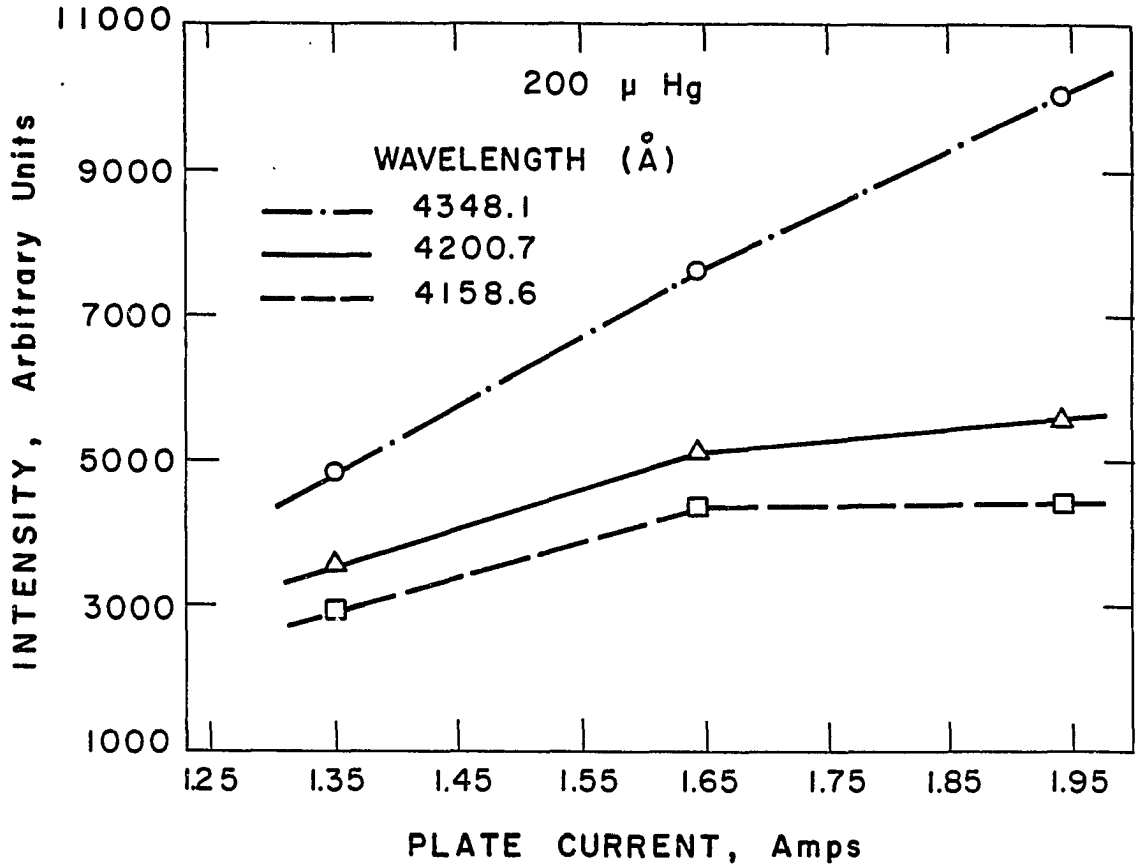


Figure 5.17 Intensity of emission of argon plasma vs power (plate current) for various wavelengths at a chamber pressure of 200 μ m Hg.

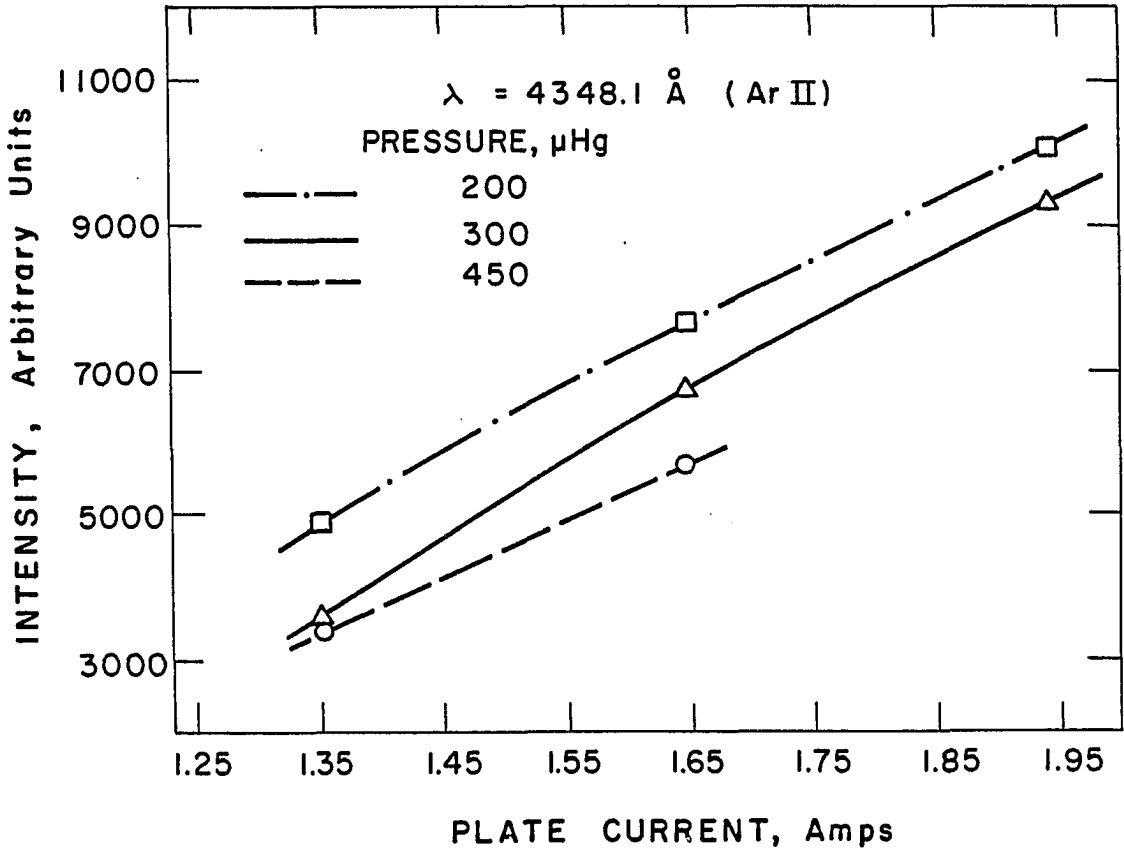


Figure 5.18 Intensity of emission of argon plasma at a particular wavelength vs power (plate current) for various chamber pressures.

(about 0.2 torr) the reduction in the population density was found to lower the intensity of plasma emission.

5.3.2 Electron temperature estimation

The electron temperature of the plasma, T_e , was measured by using equation (4.40) in which $\ln \frac{I'_{qp}}{g_q A'_{qp} v_{qp}}$ is plotted as a function of E_q . This is shown in figure 5.19 for the Fe-O(low) system in which the electron temperature was determined from the slope of the line. Similar calculations were carried out for the other systems and figure 5.20 schematically illustrates the determined values. The electron temperature of about 10^4 K is of the same order of magnitude as found in laser induced plasmas.

Because of the uncertainties inherent in the various parameters used for electron temperature estimation, a statistical analysis was carried out to estimate the accuracy of the data. The 80% confidence interval for the temperature corresponds to a temperature of 9600 ± 2400 K. The errors in electron temperature reported were calculated from the uncertainties in the slopes of the plots used to determine temperature values such as the one presented in figure 5.19. It is to be noted that the slope of the plot in figure 5.19 is a nonlinear function of electron temperature. Although statistically the slope has equal uncertainties in both upper and lower limits, this does not translate into equal errors in the upper and lower limits of temperature values because of the hyperbolic relation between the slope of the line and the temperature.

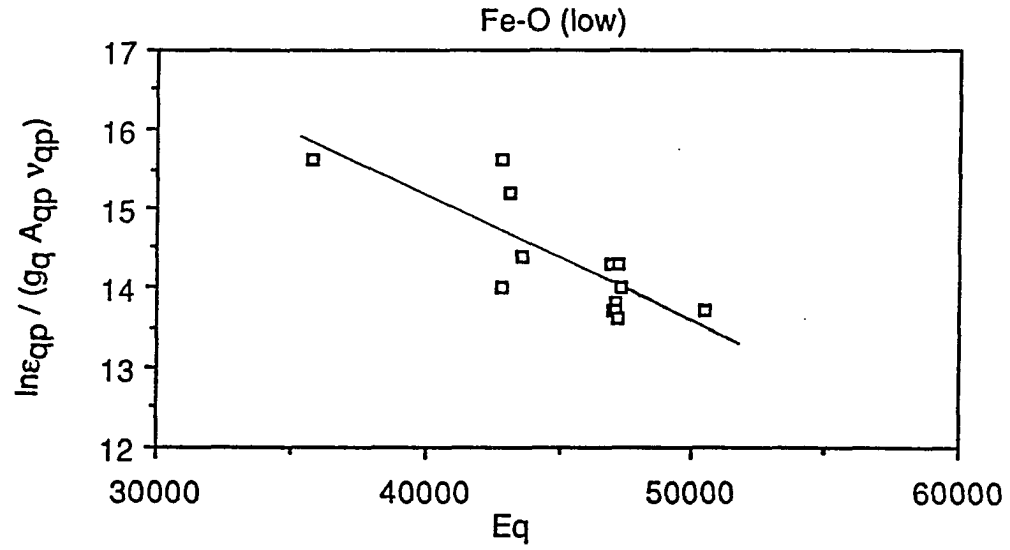


Figure 5.19 Illustration of the principle of determining the electron temperature from relative intensities of spectral lines with known relative transition probability (equation 4.40).

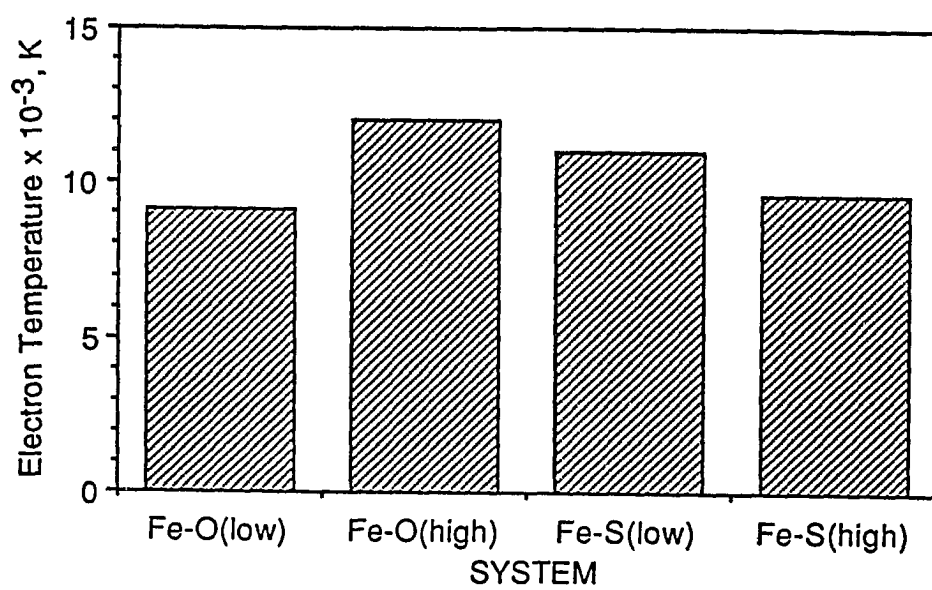


Figure 5.20 Electron temperatures calculated for various systems.

5.4 Interfacial tension measurements

Interfacial tension of pure copper and iron in argon were measured in the presence and absence of plasma. The chamber pressure selected for the experiments was such that a fairly intense plasma could be obtained. The intensity of the plasma as a function of chamber pressure was determined prior to conducting the experiments. In the absence of plasma the measured values of interfacial tension, γ , between liquid copper and argon are represented by

$$\gamma = 1.39 - 3.9 \times 10^{-4} (T - 1356) \quad \text{N/m} \quad (5.9)$$

in the temperature range 1300 to 1573 K. The data are presented in figure 5.21. The values compare reasonably well with the recent measurements of Kasama et al.⁸⁷ and the agreement indicates the appropriateness of the procedures used for the determinations. When argon plasma was present, the interfacial tension in the copper system was significantly lower than that in the absence of plasma as can be observed from the data in figure 5.21. A similar effect was also observed when experiments were conducted with pure iron droplets. The interfacial tension data with and without the presence of the argon plasma are presented in figure 5.22. Comparison of the measured values of the interfacial tension of iron in the absence of plasma with the corresponding results of Kasama et al.³³ show a small discrepancy between the two sets of values. Kasama et al.³³ measured the interfacial tension of pure iron by the levitation technique. They indicated that since the problem of container contamination is eliminated in the levitation technique, the interfacial tension values determined by this technique represent values for extraordinarily

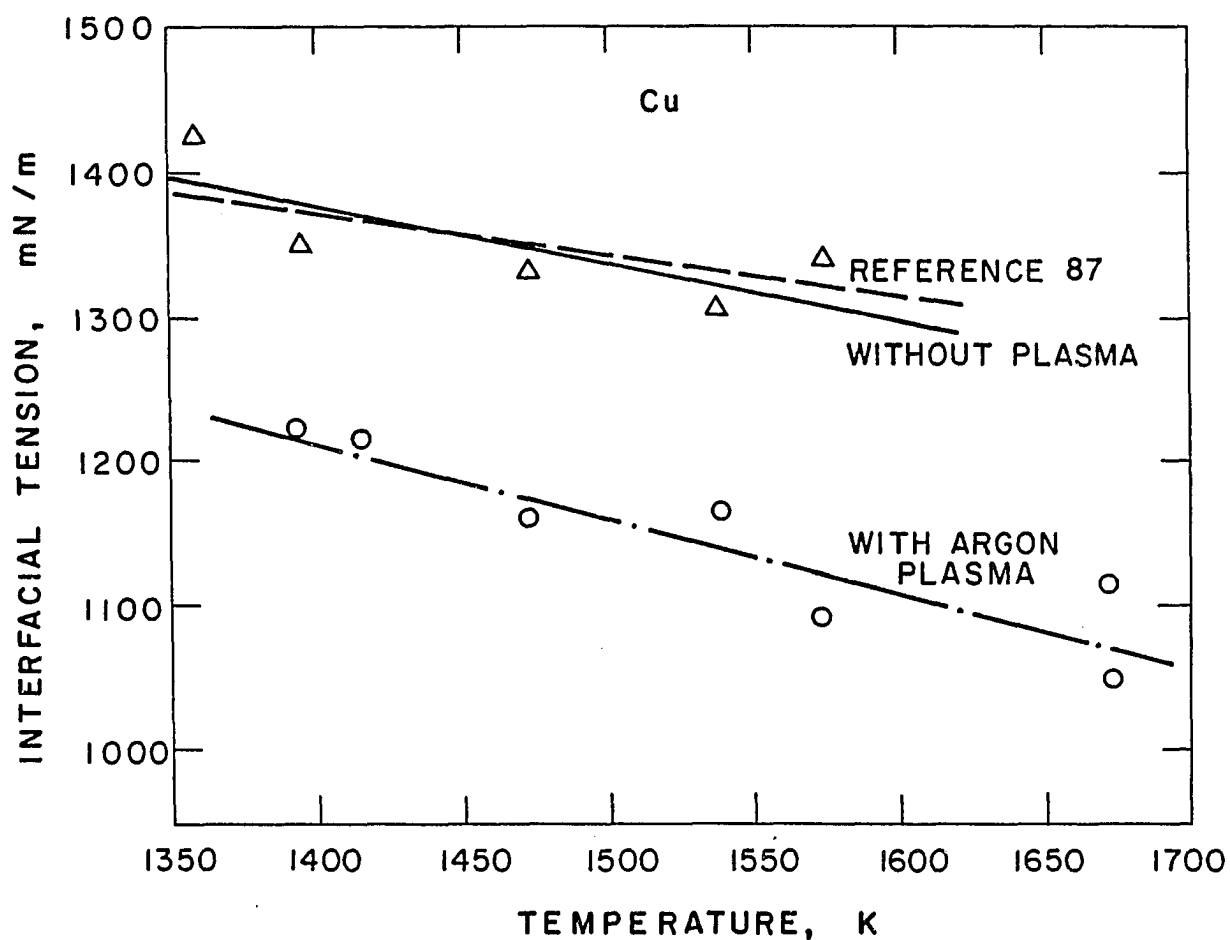


Figure 5.21 Interfacial tension between liquid copper and argon with and without the presence of plasma. Plate current and chamber pressure were in the ranges of 1.4 to 1.6 amps and 170 to 200 $\mu\text{m Hg}$, respectively.

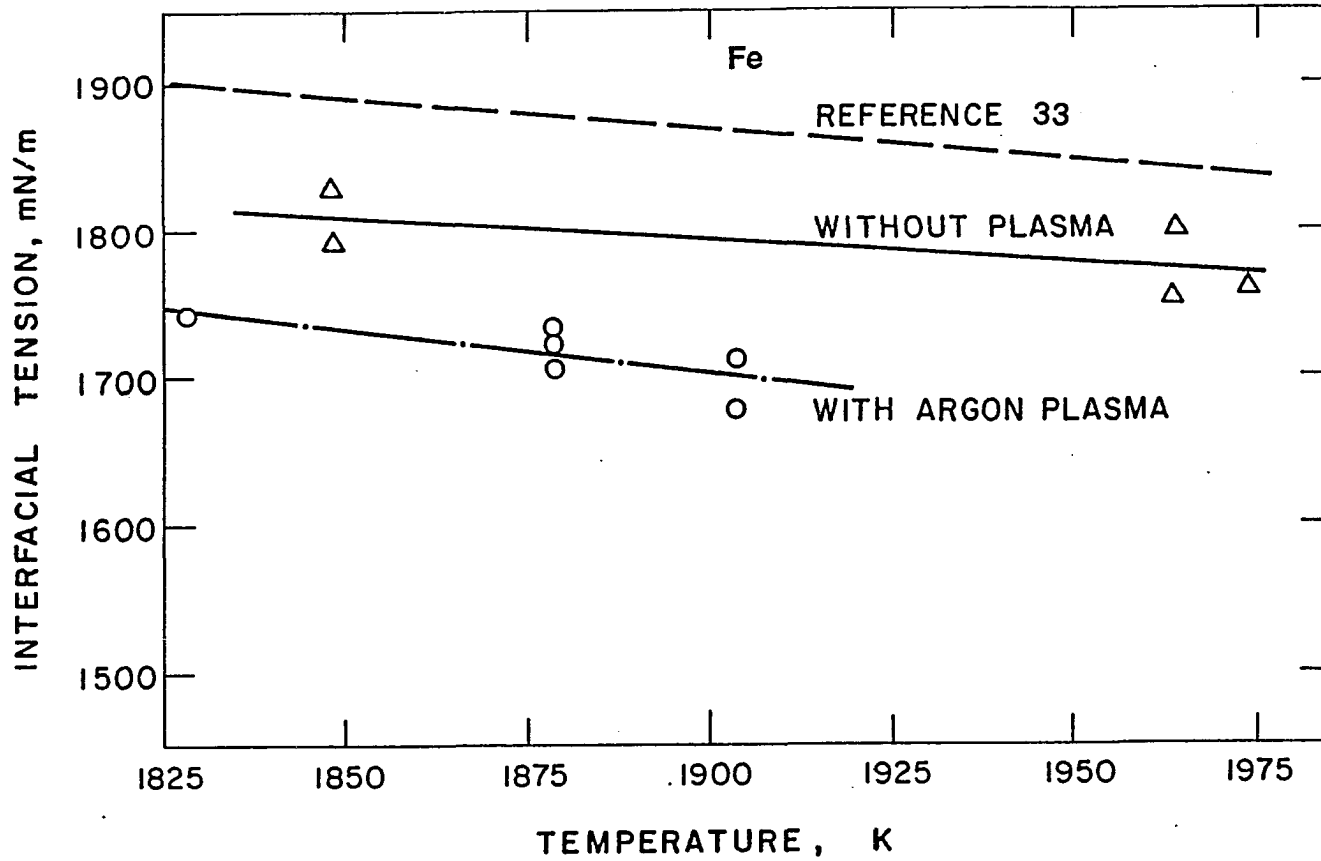


Figure 5.22 Interfacial tension between liquid iron and argon with and without the presence of plasma. Plate current and chamber pressure were in the ranges of 1.2 to 1.4 amps and 150 to 200 $\mu\text{m Hg}$, respectively.

clean metal surfaces and the values are normally higher than the values determined by other techniques. The lowering of interfacial tension of both iron and copper systems is consistent with a plasma induced surface segregation of surface active elements as will be explained in the subsequent discussions.

In the absence of plasma environment the interfacial tension, γ , in Fe-O system can be expressed by the following equation (from equation 4.32):

$$\gamma = 1.943 - 4.3 \times 10^{-4}(T - 1809) - RT \Gamma_s \ln \left\{ 1 + k_1 a_O e^{(-\Delta H^0/RT)} \right\} \quad \text{N/m} \quad (5.10)$$

where Γ_s is the surface excess at saturation which has a value of 2.03×10^{-8} kg mole/m². The symbols k_1 and ΔH^0 represent entropy and enthalpy factors in the oxygen adsorption reaction and their values are 0.0138 and -1.463×10^5 KJ/kg mole, respectively. The gas constant, R, has a value of 8.314×10^3 J/K kg mole. The interfacial tension of iron in argon plasma was found to be 1.745 N/m at 1825 K and 1.7 N/m at 1905 K. On the basis of equation 5.10 it can be shown that the reduction in the interfacial tension of iron due to plasma is equivalent to the depression in the interfacial tension caused by bulk oxygen concentrations of 13 and 23 ppm of oxygen dissolved in iron at 1825 K and 1905 K, respectively, in the absence of plasma. Similarly, for the copper system, the depression in surface tension caused by the argon plasma is similar in effect to that produced by 41 ppm oxygen at 1473 K and 94 ppm oxygen at 1673 K. Thus, in both copper and iron systems, the depression in surface tension due to plasma is equivalent to that caused by the surface segregation of oxygen that results from low concentrations of oxygen in metal in the absence of plasma. It will be argued in the following paragraphs that the presence of low pressure

argon plasma is conducive to enhanced surface segregation of oxygen; i.e., when plasma is present, a given depression in interfacial tension can be attained at a much lower oxygen concentration than normally required in the absence of plasma.

Since the ionization potentials of both copper and iron are almost half that of argon,⁷⁹ ionized metal vapors are present in close proximity of the metal droplets. The concentrations of cations in the plasma near the interface is high because of the high concentration of the metal vapor. The cations in turn facilitate the adsorption of anions on the surface of the liquid metal drop. Because of this effect, the amount of bulk oxygen concentration necessary to lower the interfacial tension of metals in argon plasma would be much lower than the bulk oxygen concentration necessary in the absence of plasma environment.

It is observed from figure 5.21 and 5.22 that the reduction in interfacial tension due to the presence of the argon plasma was more pronounced in the copper system than in the iron system. In view of the limited amount of oxygen available ($O_2 < 2$ ppm, $H_2O < 3$ ppm) in the ultra high purity argon and from the solid surface present in the experimental system, the lowering of interfacial tension is related to the surface excess of oxygen at a given oxygen concentration. Lupis⁴¹ related the tendency of surface segregation to an adsorption coefficient at infinite dilution of the surface active species. His data for the adsorption coefficient at infinite dilution for oxygen are 2500 for Fe-O system and 10,000 for the Cu-O system. Thus, qualitatively, the larger decrease in the interfacial tension of the Cu-O system than the Fe-O system is consistent

with the greater propensity of oxygen to segregate at the surface of the Cu-O system.

To investigate further the effect that oxygen present in the gas is responsible for the lowering of surface tension, experiments were conducted to measure the interfacial tension of liquid copper in the presence of a hydrogen plasma. The chamber pressure was maintained between 200 to 250 μHg . Figure 5.23 shows the surface tension of liquid copper measured as a function of temperature. For the purpose of comparison the data of Keene⁹⁴ and Kasama et al.⁸⁷ are also plotted. It is observed that unlike the argon plasma, the hydrogen plasma has little or no effect in suppressing the surface tension. This is to be expected since hydrogen will act as a scavenger for any oxygen that could contaminate the chamber.

Figure 5.24 shows the results of similar experiments using an Ar-7% H₂ plasma and measuring the interfacial tension over an extended temperature regime. The reason for conducting experiments with Ar-7% H₂ was two-fold. Firstly, diluted hydrogen will not have the cooling effect of pure hydrogen on the plasma which might affect the plasma formation. Secondly, the recombination effect of the metallic species in argon might be vastly different from the recombination effect in pure hydrogen which could disturb the segregation process of the surface active species. As shown in figure 5.24, the presence or absence of the plasma has little or no effect on the surface tension of pure copper.

This leads us to the question of what would occur if a Cu-O alloy were subjected to the plasma. In the absence of a plasma, the oxygen present in the alloy would exert its surface activity and reduce the surface tension.

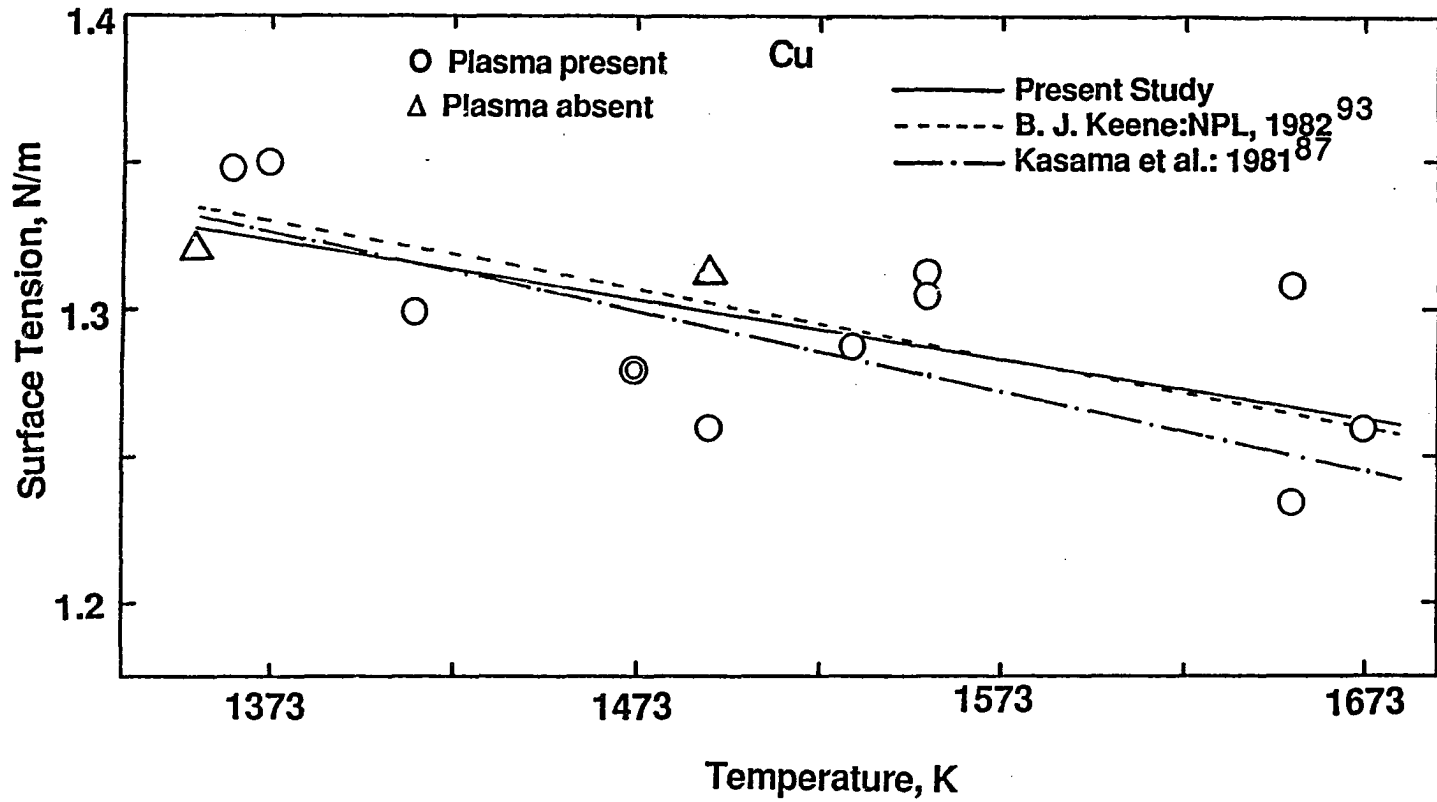


Figure 5.23 Interfacial tension between liquid copper and hydrogen with and without the presence of plasma. Plate current and chamber pressure were in the ranges of 1.5 to 1.7 amps and 200 to 300 μm Hg, respectively.

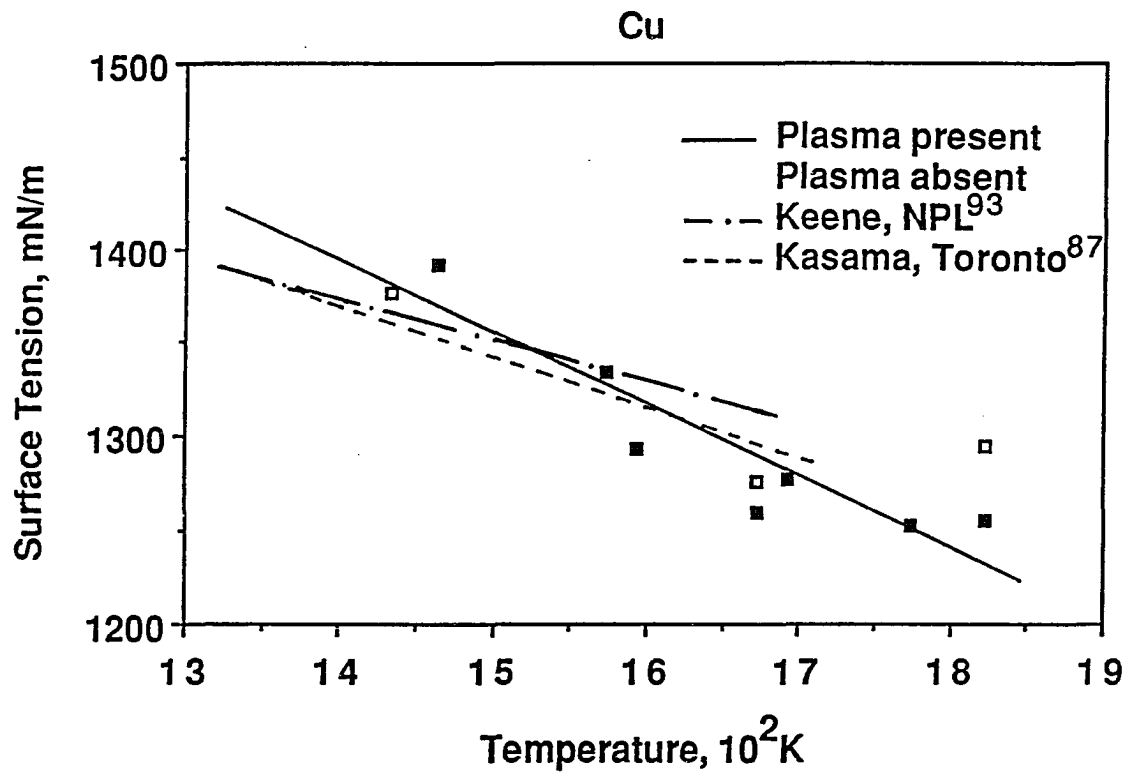


Figure 5.24 Interfacial tension between liquid copper and Ar-7% H₂ with and without the presence of plasma. Plate current and chamber pressure were in the ranges of 1.0 to 1.6 amps and 450 to 1200 μ m Hg, respectively.

Experiments were conducted using pure copper doped with 0.05 wt% oxygen to measure the interfacial tension in the presence and absence of an argon plasma at 1473 K. The results are presented in figure 5.25 with error bars corresponding to one standard deviation about the mean value. Before a thorough discussion of these results, let us conjecture as to what would occur in the γ values of such an alloy when subjected to argon plasma. In section 5.4 it was proposed that a plasma induced enhanced surface segregation of oxygen would lead to a reduction in the surface tension of pure copper. Thus, when a sample doped with oxygen is subjected to a plasma environment, the surface tension should be reduced above and beyond that would normally be accomplished by the oxygen segregating to the surface. Now, for a given amount of reduction in γ , the amount of oxygen that would be required would depend on the initial composition of the alloy. Referring to figure 5.5, it is obvious that for an initially "pure" copper sample, very slight amounts of oxygen (of the order of 10^1 to 10^2 ppm) are required to cause a significant reduction in γ . However, as the oxygen content of the initial alloy is increased, the surface tends to get saturated with oxygen, and much larger (of the order of 10^3 ppm) amounts of oxygen would be required to cause the same net reduction. In the alloy used in the present study, the oxygen content was about 0.05 wt% which corresponds to an oxygen activity of 4×10^{-4} in the alloy at 1473 K. At this composition, the surface tension with respect to pure copper has been reduced by about 26% and so any slight decrease in γ due to increase in surface segregation induced by the plasma would not be very noticeable. From the results plotted in figure 5.25, the mean of the γ values under the two conditions are different, with the mean value of γ in the absence of plasma being slightly

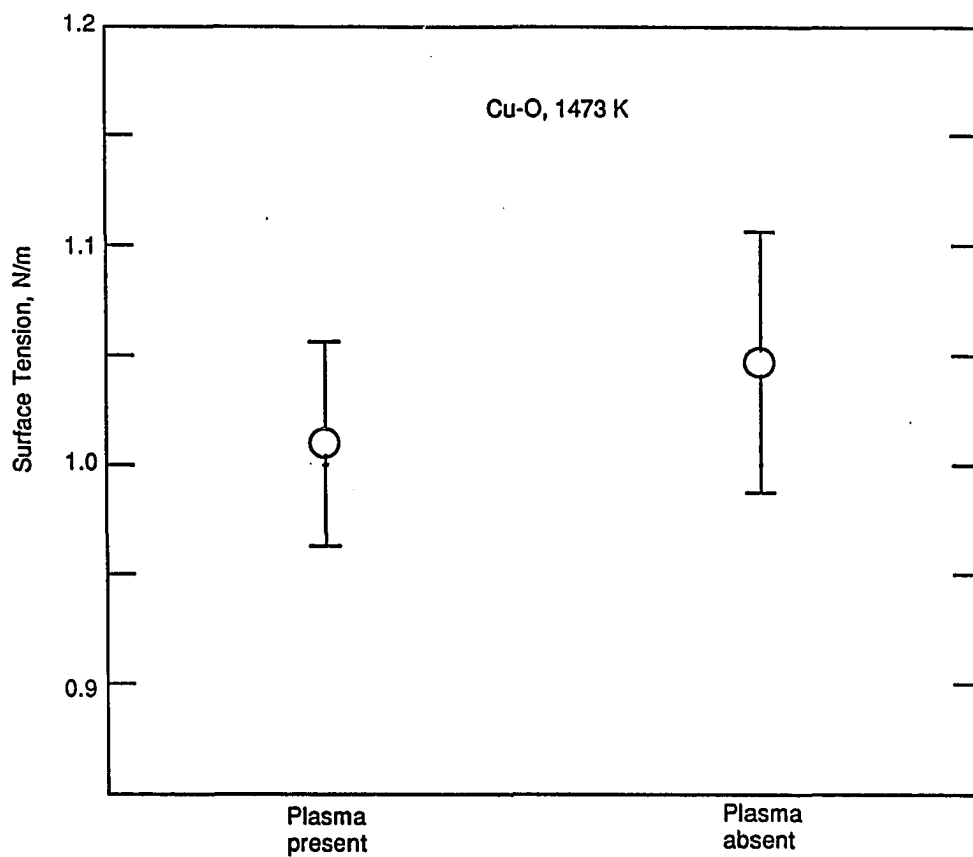


Figure 5.25 Interfacial tension between Cu-0.04 wt% O alloy and argon with and without the presence of plasma at 1473 K. Plate current and chamber pressure were in the range of 1.2 amps and 240 to 1200 $\mu\text{m Hg}$, respectively.

higher. However, from the observed data it is difficult to truly draw a statistical difference between the two sets of values.

To understand the role of plasma intensity on the surface tension of pure copper, experiments were conducted at a constant pressure level at 1473 K. The plasma intensity was adjusted by changing the input power (plate current). The interfacial tension values are presented as a function of plasma intensity in figure 5.26. A statistical analysis of the data gave a mean value of 1170 mN/m with a standard deviation of 46 mN/m. The two dotted lines on this figure indicate the precision of these determinations (± 50 mN/m) and cover most of the measured values. It appears that the interfacial tension is not significantly influenced by the intensity of the plasma.

The interfacial tensions of iron and copper in the presence of argon plasma were lower than the corresponding values in the absence of plasma. However, the temperature coefficient of surface tension did not change significantly when the plasma was present. In the welding literature the importance of both the absolute value of interfacial tension,⁴³ γ , and the temperature coefficient,^{6,10} $d\gamma/dT$, in influencing the weld penetration is well documented.^{45,88} The value of $d\gamma/dT$ is related to the intensity and direction of the recirculating flow of molten metal in the weld pool and affects weld penetration through the heat transfer process. The importance of the absolute value of interfacial tension stems from the fact that the depression of the liquid pool surface due to the arc pressure is resisted by the force due to interfacial tension. It is thought that the lowering of interfacial tension of iron due to the presence of argon plasma during arc welding would be useful in explaining the depression of the weld pool surface and the resulting weld penetration. To

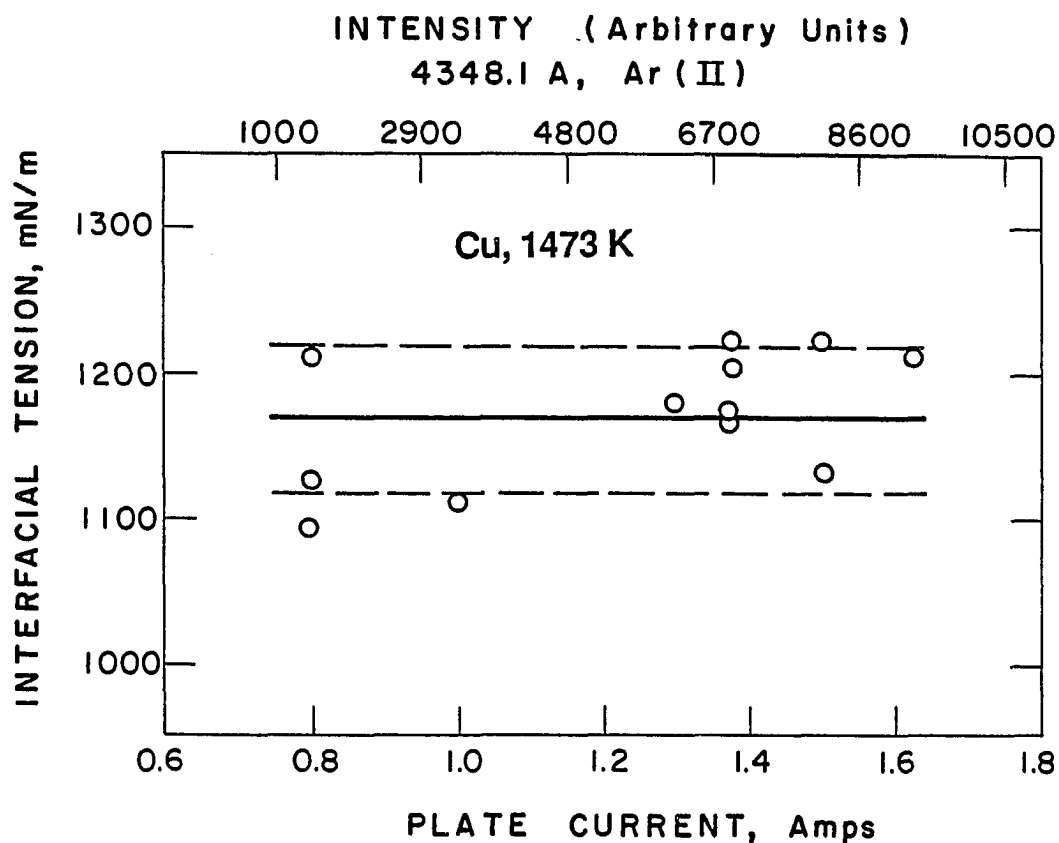


Figure 5.26 Interfacial tension between copper and argon plasma at 1473 K as a function of intensity of emission of plasma (plate current) at $200 \pm 10 \mu\text{m Hg}$.

further examine how the nature of the interface is modified in the presence of plasma, certain critical experiments were designed and conducted. These are discussed in the following pages.

5.5 Role of plasma on metal vaporization rates

The vaporization rate measurements of isothermal droplets were carried out in the set up described earlier in section 3.2. The temperature of the droplet was controlled by adjusting the position of the droplet with respect to the induction coil. A two color pyrometer was used for the temperature measurement. The chamber pressure was maintained at 80 N/m² or lower. The chamber pressures were selected to ensure a stable and intense plasma. The ultra high purity argon used for the experiments had a maximum impurity content of 10 ppm with no more than 2 ppm oxygen and 3 ppm water vapor. The gas was cleaned to remove oxygen by passing it through a bed of titanium chips at 1073 K. High purity iron and copper (maximum 10 ppm impurities) supplied by Aesar were used in the experiments. The samples weighing between 0.5 to 1.0 g were cleaned, degreased in acetone and were placed on an alumina substrate inside a vycor reaction tube. The rate of vaporization was determined from the weight change of the sample and the exposure time. In samples containing sulfur, approximately half of the initial sulfur content was lost during the experiments. However, the error in the determination of the vaporization rate due to the loss of sulfur was insignificant since the amount of sulfur in the sample was small. In some runs, a graphite susceptor was used to shield the sample from the eddy currents induced by the RF field. This ensured

that the sample surface was not disturbed, unlike the experiments where a susceptor was not used.

Sessile drop experiments

Figure 5.27 depicts the results of isothermal vaporization experiments. In this figure, the vaporization rate of copper is plotted for Cu, Cu-O and Cu-S systems, both in the presence and absence of a graphite susceptor. It is observed that for each of the three copper systems, the vaporization rate of copper is enhanced by the presence of a surface active element such as oxygen or sulfur, both in the presence and the absence of a graphite susceptor. Furthermore, the presence of a susceptor leads to a lowering of vaporization rates in all cases. Several interesting questions arise from the perusal of the data: how close are the experimental vaporization fluxes to the theoretical promise of the kinetic theory of gases (Langmuir equation)? what role, if any, does the susceptor play, especially in the vaporization of ultra high purity copper? and most important and puzzling, why do the rates increase when sulfur or oxygen is present, even at a low concentration?

5.5.1 Experimental and theoretical fluxes

The intrinsic vaporization flux from the surface of pure metal drops

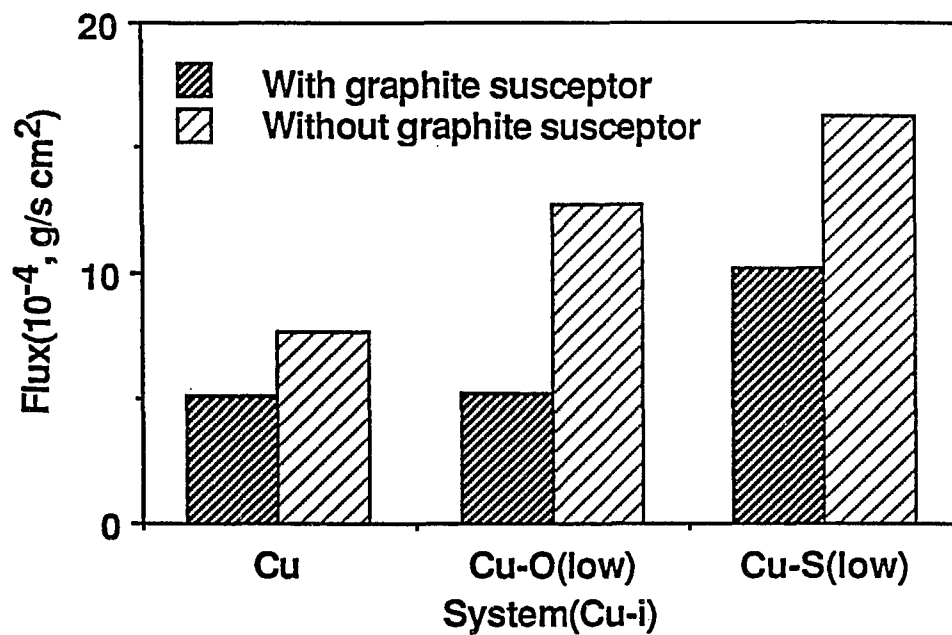


Figure 5.27 Vaporization flux at 1873 K both in the presence and absence of a graphite susceptor for copper-solute systems. The solute concentration was 0.1 wt% and the chamber pressure was maintained at 80 N/m².

under vacuum is represented by the Langmuir equation:

$$J = 4.37 \times 10^{-3} p \sqrt{MT} \quad (5.11)$$

where J is the vaporization flux in $\text{kg/m}^2\text{s}$, p is the pressure in N/m^2 , M is the molecular weight and T is the absolute temperature. The vaporization flux, calculated from equation 5.11 is compared with the experimentally determined flux values both in the presence and the absence of a susceptor in table 5.7. The calculated and the experimental values all lie within a factor of ten. However, the theoretical value is higher than the corresponding experimentally determined values. Possible reasons for this include the following: (i) lack of rapid transport in the boundary layer, (ii) surface coverage by impurities that are inevitably present at very low concentrations, even under carefully controlled experimental conditions, (iii) vacuum level in experiments insufficient for application of equation 5.11, and (iv) other factors such as experimental errors in the measurements of surface area and temperature of the drops, and insufficient accuracy in the available value of vapor pressure for use in equation 5.11. These factors are discussed in the following section.

(i) Role of gas phase mass transfer: The flux for the transport of copper vapor from the surface of the drop to the bulk gas phase through the mass-transfer boundary layer surrounding the drop, J_m , is given by:

$$J_m = (p-p^b) k_g/RT \quad (5.12)$$

Table 5.7. Rate of vaporization of copper drops.

Temperature	1873 K
Equilibrium vapor pressure of Cu	84.2 N/m ²
Vaporization flux according to Langmuir equation	6.8 x 10 ⁻² kg/m ² s
Experimentally determined flux when susceptor was used	0.76 x 10 ⁻² kg/m ² s
Experimentally determined flux when susceptor was not used	1.09 x 10 ⁻² kg/m ² s

where p and p^b are the vapor pressures of copper at the interface and in the bulk gas phase, respectively at a temperature T , R is the gas constant and k_g is the mass transfer coefficient. Calculation of p^b from the experimental data of vaporization rate and the flow rate of argon indicated that p^b was negligible compared to p . The calculated value of J_m and the data used for the calculations are presented in table 5.8. It is to be noted that the value of flux computed from mass transport considerations is higher than that predicted by the Langmuir equation (see table 5.7). Thus, if copper vapor is generated in close proximity of the droplet surface at a rate given by the Langmuir equation, the vapor can be readily transported across the boundary layer at the rate at which it is generated without any accumulation of the vapor at close proximity of the vaporizing interface. Thus, the fact that experimental values of the vaporization flux is lower than the theoretical Langmuir rate cannot be attributed to sluggish transport of the vapor through the gas boundary layer.

(ii) Surface coverage effects: If certain surface sites are occupied by surface active elements, the experimental vaporization rate can be lower than the theoretical rate. Small amounts of surface active elements such as oxygen are inevitably present even in high purity copper. Furthermore, minor amounts of impurities can be introduced in the sample from the solid ceramic substrate on which the drop rests during experiments. Calculation of surface coverage on the basis of adsorption considerations indicates that 10 ppm of oxygen in the copper drop can occupy about 50% of the surface sites at 1875 K. When the oxygen content is 0.1 wt%, more than 95% of the surface sites can be covered by oxygen. Thus, it appears that the low experimental flux can be conveniently attributed to the presence of small amounts of surface active impurities - at least

Table 5.8. Estimation of vaporization flux under gas phase mass transfer control

Temperature, T	1873 K
Tube diameter	2.54×10^{-2} m
Argon flow rate at room temperature and pressure	0.83×10^{-6} m ³ /s
Chamber pressure	80 N/m ²
Vapor pressure of copper at the surface, p	84.2 N/m ²
Diffusivity of copper vapor in argon, D	0.52 m ² s
Sherwood number,* Sh	2.37
Diameter of the copper drop, d _p	2.66×10^{-3} m
Mass transfer coefficient,** Kg	2.32×10^2 m/s
Vaporization flux under gas phase mass transport control	8.0×10^{-2} kg/m ² s

* $Sh = 2 + 0.6 Re^{1/2} Sc^{1/3}$

** $Kg = D Sh/d_p$

in principle. However, when the rates of vaporization of copper from samples that were doped with oxygen or sulfur were measured, the rates were found to be higher than those observed from pure copper drops! Thus, low values of vaporization flux cannot be attributed to only the surface coverage effects. When surface active elements are present in copper, the effect of surface coverage is outweighed by other effects that increase the vaporization rate. A more complete discussion of the role of oxygen and sulfur is deferred to a subsequent section.

(iii) Insufficient vacuum: Equation 5.11 is applicable only under perfect vacuum conditions, and it does not take into account recondensation of vapors at inadequate vacuum levels. Therefore, it is possible that the difference between the experimentally observed rate and the calculated rate results, at least in part, are due to this effect.

(iv) Other factors: The discrepancy between the experimentally determined flux and the theoretical rate computed from equation 5.11 can be contributed by errors in the estimation of surface area, measurement and control of temperature, and inaccuracies in the available vapor pressure data. The surface area of the droplet was determined from photographic measurements and appropriate relations of solid geometry and it is unlikely that the error in the estimation of surface area was significant. Small fluctuations of temperature about a mean value might have resulted in a somewhat higher experimental rate than the true rate corresponding to a constant temperature. This is because the vapor pressure is a strong function of temperature and consequently, a slight increase in temperature results in a larger increase in rate than the lowering of the rate resulting from an equivalent decrease in

temperature. Thus, the temperature fluctuation would result in the enhancement of rate and the low value of experimental rate cannot be attributed to errors in temperature control. In the calculation of theoretical vaporization flux we used the most recent vapor pressure data that was available. Indeed, some of the other commonly referred sources of vapor pressure compilations report values as high as 20% higher than the values used in the present study. Thus, the differences between the theoretically calculated and the experimental values of flux cannot be attributed to the error in the vapor pressure data.

It is to be noted that the experimental vaporization flux was lower than the vaporization flux calculated on the basis of kinetic theory of gases under perfect vacuum. However, the difference can neither be attributed to sluggish mass transport in the boundary layer nor can it be explained as a direct consequence of the presence of surface active impurities. At the pressure level maintained in the reaction chamber, 40 to 80 N/m², necessary to sustain a stable plasma, the theoretical promise of equation 5.5 cannot be met in practice, apparently due to recondensation of metal vapors.

5.5.2 Interfacial turbulence - effects of susceptor and surface active elements

Since a high frequency power source was used for the experiments, the skin depth of the induced current was very small. Thus, the presence of a graphite susceptor ensured that there was no significant electromagnetically driven flow in the droplet. The data in figure 5.27 indicate that the presence of a

susceptor decreased the vaporization rate in all the systems studied, namely Cu, Cu-O and Cu-S systems. This effect can be explained by considering the fact that even high purity copper contains very small (<10 ppm) amounts of surface active impurity and that there is a significant difference in the intensity of electromagnetically driven fluid motion in the presence and the absence of a graphite susceptor. This effect is consistent with interfacial turbulence phenomena which occurs when a surface active element is present.⁸⁹

Experiments performed by Langmuir on the evaporation of ether from water illustrate this phenomenon.⁸⁹ When talc was scattered on the surface of water, the particles exhibited abrupt local movements. This is because the eddies in the water facilitate segregation of ether to the surface where it gives rise to a local surface tension decrease. At the same time, the eddies from the ambient atmosphere remove the ether, thereby raising the surface tension as shown in figure 5.28. At any given instant the interface consists of areas of relatively low and relatively high surface tensions. The spatial variation of interfacial tension causes local flow and surface fluctuations exhibited by the motion of the talc particles. These local movements of the interface increase surface area and the rate of vaporization. The oxygen and sulfur present in the copper samples result in interfacial turbulences and lead to enhanced vaporization rates of copper.

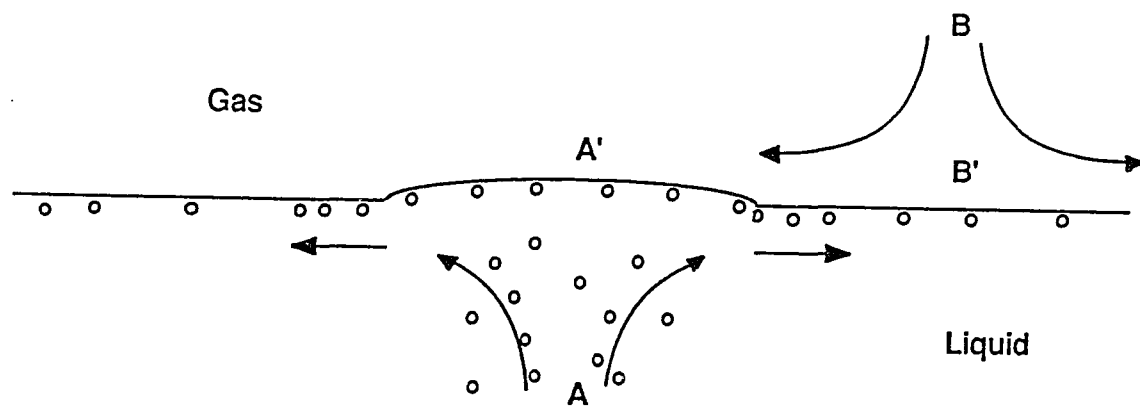


Figure 5.28 A schematic representation of interfacial turbulence phenomenon. An eddy, A, brings a small volume of solution of a surface active agent to the surface, while an eddy, B in the gas depletes the surface active solute. The surface at A' spreads towards B' and carries some underlying liquid with it (after reference 13).

Figure 5.29 shows the results of isothermal vaporization rate of iron and copper systems both in the presence and absence of a plasma. It is observed from the data that the presence of plasma lowers the vaporization rate. The reduction in the vaporization rate due to the presence of plasma is compatible with the enhanced condensation of iron vapors due to a space charge effect shown schematically in figure 5.30. The ionized and excited iron and argon atoms shown in this figure were detected in the plasma by emission spectroscopy, as shown in figure 5.31. In view of the high mobility of the electrons among the various charged species in the system, the region in close proximity of the iron surface is densely populated with positively charged iron and argon ions. Furthermore, the surface of the metal drop becomes negatively charged since the electrons strike the metal surface at a higher flux compared to that of ions.⁹⁰ The attraction between the positively charged ions and the negatively charged droplets leads to higher condensation rates. The comparatively high condensation rate, in turn, results in the reduction of the vaporization rate when plasma is present. This phenomenon is important in understanding the fundamentals of weld pool composition control, since during welding, metals vaporize from the weld pool surface which is surrounded by a plasma plume.⁴⁹

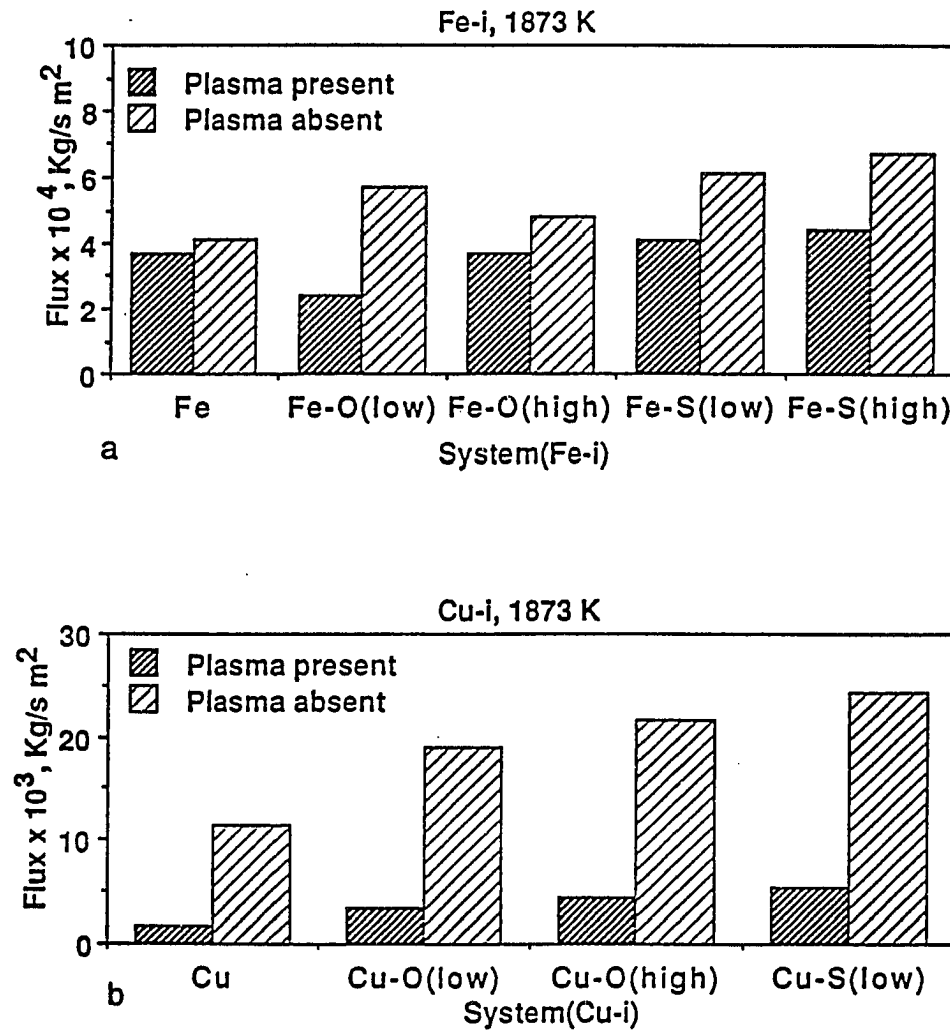


Figure 5.29 Vaporization flux at 1873 K both in the presence and the absence of plasma for (a) iron-solute systems where (low) and (high) denote solute concentrations of 0.03 and 0.25 wt%, respectively, and (b) copper-solute systems where (low) and (high) denote solute concentrations of 0.1 and 0.5 wt%, respectively. Chamber pressures were 40 N/m² and 80 N/m² for iron and copper systems, respectively.

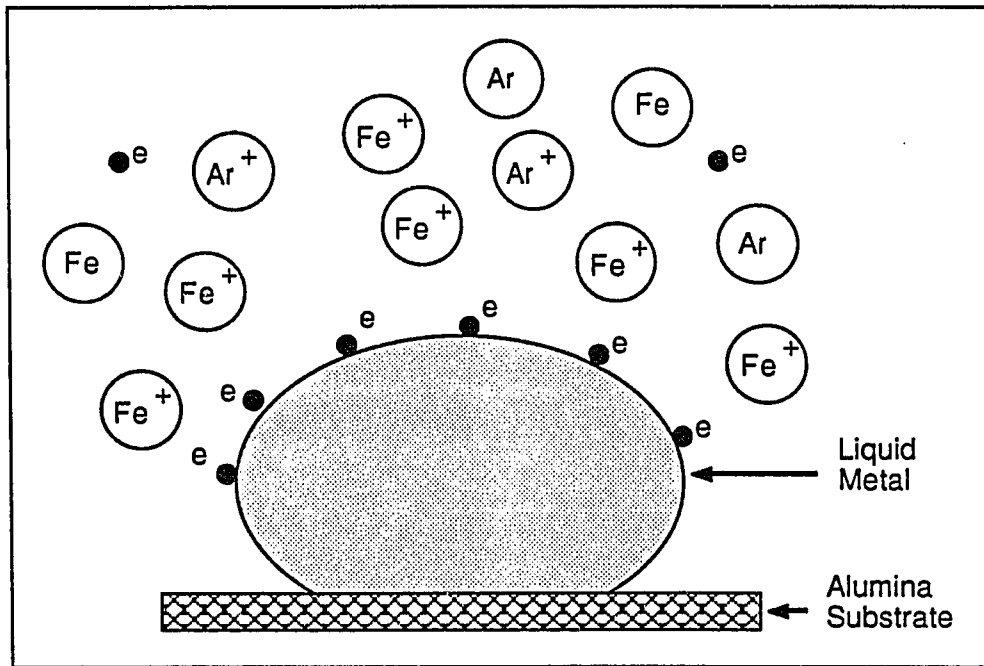


Figure 5.30 A schematic representation of the space charge effect.

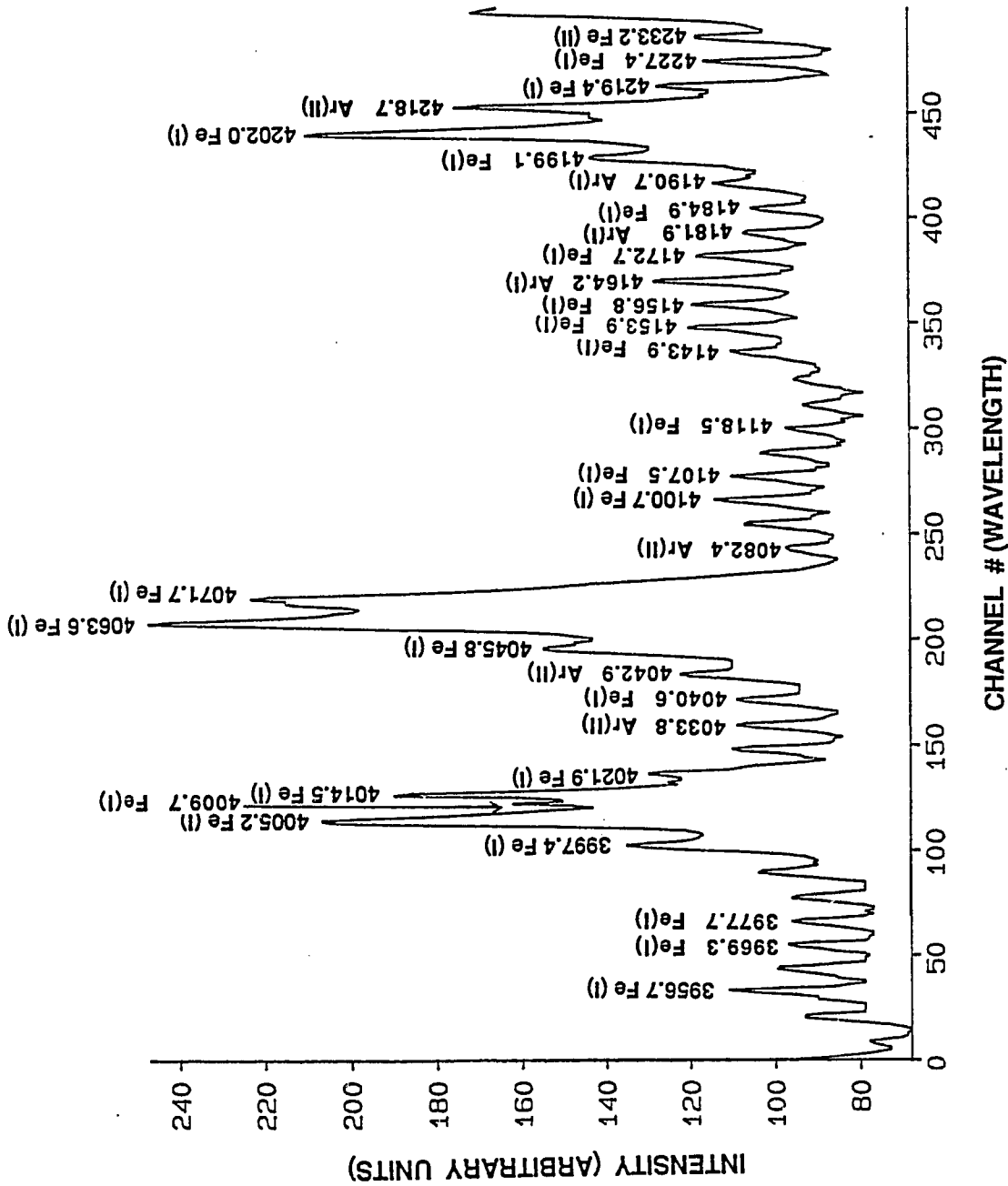


Figure 5.31 Intensity vs wavelength at a chamber pressure of 300 $\mu\text{m Hg}$ and plate current at 1.6 amps.

Previous investigations by Dunn, Allemand and Eagar⁵¹ and by Savitskii and Leskov⁵⁰ have also shown that during welding the presence of surface active elements such as sulfur enhances the rates of vaporization of alloying elements. They proposed that the enhancement in the vaporization rate of iron in the presence of sulfur is due to the formation of sulfides which have low thermal reaction and sublimation heat effects. However, with the low concentration of sulfur present in the samples used in the present study sulfide formation is not expected to play a significant role in the vaporization kinetics.

Chapter 6

CONCLUSIONS AND SUGGESTIONS FOR FUTURE WORK

6.1 Conclusions

During the course of this investigation some of the important aspects of interfacial phenomena that occur during welding were examined from theoretical and experimental standpoints. Specifically, the behavior of surface tension with respect to the temperature and composition in binary systems was established. Fluid flow behavior at the surface of a weld pool was discussed in view of this. A low-pressure low-temperature plasma was generated for the purpose of controlled experimentation and characterized by emission spectroscopy. Several interesting observations were made and the main conclusions of this study are given below.

From the analysis of the available interfacial tension data in Fe-O, Fe-S, Fe-Se, Cu-O, Cu-S, Cu-Se, Cu-Te, Ag-O and Sn-Te systems, it is demonstrated that the interfacial tension in these systems could be satisfactorily described by a formalism based on the combination of Gibbs and Langmuir adsorption isotherms. Furthermore, interfacial tensions in Cr-O, Co-S and Ni-S systems, predicted with some simplifying assumptions, agree fairly well with the limited amount of data reported in the literature. Calculations of temperature coefficients of interfacial tensions in Fe-O and Fe-S systems indicate that for these alloys, $d\gamma/dT$ can change from a positive value at relatively 'low' temperature to a negative value at 'high' temperatures when oxygen or sulfur is

present at fairly high concentrations. Under these conditions the fluid flow in weld pools is likely to be more complicated than a simple recirculation which has been traditionally assumed.

Since under actual welding conditions the interfacial tension is established between the liquid and the surrounding plasma, the interfacial tension of pure copper and iron were measured both in the presence and absence of low pressure argon plasma generated by the application of radio frequency induction current. The emission spectroscopic studies indicated the presence of ionized and excited neutral argon atoms.

The presence of argon plasma lowered the interfacial tension of both iron and copper systems. The reduction was more pronounced in the copper system than the iron system and is consistent with the plasma induced surface segregation of oxygen. The enhanced surface segregation mechanism is also consistent with the reduction of the vaporization rate of copper droplets in the presence of low pressure argon plasma observed in our laboratory. In the range of plasma intensity studied, the interfacial tension did not change appreciably with the plasma intensity.

Experiments conducted in a low pressure hydrogen plasma indicated that the plasma does not affect the interfacial tension of pure copper because of the scavenging action of hydrogen on oxygen. Furthermore, experiments conducted over an extended temperature range indicated that the temperature coefficient of surface tension remains fairly constant with temperature. Experiments to seek the effect of plasma on the interfacial tension of Cu-O samples were conducted. It was observed that although the mean γ value in the

presence of plasma was lower compared to when the plasma was absent, a true statistical difference cannot be drawn.

These results indicate several implications to practical situations. The formalism that has been developed for the surface tension behavior of binary systems can be utilized for more accurate modeling of fluid flow under surface tension driven flow conditions. Also, the variation of the temperature coefficient of surface tension of binary systems was shown to be a function of temperature and composition of the alloy. This implies that in a weld pool containing fairly high oxygen or sulfur contents, $d\gamma/dT$ may go through an inflection point somewhere on the surface of the pool. However, $d\gamma/dT$ for pure copper was found to be independent of temperature over an extended temperature range.

Based on both theoretical and experimental considerations it was observed that both the lowering of surface tension and the positive temperature coefficient of surface tension can contribute to increased depth of penetration during welding. The importance of the absolute value of interfacial tension stems from the fact that the depression of the liquid pool surface due to the arc pressure is resisted by the force due to interfacial tension. It is thought that the lowering of interfacial tension of iron due to the presence of argon plasma during arc welding would be useful in explaining the depression of the weld pool surface and the resulting weld penetration. However, for the case of laser welding the absolute magnitude of surface tension would not play a major role.

Another major problem in high power density welding, namely the loss of volatile alloying elements, was examined by conducting controlled isothermal vaporization rate experiments. Rates of isothermal vaporization of metal drops were enhanced when oxygen or sulfur were present in iron and

copper drops. The increase in the rate is consistent with the interfacial turbulence caused by the surface active elements. The vaporization rates were diminished when a graphite susceptor was used to prevent electromagnetically driven flow on the droplet surface. The presence of low pressure argon plasma led to reduction of metal vaporization rates from the drops due to a space charge effect.

6.2 Suggestion for future work

Phenomena that occur at an interface are extremely complex and their effects are multifarious. The complexity is further compounded by the presence of charged species that are present near the interface. Based on the present investigation, several suggestions are proposed for future study.

1. The formalism to quantify γ , as a function of temperature and composition, that has been developed as a result of theoretical considerations need to be buttressed by extensive experimental studies to examine its efficacy. The available experimental data have indicated the viability of the formalism but further work needs to be carried out in other systems.
2. The present investigation has also developed a relationship between the temperature coefficient of surface tension and the temperature and composition of the solution. Independent experimental studies need be performed over a wide range of temperature and composition of alloying element to examine agreement between the theoretical values and the experimental data.

3. The present work has primarily focussed on binary systems. However, in actual welding situations the materials consists of several ingredients. Future work should focus on deriving the interfacial tension of actual alloys used and the temperature coefficient of surface tension of these alloys.
4. Laboratory tests have indicated that the presence of argon plasma depresses the vaporization rate of metals. It would be important to test this finding by performing actual welding tests. One way of conducting this is to use different shielding gas mixtures with different ionization potentials. For example, Ar has a much lower ionization potential compared to He and could be used when the presence of plasma was required as opposed to using He when a plasma was not required.

REFERENCES

1. J. F. Ready: Industrial Applications of Lasers, Academic Press, New York, PP. 353-354, 1971.
2. W. B. Estill and B. D. Formisano: Proceedings of the International Congress of Applications of Lasers and Electron Optics (ICALEO), Laser Institute of America, vol. 38, pp. 67-72, 1983.
3. C. M. Banas: Proceedings of the C.E.G.B. International Conference on Welding Research Related to Power Plants, Southampton, England, September 17-21, pp. 565-573, 1972.
4. E. V. Locke, E. D. Hoag and R. A. Hella: Weld. J. vol. 51, pp. 245s-249s, 1972.
5. K. Minimada, S. Yamaguchi, H. Sakurai and H. Takafuji: ICALEO, vol. 31, pp. 65-72, 1982.
6. C. R. Heiple and J. R. Roper: Welding Journal, vol. 61, pp. 97s-102s, 1982.
7. C. R. Heiple, J. R. Roper, R. T. Stagner and J. J. Alden: Welding Journal, vol. 62, pp. 72s-77s, 1983.
8. S. Kou and D. K. Sun: Metall. Trans. A, vol. 16A, pp. 203-213, 1985.
9. R. A. Woods and D. R. Milner: Weld. J., vol. 50, p. 163s, 1971.
10. C. R. Heiple and J. R. Roper: in Trends in Welding Research in the United States, S. A. David, ed., ASM, Metals Park, OH, pp. 489-515, 1982.
11. C. R. Heiple and J. R. Roper: Weld. J., vol. 60, pp. 143s-145s, 1981.
12. C. R. Heiple, P. Burgardt and J. R. Roper: Modeling of Castings and Welding Processes II, J. A. Dantzig and J. T. Berry, ed., TMS-AIME, Warrendale, PA, PP. 193-205, 1984.
13. C. R. Heiple and P. Burgardt: Weld. J., vol. 64, p. 159s, 1985.
14. J. K. Brimacombe and F. Weinberg: Metall. Trans., Vol. 3, pp. 2298-2299, 1972.

15. R. E. Sundell, S. M. Correa, H. D. Solomon, L. A. Wojcik, D. W. Walsh and W. F. Savage: 1985 NSF Manufacturing Systems Research Conference, May 14-17, University of Wisconsin-Madison.
16. R. C. Crafer: Weld. Inst. Res. Bull., vol. 17, pp. 29-33, 1976.
17. P. A. A. Khan and T. DebRoy: Metall. Trans. B., vol. 15B, pp. 641-644, 1984.
18. D. W. Moon and E. A. Metzbower: Welding Journal Research Supplement, vol. 62, pp. 53-58, 1983.
19. L. R. Hettche, E. A. Metzbower, J. D. Ayers and P. A. Moore: Naval Reviews, vol. 28, pp. 4-20, 1981.
20. P. Sahoo and T. DebRoy: Metall. Trans. B, vol. 18B, pp. 597-601, 1987.
21. F. Bashforth and J. C. Adams: An Attempt to Test the Theory of Capillary Action, Cambridge University Press and Deighton Bell and Co., Cambridge, 1892.
22. Y. Rotenberg, L. Boruvka and A. W. Neuman: J. Colloid and Interface Science, vol. 93, pp. 169-183, 1983.
23. R. Sangiorgi, G. Caracciolo and A. Passerone: J. Materials Science, vol. 17, pp. 2895-2901, 1982.
24. D. W. G. White: Trans. ASM, vol. 55, pp. 757-777, 1967.
25. B. Gallois and C. H. P. Lupis: Metall. Trans. B, vol. 12, pp. 549-557, 1981.
26. M. E. Fraser, W. K. Lu, A. E. Hamilec and R. Murarka: Metall. Trans., vol. 2, pp. 817- , 1971.
27. R. N. Murarka, W. K. Lu and A. E. Hamilec: Can. Met. Quart., vol. 14, pp. 111-115, 1975.
28. H. Soda, A. McLean and W. A. Miller: Trans. JIM, vol. 18, pp. 445- , 1977.
29. H. Soda, A. McLean and W. A. Miller: Metall. Trans. B, vol. 9B, p. 145, 1978.
30. B. J. Keene, K. C. Mills, J. W. Bryant and E. D. Hondros: Can. Met. Quart., vol. 21, pp. 393-403, 1982.

31. Lord Raleigh: Proc. Roy. Soc. vol. 29, p. 71, 1879.
32. G. R. Belton: Metall. Trans. B, vol. 7 B, pp. 35-42, 1976.
33. A. Kasama, A. McLean, W. A. Miller, Z. Morita and M. J. Ward: Can. Met. Quart., vol. 22, pp. 9-17, 1983.
34. K. Ogino, K. Nogi and O. Yamase: Trans. ISIJ, vol. 23, pp. 234-239, 1983.
35. Z. Morita and A. Kasama: Trans. JIM, vol. 21, pp. 522-530, 1980.
36. S. P. Mehrotra and A. C. D. Chaklader: Metall. Trans. B, vol. 16, pp. 567-575, 1985.
37. B. Von Szyszkowski: Z. Phys. Chem., vol. 64, pp. 384-414, 1908.
38. J. H. Clint, J. M. Corkill, J. F. Goodman and J. R. Tate: J. Colloid Interface Science, vol. 28, pp. 522- , 1968.
39. G. Bernard and C. H. P. Lupis: Surf. Sci. vol. 42, pp. 61-85. 1974.
40. R. H. Fowler and E. A. Guggenheim: Statistical Thermodynamics, MacMillan, New York, p. 430, 1939.
41. C. H. P. Lupis: Chemical Thermodynamics of Materials, Elsevier Science Pub. Co., New York, 1983.
42. C. Marangoni: Annalen der Physik und Chemie, vol. 143, p. 337, 1871.
43. E. Friedman: Weld. J. Res. Suppl. vol. 57, pp. 161- , 1978.
44. P. Burgardt and C. R. Heiple: Weld. J., vol. 65, pp. 150- , 1986.
45. B. J. Keene, K. C. Mills and R. F. Brooks: Mat. Sci. Tech., vol. 1, pp. 568-571, 1985.
46. R. E. Sundell, H. D. Walsh, L. P. Harris, S. M. Coorrea, D. W. Walsh and W. F. Savage: Proceedings of the Conference in Resolving Undesirable Trace Element Effects on the Weldability of Steel, ed., C. R. Heiple, Rocky Flats Plant, pp. 10-29, 1986.
47. B. Pollard: Ibid, pp. 30-41.

48. A. A. Romanov and V. G. Kochegarov: *Phys. Met. Metallogr.*, vol. 17, p. 136, 1964.
49. M. M. Collur, A. Paul and T. DebRoy: *Metall. Trans. B*, vol. 18B, pp. 733-740, 1987.
50. M. M. Savitskii and A. I. Leskov: *Autom. Weld.* vol. 33, pp. 11-16, 1980.
51. G. J. Dunn, C. D. Allemand and T. W. Eagar: *Metall. Trans. A*, vol. 17A, pp. 1851-1863, 1986.
52. E. T. Turkdogan, S. Ignatowicz and J. Pearson: *J. Iron and Steel Inst.*, p. 349, 1955.
53. T. Rosenqvist and B. L. Dunicz: *Trans. AIME*, p. 605, 1952.
54. L. Coudurier, D. W. Hopkins and I. Wilkomirsky: *Fundamentals of Metallurgical Processes*, Pergamon Press, 1978.
55. A. W. Adamson: *Physical Chemistry of Surfaces*, Wiley, New York, 1976.
56. J. W. Gibbs: *The Collected Works of J. W. Gibbs*, Longmans, Green, New York, 1931, vol. I, p. 219.
57. J. Oudar: *Physics and Chemistry of Surfaces*, Blackie & Son, London, 1975.
58. L. H. Germer, R. M. Stern and A. V. Mac Rae: *Metals Surfaces: Structure, Energetics and Kinetics*, *Am. Soc. Met.*, p. 287, 1963.
59. A. V. Mac Rae: *Surf. Sci.*, vol. 1, p. 319, 1964.
60. G. V. Marr: *Plasma Spectroscopy*, Elsevier Pub. Co., p. 1, 1968.
61. T. B. Reed: *International Sci. Tech.*, vol. 42, pp. 42-47, 1962.
62. V. M. Goldfarb and D. H. Douglas-Hamilton: *Proc. of the First Annual International Conf. of Plasma Chemistry and Technology*, H. V. Boenig, ed., pp. 33-39, 1982.
63. R. C. Johnson: *Atomic Spectra*, John Wiley and Sons, New York, 1961.
64. Adir Jacob: *Proceedings of the First Annual International Conference of Plasma Technology*, H. V. Boenig, ed., p. 190, 1982.

65. P. Friedel and S. Gourier: *J. Phys. Chem. Solids*, vol. 44, pp. 353-364, 1983.
66. P. W. J. M. Boumans: *Theory of Spectrochemical Excitation*, Plenum Press, New York, 1966.
67. G. Bernard and C. H. P. Lupis: *Metall. Trans.*, vol. 2, pp. 2991-2998, 1971.
68. B. C. Allen: *Trans. Met. Soc. AIME*, vol. 227, pp. 1175-1183, 1963.
69. H. P. Papazian: *Scripta Met.*, vol. 18, pp. 1401-1403, 1984.
70. F. A. Halden and W. D. Kingery: *J. Phys. Chem.*, vol. 59, pp. 557-559, 1955.
71. P. Kozakevitch: *Surface Phenomena of Metals*, Society of Chemical Industry Monograph 28, pp. 223-245, 1968.
72. P. Kozakevitch, S. Chatel, G. Urbain and M. Sage: *Rev. Met.*, vol. 52, pp. 139-160, 1955.
73. G. S. Ershov and V. M. Bychev: *Russ. Metall.*, vol. 4, pp. 45-46, 1975.
74. P. Kozakevitch and G. Urbain: *Mem. Sci. Rev. Met.*, vol. 58, pp. 517-534, 1961.
75. K. Monma and H. Suto: *J. Jpn. inst. Met.*, vol. 2, pp. 377-399, 1961.
76. C. F. Baes and H. H. Kellog: *Trans. AIME*, vol. 197, pp. 643-648, 1953.
77. K. Monma and H. Suto: *Trans. Jpn. Inst. Metals*, vol. 2, pp. 148-153, 1961.
78. K. Monma and H. Suto: *J. Japan Inst. Metals*, vol. 24, pp. 374-377, 1960.
79. K. H. Wedepohl (Executive ed.): *Handbook of Geochemistry*, Springer-Verlag, 1969.
80. R. G. Ward: *An Introduction to the Physical Chemistry of Iron and Steel Making*, Edward Arnold Ltd., London, 1962.
81. S. Otsuka and Z. Kozuka: *Metall. Trans. B*, vol. 11, pp. 119-124, 1980.

82. K. Nogi, W. B. Chung, A. McLean and W. A. Miller: Private Communication, 1985.
83. K. Monma and H. Suto: J. Japan Inst. Metals, vol. 24, pp. 611-614, 1960.
84. M. Bramson: Infrared Radiation, A Handbook for Applications, Plenum Press, New York, p. 127, 1968.
85. B. F. Dyson: Trans. Met. Soc. AIME, vol. 227, p. 1098, 1963.
86. B. C. Allen and W. D. Kingery: Ibid, vol. 215, p. 30, 1959.
87. A. Kasama, A. McLean and W. A. Miller: Can. Met. Quart., vol. 19, pp. 399-401, 1981.
88. A. Paul and T. DebRoy: Advances in Welding Science and Technology, S. A. David, ed., ASM, Metals Park, OH, pp. 29-33, 1986.
89. F. D. Richardson: Physical Chemistry of Melts in Metallurgy, Academic Press, vol. 2, pp. 452-453, pp. 452-453, 1974.
90. B. Chapman: Glow Discharge Processes, Wiley-Interscience, John Wiley and Sons, pp. 51-57, 1981.
91. Y. Arata, S. Miyake, H. Matsuoka and H. Kishimoto: Trans. JWRI, vol. 10, pp. 33-38, 1981.
92. B. C. Allen: Liquid Metals-Chemistry and Physics, S. Z. Beer, ed., pp. 161-212, M. Dekker, Inc., New York, 1972.
93. B. J. Keene: National Physical Laboratory, Teddington, Report NPL-DMA-a-56, 1982.

Appendix

CALCULATION OF BOND NUMBER

The buoyancy force, F_b , is expressed as:

$$F_b = -\rho\beta g (T - T_0) \quad (\text{A.1})$$

and the surface tension force, F_γ , is expressed as

$$F_\gamma = - \frac{\partial \gamma}{\partial T} \frac{dT}{dx} \quad (\text{A.2})$$

where

ρ = density of liquid metal

β = thermal expansion coefficient of liquid metal

g = acceleration due to gravity

T = Temperature

T_0 = reference temperature

γ = surface tension of liquid metal

For the case of laser welding thin iron plates with a 0.5 KW CO₂ laser, some typical values of the various parameters are listed in table A.1. The Bond number, B_0 , is given as the ratio of the buoyancy force to the surface tension force.

Table A.1 Typical values of various parameters for laser welding of thin iron plates using a 0.5 KW CO₂ laser.

Parameter	Value
ρ	$6.8 \times 10^3 \text{ kg/m}^3$
β	$3.6 \times 10^{-6} \text{ m/mK}$
g	9.8 m/s^2
T	3000 K
T_0	2000 K
dy/dT	$-4.3 \times 10^{-4} \text{ N/mK}$
l	10^{-3} m

Noting that F_b is a volumetric force and F_γ is a force per unit area, we have

$$B_o = \frac{F_b}{F_\gamma} = \frac{-\rho \beta g (T - T_o) V}{\frac{\partial \gamma}{\partial T} \frac{dT}{dx} A} \quad (\text{A.3})$$

$$= \frac{-\rho \beta g (T - T_o) l}{\frac{\partial \gamma}{\partial T} \frac{dT}{dx} A} \quad (\text{A.4})$$

where l is a characteristic length.

Substituting values from table A.1 into equation A.4 gives B_o approximately equal to 0.006. This means that the buoyancy force is less than 1% of the surface tension force.

Vita

Born: Cuttack (INDIA), March 16, 1959.

High School Graduation: Hijli High School (Kharagpur, India), 1976.

College:

I.I.T. Kharagpur, B.Tech(Honors), Metallurgical Engineering, 1981.

University of Nevada-Reno, M.S., Metallurgical Engineering, 1984.

Pennsylvania State University, Ph.D., Metals Science and Engineering.

Employment: Worked as process engineer at Mukand Iron & Steel Company,
Bombay, India, 8/81 to 7/82

Publications:

1. Effect of oxygen and sulfur on alloying element vaporization rates during welding: Submitted to Metallurgical Transactions, 1988.
2. Interfacial Tension Between Low Pressure Argon Plasma And Molten Copper And Iron: Metallurgical Transactions B, pp. 597 601, September 1987.
3. Surface Tension Of Binary Metal-Surface Active Solute Systems Under Conditions Relevant To Welding Metallurgy: To be published in Metallurgical Transactions B, 1988.
4. Activity Coefficient Of Nickel Oxide In FeO-NiO-FeO_{1.5}-AlO_{1.5}-SiO₂ Slag At 1573K: Second International Symposium On Metallurgical Slags And Fluxes, Eds., H. A. Fine and D. R. Gaskell, 1984.

Professional affiliations:

VICE-CHAIRMAN: The Penn State Chapter of the AWS.

STUDENT MEMBER: The American Welding Society.

STUDENT MEMBER: The Metallurgical Society of AIME.